Multispectral Segmentation of Magnetic Resonance Images of the Human Brain

by

S. M. Javad Alirezaie

A thesis
presented to the University of Waterloo
in fulfilment of the
thesis requirement for the degree of
Doctor of Philosophy
in
Systems Design Engineering

Waterloo, Ontario, Canada, 1996

The University of Waterloo requires the signatures of all persons using or photocopying this thesis. Please sign below, and give address and date.

Abstract

Segmentation is an important step in the interpretation of Magnetic Resonance (MR) images of the human body. MRI reveals an unequaled view of the anatomy of the brain in terms of spatial and contrast resolution, and its multispectral nature has been exploited to obtain better performance in the segmentation process. This thesis presents new techniques based on artificial neural network (ANN) architectures for automatic segmentation and tissue classification of MR images of the human brain. Two different methodologies were adapted for supervised and unsupervised segmentation.

The Learning Vector Quantization (LVQ) ANN is utilized for multispectral supervised classification of MR images. The original LVQ was modified for better and more accurate classification. LVQ ANN segmentation results are compared to those achieved with a backpropagation ANN and a conventional Maximum Likelihood Classifier (MLC).

In the second scheme a fully automated technique was developed for segmentation. The scheme utilizes the Self Organizing Feature Map (SOFM) ANN for feature mapping and generates a set of codebook vectors for each tissue class. An additional layer then completes the classification process. To minimize clustering artifacts, an algorithm has been developed for isolating the cerebrum prior to segmentation. The cerebrum is extracted by stripping away the skull pixels from the T2 weighted image. The network is tested for different sets of image slices from normal and abnormal brain studies. Images were selected from 54 axial images of the whole head.

Twenty nine brain studies were analyzed using the techniques developed in this thesis. Three tissue types of the brain are segmented: white matter, gray matter

and cerebrospinal fluid (CSF); in case of abnormality, the tumor or other unknown tissues were also segmented. From the evaluation of segmentation results, the advantages and disadvantages of each method are discussed.

Acknowledgements

I wish to express my gratitude to my supervisors professor Ed Jernigan and professor Claude Nahmias, for their continuous help, encouragement, and supportive attitude throughout my research. Their guidance and understanding helped to elevate and promote my work to a level that would not have been otherwise possible. Their assistance and inspiration are gratefully appreciated.

I would like to thank the members of my advisory committee Dr. Vrscay, Dr. Stacey, Dr. Robinson and Dr. Sid-Ahmed for their considerable efforts and advice.

I would also like to thank the administrative assistants Sue Gooding, and Annette Dietrich for their generous help.

The support of special friends and colleagues in VIP and MIND lab has been greatly appreciated and will always be remembered.

I sincerely appreciate the Ministry of Culture and Higher Education of Islamic Republic of Iran and professor Ed Jernigan for the financial support and sponsorship.

I thank my parents for the continuous support of my endeavours. Finally, special thanks to Mehri my wife. Her patience, love, and understanding were instrumental for successful completion of my dissertation.

Dedicated to the most

important people in my life:

Mehri, Mahdi, Mohammad Saeed, and my parents.

Contents

List of Figures

Chapter 1

Introduction

Magnetic Resonance Imaging (MRI) is fast becoming the technique of choice to study the brain in health and disease [16]. It reveals an unequaled view of the anatomy of the brain in terms of spatial resolution as well as contrast resolution. Segmentation is the first step in the analysis of brain morphometry ; subsequently, volumes, shapes and positions can be determined [63]. Automating the feature extraction process provides for an objective and reproducible method of analysis. While there were many possible approaches to image segmentation, a *neural network* approach is appropriate because it draws directly on human experience to develop the necessary algorithms.

This thesis describes a neural network approach to the automatic segmentation of magnetic resonance brain images. This chapter describes the nature and significance of the problem domain and then outlines the proposed solution.

1.1 Segmentation of MR brain images

1.1.1 Magnetic resonance brain imaging

Figure 1.1 shows three slices from an MR study of the brain of a human subject. The slices are obtained at the same level in the brain, but using different pulse sequences, an MR technique that allows for the manipulation of contrast between different tissues. A typical examination consist of 54 axial slices each 5mm thick. The brightness of each voxel (volume pixel; 1mm by 1mm by 5mm in this case) reflects an average measurement of the tissue characteristics over that volume of the brain. While a detailed description of the magnetic resonance imaging (MRI) technique itself is beyond the scope of this thesis, a brief discussion of the imaging process should provide sufficient background to introduce the multispectral nature of the MR examination.

1.1.2 The physics and nature of MRI data

This discussion presents the classical interpretation of the behavior of nuclear magnetic moments by using the hydrogen nucleus (i.e., a single proton) as a model. In the classical interpretation, the position of the hydrogen nucleus can be specified with any desired degree of precision, and its movements are assumed to be continuous and completely predictable. Each proton behaves as a small magnet with a magnetic moment that has both magnitude and direction. In any sample of material containing hydrogen (such as the human body), the magnetic moments of the individual hydrogen nuclei are oriented in random directions. If a strong magnetic field is applied to the sample, the magnetic moments of the nuclei align in the direction of the applied magnetic field in a manner similar to that of a compass

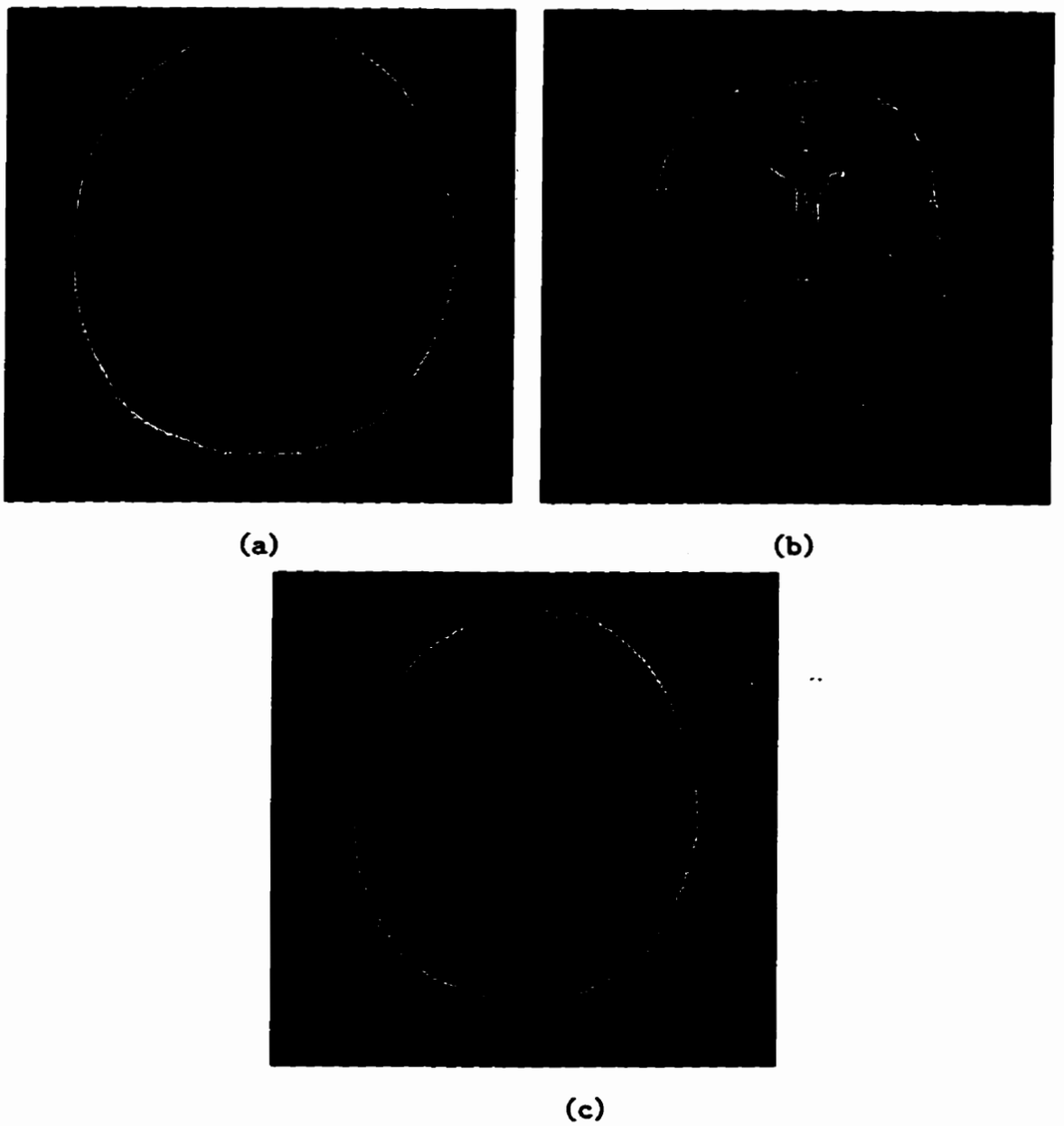

Figure 1.1: (a): A T1-weighted image (b) A T2-weighted image (c) A PD-weighted image.

needle aligning with the earth's magnetic field. The field provided by the main magnet of an MR system is of the order of 1 tesla (compared to 0.5×10^{-5} tesla for the Earth's magnetic field).

In addition to aligning itself with the applied magnetic field, the magnetic moment will also precess about this field. The frequency f_L of precession of a proton depends upon its gyro-magnetic ratio γ and the strength of the static magnetic field B_0. This relation is described by the Larmor equation.

$$f_L = \frac{\gamma}{2\pi} B_0 \qquad f_L \text{ in MHz, } B_0 \text{ in tesla (T)}$$

Different nuclei have different gyro-magnetic ratios, and the resonant frequency of a specific nucleus will vary with the magnitude of the applied magnetic field. A radio-frequency, RF, pulse at the resonant frequency (f_L) can excite the precessing nucleus to a higher energy state in which its magnetic moment is aligned in the opposite direction to the magnetic field. The nucleus then returns to the lower energy state by transferring its excess energy to the neighboring nuclei or to the surrounding lattice.

The collective effect of the applied magnetic field on many nuclei is described by a magnetization vector whose direction is given relative to the direction of the main magnetic field. At equilibrium the longitudinal component of the magnetization vector has a maximum value M_o that depends on the number of nuclei aligned anti-parallel to the field. For any tissue, this value depends on the concentration of the MR visible protons, or *proton density*, in the tissue. When the RF pulse is turned on, the longitudinal magnetization, M_z, decreases with the number of nuclei flipping to the excited state. At the same time, the transverse magnetization, M_{xy}, appears as a result of the synchronization of the precessing nuclei induced by the RF pulse. M_{xy} will precess around B_o, thus creating an oscillating magnetic field

that will induce a current in an antenna near by. This is the MR signal. When the RF pulse is switched off, the nuclei are flipped back to the original state, allowing the longitudinal magnetization to return to its equilibrium position (see Figure 1.2).

There are two basic relaxation processes at work in the sample as the protons return to the state that existed before the RF pulse was applied. Both processes account for the observed decay of the MR signal. One relaxation process involves a return of the protons to their original alignment with the static magnetic field. This process, called longitudinal or spine-lattice relaxation, is characterized by a time constant T1 (see Fig 1.3 (a)). The other relaxation process is a loss of synchrony of precession among the protons. Before a radio wave is applied, the direction of magnetization of the protons within their precession is random. Immediately following the application of a radio wave, the protons rotate synchronously, or in phase. When the radio frequency is switched off, the protons begin to interact with their neighbors and give up energy in random collisions and so revert to a state of random phase. As the protons return to random orientation, the bulk signal decreases. This process is called transverse or spin-spin relaxation and is characterized by a time constant T2 (Fig. 1.3 (b)).

In any sample undergoing MRI both relaxation processes, longitudinal and transverse, occur at the same time, although the transverse or T2 relaxation is always much shorter than the longitudinal or T1 process. For typical biologic materials, T1 may be on the order of several hundred milliseconds while T2 is a few tens of milliseconds.

The influence of the relaxation parameters on the MR signal is one of the central principles of tissue contrast in MRI. Contrast in MRI is influenced by differences in relaxation parameters, T1 and T2, and nuclear spin density (proton density (PD) number of MR visible protons per unit volume of tissue), among tissues. Since

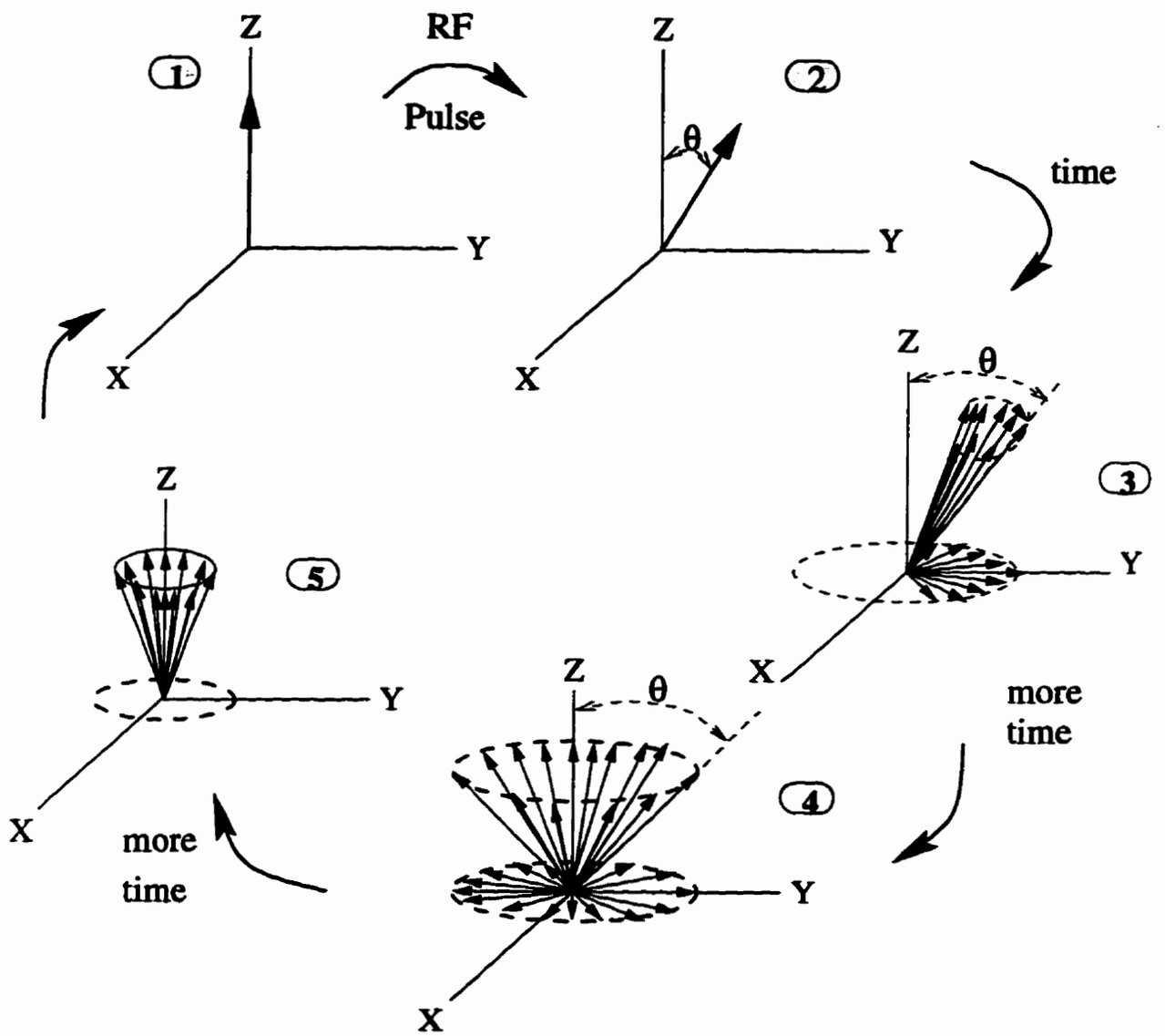

Figure 1.2: **1.** Magnetic moment of the sample is aligned with the magnetic field. **2.** Immediately after an RF pulse, the magnetic moment of the sample can be represented by a single vector. **3.** As the magnetization vector begins to break up or dephase as a result of localized non-uniformities in the applied field, components of the vector begin to fan out in the xy plane. **4.** When there are an equal number of components in all directions in the xy plane, the components cancel one another and the MR signal disappears. **5.** As time passes, the cone representing the processing but dephased magnetic moment continues to narrow because of spin-lattice relaxation. **1.** Finally the magnetic moment once again is realigned with the applied field.

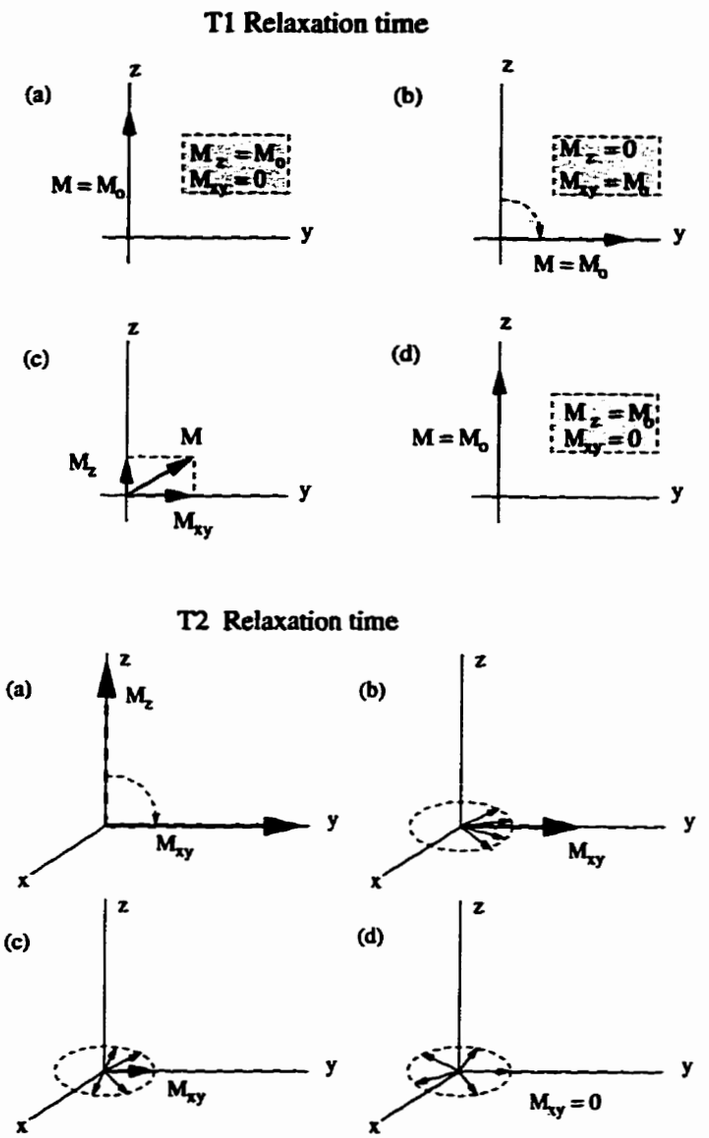

Figure 1.3: Longitudinal and transverse relaxation process

different tissues have different T1, T2 and proton density values, these parameters can be used to discriminate between tissues in the image. Measurement techniques that exploit differences in T1, T2, and PD among tissues are described in [58], [30], [100] and [102].

1.1.3 Segmentation and tissue classification

Image segmentation refers to the decision process whereby similar pixels of an image are grouped into regions that correspond to objects or pieces of objects in a scene. For the purpose of this thesis, segmentation refers to the pixel by pixel labeling of regions as gray matter, white matter, cerebrospinal fluid, bone, skin & fat, background, and tumor (if present).

Major problems with segmentation of MRI

Looking at Figure 1.1 (b), it might seem easy even for an untrained observer to decide which regions to assign to the tissue class of gray matter, white matter, CSF, etc. The task seems trivial because we take for granted the human visual system's astonishingly effective segmentation abilities. Marr [81] argues that the task of seeing only seems easy. He states that, "The reason for this misperception is that we humans are ourselves so good at vision". He remembers that in his attempts to solve computer vision problems in general "The first great revelation was that the problems are difficult. (p.16 [81])"

Figures 1.1 and 1.4 demonstrate the difficulty of this task. One reason the task is difficult is because a single image intensity threshold cannot be selected to distinguish gray matter from white matter. It can be seen that no single contour line can be chosen that will adequately divide, for instance, the gray and white matter in Figure 1.1(a). It is easy to pick out the sweeping dark lines that divide the white matter from gray matter in Figure 1.1(b) but much more difficult to find them. The pixels that our eyes somehow group into a single dark line actually span a large range of intensities. By looking at the image histograms in Fig. 1.4, it is clear that labeling all pixels below a given threshold would certainly not achieve

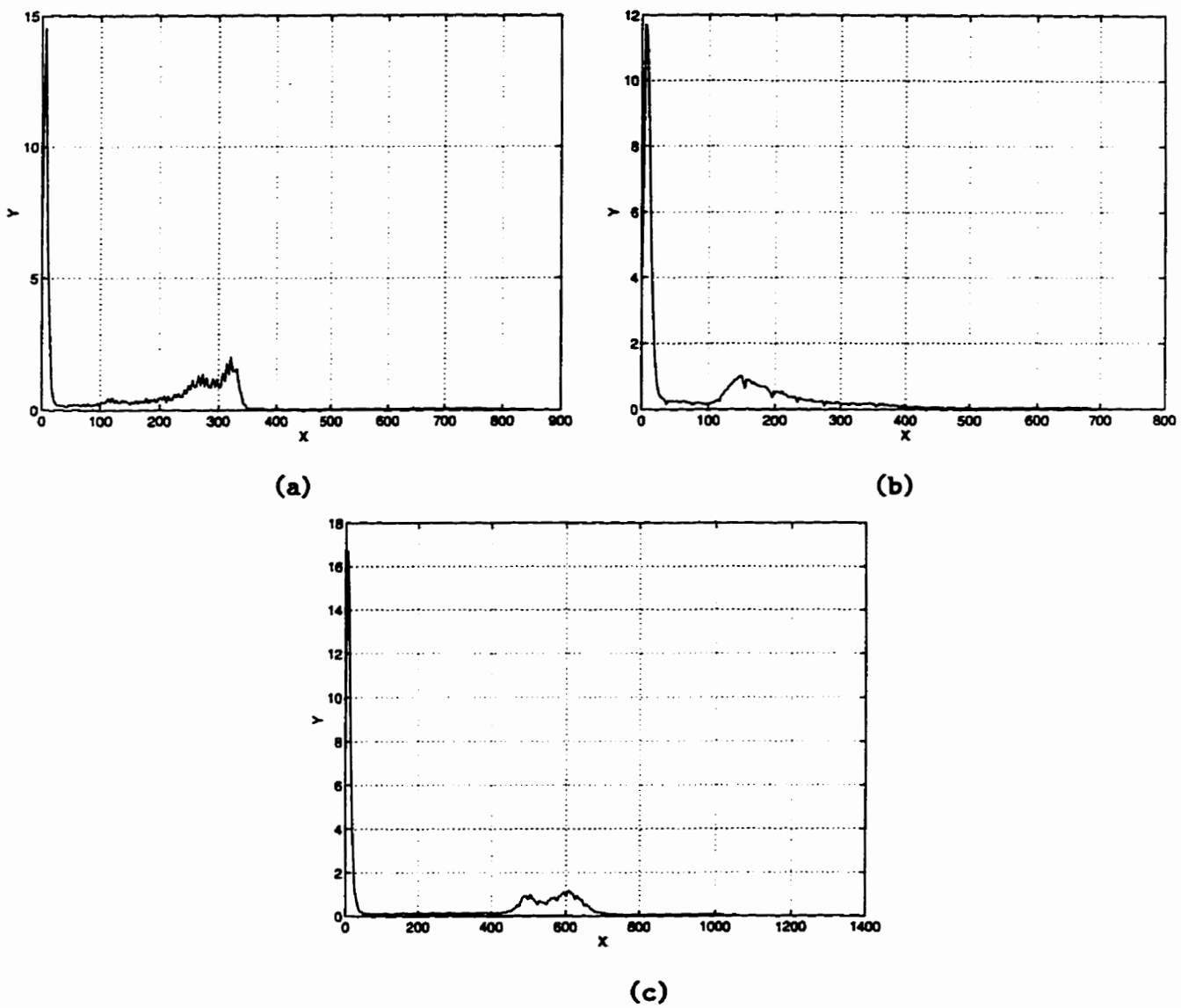

Figure 1.4: (a): Histogram of T1-weighted image (b) Histogram of T2-weighted image (c) Histogram of PD-weighted image.

the desired result.

The lack of a single threshold for segmenting an image is only the beginning of the difficulties. If such a threshold could be found for a particular image it

would not necessarily be the same for other images because the many sources of variation in the MRI process do not allow intensity to be an absolute measure. As a matter of fact one of the major problems in the segmentation of MR images is the intensity variations introduced by inhomogeneities in the magnetic field [26]: These occur within a slice, between slices in the same patient study, and between patient studies.

Another problem is what is known as the partial volume effect. This occurs because the MRI technique samples the tissue characteristics across discrete 3-dimensional volume elements (voxels) at a certain resolution, and the resulting signal intensity reflects the average tissue characteristics over this volume. This causes transitions in tissue characteristics to seem blurred: the edges, for instance, between gray matter and white matter are not ideal step edges, but could more accurately be approximated by a ramp [91].

There are also problems which may not be solvable, for instance labeling the segmented regions by their anatomical name. This task requires information that is not directly obtainable from the image. When tackling this kind of problem, the conclusion drawn by many researchers is that there is need for high level information or knowledge (see, for example: [48], [9], [111], [73] and [86]). Still another problem is that this high level knowledge must be specific for a given application in order to be useful.

1.2 Importance of segmentation

Automatic segmentation and tissue classification of MR brain images are important tasks because segmentation is fundamental to a quantitative analysis of the brain and because automation can increase the reliability of this analysis. Stiehl in [115]

describes the significance of segmentation: "Segmentation of primitives and subsequent grouping to anatomically meaningful objects is the building-block for feature measurement (*e.g.*, via tissue characterization, shape recovery, and morphometry), organ recognition, as well as 3D representation and graphics display. At present no generally applicable, parameter-free, or even self-adaptive automatic segmentation scheme exists that is completely independent of the image class, the object class, the domain and the task for the SISU [1] system (p. 25 [115])".

Quantitative measurements from MR brain images can provide an unequaled view into the understanding of human brains through morphological analysis [16]. Segmentation is the first step to providing this analysis. Subsequent to segmentation, the volume, shape, location and homogeneity of component brain structures can be calculated. Segmentation and subsequent analysis can lead to a better understanding of the development of the brain. Since MRI is non-invasive, morphological studies can be performed at regular intervals during development. Previous research using these kind of techniques include characterization of the normal population as a function of age [35], [56], anatomical variability of primary visual cortex [62] [130], Alzheimer's disease [8], [14], and developmental disorders [34], [36].

An automatic MRI brain segmentation system also has another potential clinical application: the diagnosis of brain trauma. White matter lesions which are typical of diffuse axonal injury, a signature of traumatic brain injury, may potentially be identified in moderate and possibly even mild cases. These methods, in turn, may require correlation of anatomical images with functional metrics to provide sensitive measurements of brain trauma [54].

Automatic segmentation is a natural extension of the use of computers in

[1]SISU stands for Spatial Image Sequence Understanding

medicine. The improvement from a purely visual, qualitative analysis to three-dimensional tomographic analysis and then to automated analysis can make physicians' and researchers' image analysis tasks easier and possibly more accurate [115].

Automatic segmentation not only requires less time from human experts, but can also provide less variable results. For instance, in the study of Alzheimer's disease where the quantities of interest are the volumes of white matter and gray matter, if manual delineation is considered the analysis would be time consuming and tedious, and would require a qualified observer [63]. Detection of white and gray matter structures on a large number of MR images is impractical, and will only become possible if reliable and robust automated methods are developed to assist human experts. In a discussion of the use of automated MRI diagnosis of multiple sclerosis, Mitchell *et al.* [87] state that, "manually quantifying the number of lesions and determining their changes between exams are arduous and time consuming procedures (p.4211)". Automation could not only eliminate errors resulting from fatigue or lack of concentration, but with increasing computational capabilities, the analysis would be provided in less overall time and would even allow additional analyses that are currently impractical. As Fleagle *et al.* state in their article [38], "Magnetic Resonance (MR) imaging, although capable of producing superb images of cardiac structure, is not widely used as a diagnostic cardiovascular tool. One reason for this is the need to assess cardiac structure and function based on manual tracing of endocardial and epicardial borders on individual images, a tedious and time consuming process (p.4226)". These authors go on to describe an excellent correlation between their semi-automatic results and those of an independent observer demonstrating that automation can be used effectively [38].

Stiehl in his article [115] emphasizes that it is time for automation: "Tedious,

fatiguing, and time-consuming as well as error-prone interactive object definition for a large number of slice images per patient sequence, as a methodic prerequisite for the generation of 3D body geometry model, may take up to one hour or more in turn-key systems. Thus, such working conditions do usually not attract or convince physicians to use such technologies as a common tool in daily routine. The quest for a certain amount of automation, or at least semi automation, of such tools is straightforward. The existing gap has been widely recognized between the theoretical state-of-the-art in general computational vision and the state-of-the-technology in operational turn-key systems, with respect to segmentation schemes and image analysis/interpretation paradigms that are presently in common use. In particular, purely interaction-driven image segmentation has been identified as being a severe bottleneck of such operational systems (p.25)".

1.3 Goal

The goal of this thesis work is to automate the anatomic segmentation of magnetic resonance brain images. For the purpose of this thesis anatomic segmentation refers to the characterization of pixels as gray matter, white matter, cerebrospinal fluid (CSF) and skull. A completely automatic system would by definition eliminate all user interaction; however, this goal is neither attainable for a close ended research project, nor desirable from the stand point of clinical verification. Therefore the system described herein is designed with the goal of becoming completely automatic with the realization that confirmation and corrections from human experts are inevitable.

Twenty nine MRI studies will be considered for segmentation in this thesis. The following table shows the imaging parameters and the total number of images in

each study. The two approaches developed, namely modified LVQ and extended SOFM, will be used to segment the MR images in a supervised and unsupervised fashion respectively.

	# studies	T1	T2	PD	Thickness	# Total images
TR/TE	18	600/16	2916/119	2916/17	5/2.5	972
TR/TE	6	600/16	2800/90	2800/30	5/2.5	324
TR/TE	1	600/25	3083/112	3083/16	5/2.5	54
TR/TE	2	700/25	3500/102	3500/17	5/2.5	108
TR/TE	1	636/16	2700/90	2700/30	5/0	66

An adaptive training scheme will be utilized to overcome intensity variation within a slice and between image slices. The acquired results from the two approaches will be compared with standard backpropagation ANN and maximum likelihood classifier for the supervised, and c-means clustering technique for the unsupervised scheme.

In an attempt to automate the segmentation process, the artificial neural network based image segmentation and classification schemes were investigated. There are potentially many situations in which a clinician would use more than one image spectrum to define an anatomical structure or tumor volume [92], [101]. Using the same idea, multispectral classification techniques were adapted. Supervised and unsupervised classification schemes were utilized and the neural networks architectures were designed.

The design objectives for the supervised segmentation scheme included:

1. the design of the learning vector quantization (LVQ) artificial neural network classifier for the supervised segmentation of MR images of the brain.

2. the evaluation of results obtained using multispectral images versus single spectral images for segmentation purposes.

3. the comparison of the technique with the Bayes maximum likelihood classifier (MLC) and a back-propagation artificial neural network.

4. the ability to adapt to variations in the data (the proposed system must be able to modify the segmented images by controlling the neural net parameters and retraining the neural net).

5. the provision of a user interaction capability for cases where the system cannot adapt to variations in the data and cannot proceed with the recognition process for the other slices.

The objectives of the fully automated segmentation scheme were:

1. the design of the self-organizing feature maps (SOFM) artificial neural network for unsupervised tissue classification of MR images.

2. the reduction of the number of clusters in segmentation by extracting the cerebrum from the MR images of the head prior to segmentation.

3. the application of statistical pattern recognition approaches like c-means or fuzzy c-means techniques to the problem.

4. the evaluation of the relative advantages and drawbacks of the neural network approach versus a statistical pattern recognition approach for unsupervised MRI tissue characterization.

The quantitative assessment of performance is complicated by the lack of a gold standard. The problem that one faces includes the inability to segment manually

the images, the subjective nature of any manual segmentation procedure, and the lack of realistic phantoms which could be used as reference. Therefore, all the segmented images in this thesis were evaluated by at least two individual observers. The receiving operator characteristic (ROC) analysis can provide a quantitative evaluation but because of the considerable number of observations required, this has not attempted in this thesis and is left for future work.

1.4 Discussion

A number of imaging tools have been developed that can provide topographic information about the intact human body. Each characterize different tissues, or their function, according to certain properties. For example, X-ray Computerized Tomography (CT) measures the attenuation by tissue of an incident beam of X radiation. The technique classifies tissues according to their attenuation properties. Positron tomography relies on the detection of the time course and spatial distribution of certain specific molecules, such as analogue of glucose or neurotransmitters labeled with positron emitting isotopes, to measure blood flow or rates of chemical reaction. Magnetic resonance imaging (MRI) relies on the nuclear properties of the hydrogen atom to study the distribution of hydrogen atoms, or their chemical environment. In general, a particular imaging modality may be more useful to diagnose certain type of abnormalities such as differentiation between scar tissue and recurring tumor using FDG and PET , or would emphasize certain anatomical features better, such as gray/white matter differentiation in proton weighted MR images. However, more than one imaging technique is often used because each provides complementary information. Automated segmentation and co-registration techniques are essential in order to take full advantage of this capability. The im-

portance and the difficulties of the automatic segmentation task are discussed in several medical imaging articles, [10], [12], [21], [72], [96], [103], and [115].

In general, the segmentation of brain images involves the discrimination between different types of tissues and fluids (e.g., white matter, gray matter, cerebrospinal fluid (CSF), skin, etc.). Many techniques have been developed over the years to extract different tissue components from biological images. Classical methods range from simple techniques that rely on pixel intensity thresholding to more sophisticated techniques that rely on the calculation of the median, the variance, or the gradient of the pixel intensity distributions to characterize local statistics [9], [51], and [116]. Because MRI permits the measurement of more than one independent tissue-specific parameter, each image pixel can be segmented as a multidimensional pattern whose components are the intensity values for each of the parameters. Three types of images are acquired routinely for diagnostic purposes, T1 weighted images (sensitive to variations in spin-lattice relaxation time), T2 weighted images (sensitive to variations in spin-spin relaxation time), and proton density (PD) weighted images. This multidimensional feature of an MR examination can be used to enhance the pattern recognition and image processing technique.

Multidimensional data classification has been used extensively in the area of remote sensing. The parallel between multispectral images of the earth (LAND-SAT images) and MRI was made as early as 1985 [94], [107], [122], and pattern recognition techniques developed by NASA for the automatic classification of multispectral images have been applied to MR images. Since then, several other classification approaches have been tried, some of which will be surveyed in chapter 2.

Chapter 2 is a survey of the work related to the segmentation of MR images. Previously developed systems for MR image segmentation are reviewed, and their results, potential, and limitations are discussed. Multispectral segmentation tech-

niques are emphasized. Recognition and/or classification tasks performed using artificial neural networks are also mentioned to illustrate neural network capabilities.

Chapter 2

Literature Review

The techniques used to segment multispectral images can be divided into supervised and unsupervised methods [20], [12], [48] and [50]. Supervised methods require that an operator identifies selected features on training data by using a human-machine interface such as a mouse [6], [5],[25], [52] and [123]. Unsupervised methods define regions in the image without any operator intervention [110] and [128], although human intervention may be required to complete the process. The regions identified by the algorithm will not have an anatomical label associated to them; however a label could be attached to the clustered region in a subsequent step.

2.1 Supervised segmentation methods

2.1.1 Statistical pattern recognition methods

The design of a statistical pattern recognition technique requires complete knowledge of the probabilistic structure of the data. Parametric methods assume partic-

ular distributions of the features. For example, the maximum likelihood method usually assumes multivariate Gaussian distributions [1], [23], [29], [43], [99], [87], [108], [118] [122], [121], and [124]. In this approach, the mean and covariance matrices for each of the tissue classes are estimated from a training set provided by the operator. The training data is usually specified by drawing regions of interest on the images using a mouse driven interface. The remaining regions (pixels) are then classified by calculating the likelihood of each pixel belonging to a tissue class, and assigning the pixel to the tissue type with the highest probability. This parametric approach is useful when the feature distributions for different classes are well known; however, this is not necessarily the case for magnetic resonance images [19], [21], [107] and [125].

There are other statistical methods, called non-parametric methods, which do not rely on predefined distributions. The k-nearest neighbor, or k-NN, method relies on actual distributions of the training samples themselves [21], [54],[64], and [88]. There are other reports in the literature that use statistical pattern recognition techniques such as shape recognition [127], contour and connectivity [31], [57], region growing [2], Markov random field [17], [75], [76], gray level co-occurrence matrix [106], and gray level histogram [37], [83], [117].

Gerig *et al.*(1991) [41] presented the application of a maximum likelihood classifier (MLC) for the segmentation of MR images and compared their results with unsupervised clustering techniques. A Parzen window approximation was used to estimate the continuous density function from the discrete scatter plot of the two echoes in a double echo sequence (PD, T2). They used knowledge from their supervised classification technique (MLC) to find the cluster centers, although this strategy made the approach not fully unsupervised. Moreover, preliminary results published by Dudewicz *et al.* [29] indicate that although the distributions of T1 and

T2 values can be considered as jointly normal, the distribution of proton density values is not normal. Also, the variations in the intensity values of the different tissue types, across the volume, is so high that the probabilistic decision functions usually overlap to produce conflicting results.

Three problems associated with the unsupervised clustering technique were identified by Gerig *et al.*[41]: 1) choosing a good criterion to split and merge clusters, 2) determining the number of classes, and 3) correcting the classification errors due to the complexity of the problems.

Mitchell *et al.* (1994) [88] reported the application of maximum-likelihood and k-nearest-neighbor (k-NN) classifiers for the segmentation of multiple sclerosis lesions in MR brain images. They generated a set of data by labeling regions of interest (ROIs): CSF, white and gray matter regions in the frontal and occipital lobes and the corpus callosum. From the labeled regions a 2D histogram of those tissues of interest was calculated and displayed. The mean and covariance of the region histogram were used to estimate the mean and covariance of the tissue distribution. Principal components of the distribution estimate were calculated and used to define an elliptic region centered about the estimated mean. A k-NN classifier was then used to differentiate the lesion and brain distributions.

Lang *et al.* (1994) [75] presented a statistical method which assumes that the underlying tissue regions are piecewise contiguous and can be characterized by a Markov random field prior. In classifying the tissues, the method models the likelihood of realizing the images as a finite multivariate-mixture function. The method was tested on sets of T1, T2, and PD weighted images of the brain. Their results were verified visually. The authors state that "quantitative validation on the accuracy and stability of the method needs further experimental studies using different acquisition protocols, realistic anthropomorphic phantoms, and a large

number of clinical scans" (p.448).

Taxt *et al.* (1994) [117] proposed a segmentation technique that requires five differently weighted MR images for the segmentation process. The authors conclude that increasing the feature dimension by varying the image acquisition parameters improves the segmentation scheme. The classification was done using the Bayesian framework. Quantitative validation was made in two steps by using all the labeled pixels of the imaged head and a surrounding rim of air. In the first step, they labeled the test image manually using the same clustering and manual labeling technique for the training image. However, the labeling of the training image and the test image was done independently, and by a different expert to avoid bias. In the second step they computed a confusion matrix based on the true manual labeling and the automatic classification of the test image.

2.1.2 Algebraic methods

Outside the field of pattern recognition, algebraic approaches have been reported [61], [65], [114], and [112]. For images with clearly identified signature vectors these methods provide very good solutions to the partial volume effect, which may have some influence on measurement of tissue volumes. Algebraic approaches, however, may become impractical for images showing complex pathology. Since these methods work with projections of feature vectors, the number of more or less uncorrelated features that need to be acquired to determine the eigen-images for every tissue becomes very large, potentially leading to impractical processing times. Kao *et al.* (1994) [61] have presented a possible solution for the dimensionality, however, the method is optimal for signature vectors that are more or less orthogonal, which may not be the case for pathologic tissues that exhibit similar relaxation behavior.

2.1.3 Manual feature space segmentation methods

Other supervised segmentation methods include feature space based segmentations that utilize operator defined decision boundaries [39], [59], and [113]. Researchers have emphasized the feature extraction and selection step, and they display these features in some multi-dimensional graph. The area of higher density that are visible in this graph are then manually outlined and associated with tissue types. Just *et al.* [59] impose an ellipsoid containing a predefined fraction of known samples to delineate the decision boundaries, while other investigators have used a nearest centroid classifier where the centroid is defined at the middle of a region of interest in feature space [113]. Fletcher *et al.* [39] reported a manual selection of thresholds in each feature for each tissue type, which forces clusters in rectangular boxes in the feature space.

2.1.4 Knowledge-based segmentation methods

Li *et al.* (1993) [73] presented a knowledge-based approach to automatic classification and tissue labeling of MR images of the human brain. Their system consists of two components: an unsupervised clustering algorithm and an expert system. MR brain data were first segmented by the unsupervised fuzzy c-mean clustering (UFCM) algorithm, then an expert system located a landmark tissue or cluster and analyzed it by matching it with a model. First they separated the skull tissues using a quadrangle model for the head and applying "IF" and "ELSE" rules. such as:

- " IF (The number of the foreground pixels within the quadrangle is small)
- THEN (It is a skull class)

- ELSE (It is a class of white or gray matter) "

They used different models for white matter, CSF and gray matter, and split them according to their shape and tissue structures. A polygonal approximation model along with rules specific to each tissue class was presented to segment the ventricle area and the CSF. They also proposed an approach which was semi-supervised FCM. In this approach the information about the known clusters (labeled tissues) was given to UCFM, essentially, using the cluster centers of the known tissues for initialization of clusters. Initialization has major effects on how fast FCM converges and how accurate a result it provides. The authors used different variables as thresholds, but did not provide any information on how to validate them.

2.1.5 Rule-based segmentation methods

Raya (1990) [104] extracted features from PD and T2 MR images and used them to calculate confidence levels for the properties of a voxel. Six simple low-level features were calculated; 1) PDT2-Ratio $(PD + T2)/(PD - T2))$, 2) T2, 3) CSF gradient (magnitude of local gradients on T2), 4) $(PD - T2)$subtracting T2 image intensity from PD image intensity, 5) (PD - T2)-Gradient (Magnitude of local gradients on $(PD - T2)$, and 6) PD, proton density image. The features were heuristically derived to enhance the separability of features and are closely linked to the specific brain areas to be segmented. Rules were then used to perform the segmentation. The first rule focuses attention by deciding what is foreground and background. Afterwards very specific rules are applied to extract areas of interest within the brain. Finally, additional rules are used to correct mistakes.

2.1.6 Neural network based segmentation methods

A backpropagation neural network was presented by Ozkan *et al.* (1993) [95]. This network consists of one input layer, one or two hidden layers, and one output layer. Four different image modalities were used. In addition to T1, T2 and PD weighted MR images, a CT image was also used as another feature for the ANN classifier. The authors claim that the use of the three MR modalities is useful for the segmentation of soft tissues, and that the use of the CT image permits a good segmentation of bony structures and improves the separation of white and gray matter. The neural network was sensitive to the sizes of the training set. However it performed better classification accuracy for the white and gray matter classes than the MLC classifier when the size of the training sets were small. For the CSF class both the ANN and the MLC classifier faced reduction in the classification accuracy for large training sets.

Dawant *et al.* (1993) [26] reported a new approach to the correction of inter-slice intensity variations in MR images which enhanced the performance of back-propagation neural network classifiers designed for the segmentation of the images. They presented two different methods for the correction of intensity variations and reported results from several studies. Two different techniques, namely "direct" and "indirect" fit models, were proposed. In the direct method, an interpolation technique was used to fit the intensity surface directly to the labeled points. In the indirect approach, a classifier is trained on the labeled points, a preliminary classification of the images is performed, reference points were selected from these classified images, and an intensity surface is fitted to these points in a least-squares sense. Their indirect fit method was sensitive to the training data. The difficulty of generating a reliable set of reference points to which the surface could be fitted was

a crucial problem. Because of this, the direct fit method was used in their routine studies. The direct method fits an intensity correction surface directly to reference points selected by the user in the images. Their results show improvement in segmentation of MR images when using the backpropagation artificial neural network, but the methods rely heavily on the user interactions and is fully supervised.

2.2 Unsupervised segmentation methods

2.2.1 Statistical pattern recognition approaches

Bomans and Riemer (1990) [9] applied the Marr-Hildreth [55] operator for edge detection. They extended the zero-crossing edge detection scheme to three dimensions and used a morphological filtering to recover 3D surface of skin, bone, brain and the ventricular system from MR images. The Marr-Hildreth operator was approximated by a 3-D "Difference of Gaussian " (DOG). The authors admit that the convolution and the morphological filtering are computationally expensive, and time consuming. They also reported problems in finding the correct borders: for example the gray-white matter border may be found instead of the gray-CSF border. The authors conclude that for a fully automatic process, knowledge-based methods should be used for the assignment of labels to the constituents of the head. However, Raya [104] points out that the 3-D operations cannot be used directly if the scans have different spatial resolutions in different spatial dimensions.

Alaux and Rick (1990) [4] compared supervised and unsupervised techniques. They used principal components analysis, supervised Bayesian classification, and clustering techniques for classification and segmentation of MR brain images. No information was provided about the clustering scheme. The authors reported that

typically, both supervised and unsupervised techniques perform at least as well as a trained radiologist in segmenting the images. However, no significant difference between the performance of the supervised and the unsupervised methods was found.

Herskovits (1990) [51], combined the Bayes Maximum Likelihood classifier and an unsupervised clustering algorithm (ISODATA) to ease the task of region drawing (labeling) and to start with more reasonable seed points for ISODATA. Such an approach was required since the distance measures used in the unsupervised methods are not necessarily clinically relevant. The clustered regions could be screened to form good training points for the Maximum Likelihood classifier. However, the underlying assumption was again the normal distribution of the data.

Liang (1993) [74] showed the application of Gaussian Markov random field (GMRF) for unsupervised segmentation of MR images. His method estimates the model parameters by fitting all voxel values to the mixture by using the maximum likelihood principle. He showed results from a few images and no evaluation was reported. He concluded that "the key feature of statistical approaches toward automatically classifying tissues and segmentation of MR images is determination of the number of image classes and the model parameters of these classes from the image data by a computer".

Lundervold *et al.* (1995) [79] presented a new method for segmentation of brain tissues and CSF in routine axial MR images. The algorithm uses information about anatomical boundaries and intensity value of tissues in the brain. They divided the head and brain into four regions and seven tissue types. Each tissue type was modeled by a multivariate Gaussian distribution. The k-means algorithm was used for initial estimation of tissue parameters. Their segmentation method is restricted to slice images where the brain tissues and CSF spaces form connected

regions. Because of this assumption, segmentation fails when the structures to be segmented are not connected or do not form closed contour boundaries. They did not perform any clinical evaluation, though results were visually satisfactory.

Yan and Karp (1995) [129] presented a technique for 3D brain image segmentation using an adaptive k-means algorithm. CSF, white matter and Gray matter were segmented in each image slice. Each tissue type was modeled by a Markov random field with the second order neighborhood in a 3-D lattice. They presented results from 2-D image slices; however validation of the technique was left for future work.

2.2.2 Fuzzy clustering approaches

Hall *et al.* (1992) [47] compared the neural network and fuzzy clustering techniques for segmentation of MR images of the brain. They implemented the fuzzy c-means (FCM), and the approximate fuzzy c-means (AFCM) algorithms for fuzzy clustering and compared results with the standard feed-forward backpropagation computational neural network called cascade correlation (FFCC). They claimed that supervised and unsupervised segmentation techniques provide similar results. They report that unsupervised fuzzy algorithms were observed visually to show better segmentation when compared with raw image data from volunteer studies. However, for a more complex segmentation problem with tumor/edema or cerebrospinal fluid boundary, where the tissues have similar MR relaxation behavior, inconsistency in rating among experts was observed, with fuzzy c-means approaches being slightly preferred over feed-forward cascade correlation results after several iterations in the selection of training regions. They claim both FFCC and AFCM/FCM provide results acceptable to the radiologists, however, the advantages and limita-

tions of each approach were not discussed.

Clark *et al.* (1994) [18] presented a hybrid technique combining knowledge based approaches with unsupervised fuzzy clustering to detect tumor abnormalities and label normal volumes in the brain. Each slice within an input volume was processed separately using the fuzzy c-means algorithm to segment MRI data into ten classes or regions. After fuzzy clustering, an expert system used model-based recognition and image processing techniques on the ten classes to locate a landmark tissue and to look for expected features. The process was repeated until an abnormality was detected, or all the tissues in the slice are labeled. The authors conclude: "The absolute accuracy of the segmentations has not been rigorously established. The relative accuracy appears acceptable as discussed in the paper (p.730) [18]".

2.2.3 Neural network based clustering approaches

Amarture *et al.* (1992) [7] described the application of Hopfield neural network for the multispectral unsupervised classification of MR brain images. They used "winner-take-all" neurons to obtain a classification map using PD and T2-weighted images of the head. The results were qualitative, and the authors reported the following observation: "The technique is at present not robust enough to handle images corrupted by non-stationary sensitivity of the image acquisition and partial volume effects" ([7]-p.220).

2.3 Discussion

It is clear from reviewing the recent literature on segmentation of MR images that there is no technique that is available to segment automatically MR brain images

satisfactorily.

A number of the segmentation systems which appear in the literature tend to be domain specific, and often involve the use of some tricks in order to accomplish successfully each specific task (Raya, 1990 [104] ; Bomans, 1990 [9]; Li, 1993 [73]). Making a system work autonomously in all cases requires the system to learn and to be able to receive new information. Rule based systems often are not set up to learn new rules.

In response to this conclusion, and as a way to incorporate application of learning systems for the work described in this thesis, the artificial neural networks based image segmentation and classification schemes were investigated. There are many situations in which a clinician would use more than one image modality to define an anatomical structure or tumor volume [92], [101]. By analogy, multispectral classification techniques were adapted. Supervised and unsupervised classification schemes were utilized, and the architecture of the neural networks was designed.

The segmentation techniques described in this thesis address the problem of more basic segmentation methods by using artificial neural networks. The computation time and reduction of operator dependence are other issues which have been considered in this dissertation. The next chapters describe a system that performs feature extraction, segmentation and automatic segmentation of MR brain images.

Chapter 3

Image Analysis Segmentation Methods

3.1 Introduction

Image analysis is a process that can be used to discover, identify, and understand patterns that are relevant to any image-based task. Figure 3.1 shows a representative diagram of the most common parts of an image analysis system [44]. Preprocessing improves the quality of the data by reducing artifacts and noise. Feature extraction provides the measurement vectors on which image segmentation is based. Segmentation is the process by which an image is subdivided into its constituent parts or objects. Classification, description and recognition are steps from which objects or other entities of interest are extracted. Segmentation is one of the crucial steps in the overall process.

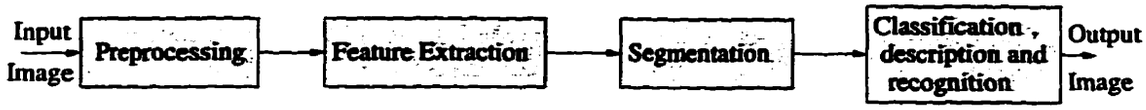

Figure 3.1: Components of an image analysis system.

3.2 Preprocessing

Preprocessing improves the quality of the data by reducing artifacts and noise. Examples of preprocessing are noise suppression by adaptive filtering, contrast enhancement, and image restoration.

3.3 Feature extraction

Features that can be extracted from the image form the basis for image segmentation. These features can be, for example, pixel intensities, edges or textures. Rather than using all the information in the images at once, feature extraction and selection breaks down the problem of segmentation to the grouping of feature vectors. Selection of good features is the key to successful segmentation. This issue is still under investigation [20].

Many segmentation approaches use the gray scale values of the pixels [21], [54], [47], [88], [123]. The pixel intensity as a feature vector can be obtained from a single spectral image (i.e., T1, T2 or PD images) or a multispectral representation of the object from the same anatomical location. If more images become available, they can simply be added to the feature vectors to form a higher dimensional feature space. The advantages of higher dimensional feature space will be discussed in the next section.

The use of edge detection methods have been reported in [9], [31], [119],[127].

(a) (b) (c)

Figure 3.2: (a): smooth, (b) coarse, and (c) regular textures.

For segmentation, edge detection can be used when the gray-levels of the boundary between two regions are relatively distinct. This means that the regions in question should be sufficiently homogeneous so that the transition between two regions can be determined on the basis of gray-level discontinuities alone. Another feature is texture [37], [106]. However, texture features are mainly applied on a large number of pixels rather than pixel by pixel [37], [106]. Although no formal definition of texture exists, intuitively this description provides measures of properties such as smoothness, coarseness, and regularity (Figure 3.2 shows some examples). The three principal approaches used in image processing to describe the texture of a region are statistical, structural, and spectral [28]. Statistical approaches yield characterization of textures as smooth, coarse, grainy, and so on. Structural techniques deal with the arrangement of image primitives, such as the description of texture based on regularly spaced parallel lines. Spectral techniques are based on properties of the Fourier spectrum and are used primarily to detect global periodicity in an image by identifying high-energy, narrow peaks in the spectrum. Texture features necessarily derive from a large number of pixels usually size of (8×8) to (64×64); hence it is not suited for pixel classification [31], [44].

The pixel intensities in a neighborhood can be used as an additional feature. For example, the mean and standard deviation of pixels in a region of (3×3) attempt to quantify the texture of that region. The nine element feature vector can also be obtained using the eight nearest neighbors around the centered pixel.

Feature selection becomes important if the dimensionality of the data affects the computational load; however, the criteria for feature extraction and selection have not been extensively studied but will become an important area as the number of features increases due to advances in MR imaging methods [20].

3.4 Image segmentation techniques

The literature on MR image segmentation can be roughly divided into two categories: 1) a single spectral image segmentation, 2) multispectral image segmentation. In the former category, a single image such as T1, T2, or proton density weighted image will be used while, in the later category, multiple MR images obtained on the same level in the object bue using different acquisition parameters, and hence with different gray scale contrasts will be employed.

3.5 Single spectral image segmentation

3.5.1 Segmentation methods based on thresholding

Single image segmentation methods which have been applied to the problem of MR image segmentation can be subdivided as follows (Fig. 3.3.) One of the simplest techniques for segmentation is the partitioning of the image histogram by using single or multiple thresholds. Generally, multiple thresholding is less reliable than

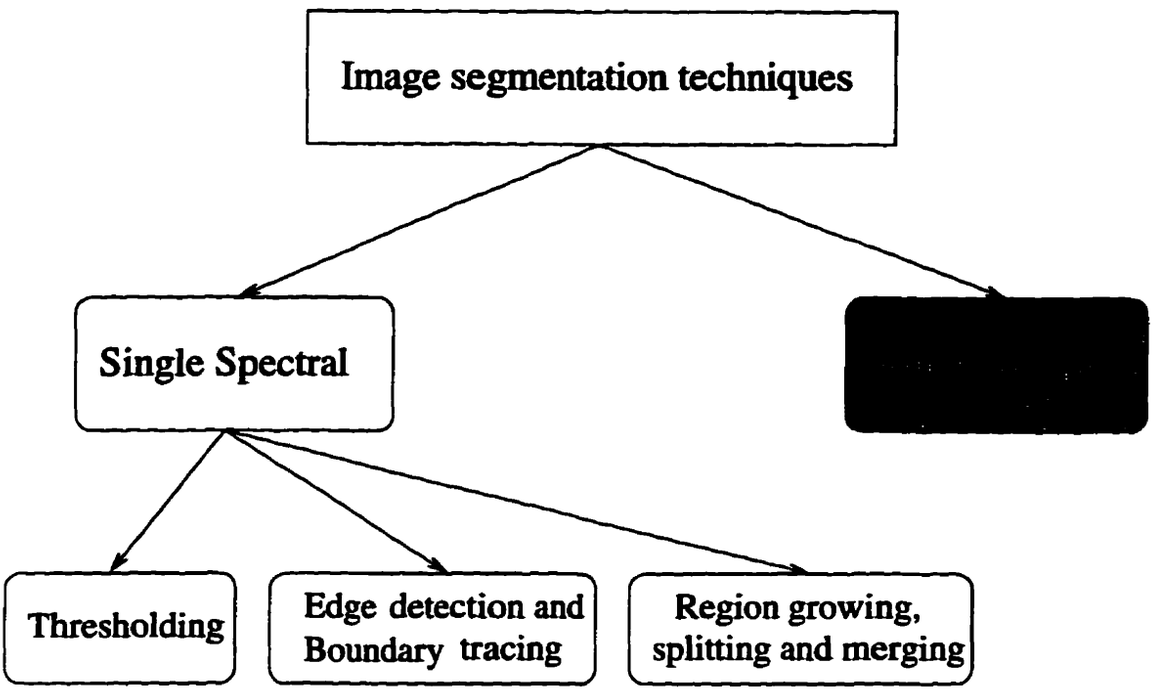

Figure 3.3: Classification of single spectral image segmentation methods.

single thresholding, because it is difficult to establish multiple thresholds that effectively isolate regions of interest, however, if the histogram can be well partitioned, a very "clean" segmentation can be achieved.

Figure 3.4 shows an example of multilevel thresholding in which the histogram can be partitioned very well, and three different clusters can be found. Figure 3.4(a) shows four planes through a peeled hard-boiled egg in gelatin obtained using a fast spin echo gradient sequence (TE/TR= 25/500 ms). Figures 3.4(b) and 3.4(c) show the image histogram and the result of segmentation respectively. In this example the thresholds are set to 50 ($s1$) and 160 ($s2$). Segmentation is accomplished by scanning the image pixel by pixel and labeling each pixel as gelatin (0) , egg-yolk (100), or egg-white (200) depending on the gray level of the pixel. Assuming $f(x, y)$ is the gray level of pixel (x,y), then the thresholded image $g(x, y)$

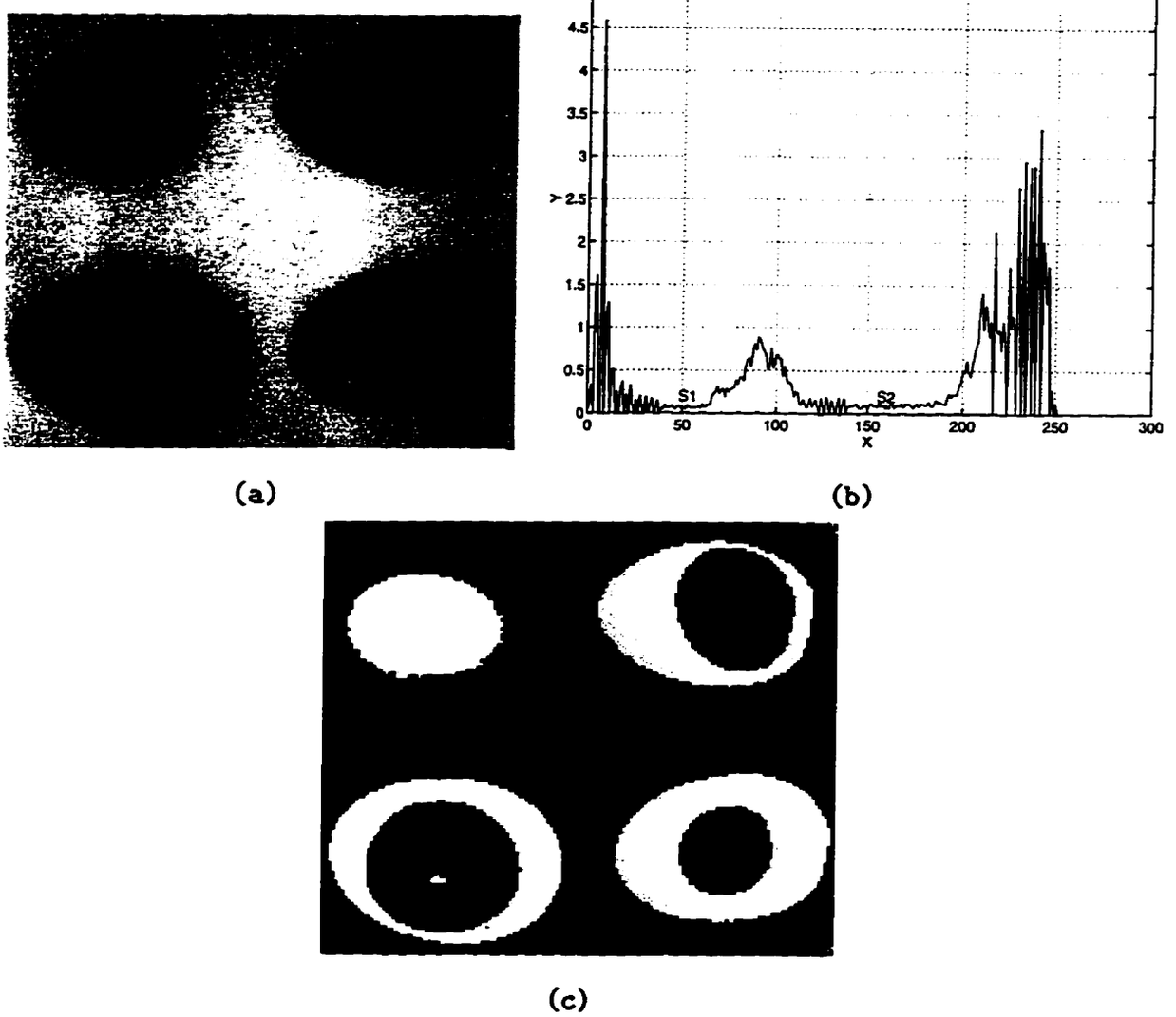

Figure 3.4: (a): Original image (b) image histogram and, (c) result of segmentation.

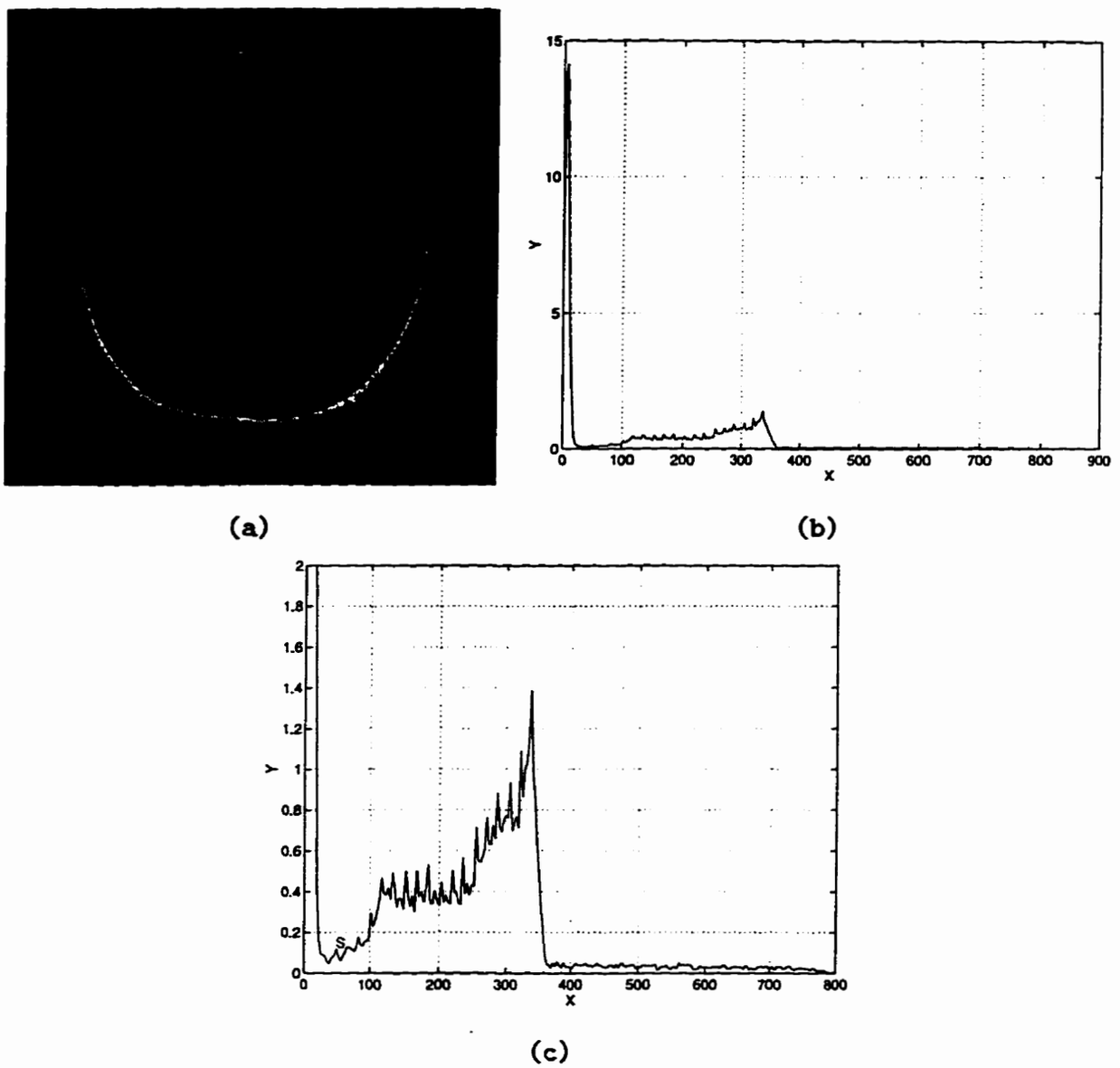

Figure 3.5: (a): Original image, (b) image histogram, and (c) expanded image histogram .

is defined as

$$g(x,y) = \begin{cases} 0 & \text{if } f(x,y) < s1 \\ 200 & \text{if } s1 \leq f(x,y) < s2 \\ 100 & \text{if } f(x,y) \geq s2 \end{cases} \tag{3.1}$$

As indicated earlier, the success of this method depends entirely on how well the histogram can be partitioned. In order to illustrate the problems associated with the multilevel thresholding technique for the segmentation of MR images of the head, an example is given in Fig. 3.5. Figure 3.5(a) shows a plane through the head of a human obtained using a T1 weighted technique, and Fig. 3.5 (b) the corresponding histogram. As can be seen, the histogram can be partitioned only into two regions (background and whole head), therefore, the histogram thresholding by itself cannot be used for the segmentation.

3.5.2 Edge based segmentation methods

An edge is the boundary between two regions in an image with relatively distinct gray-level properties. Usually for the edge based image segmentation, the assumption is that the regions in question are sufficiently homogeneous that the transition between two regions can be determined on the basis of gray-level discontinuities alone.

The basic idea underlying most edge detection techniques is the computation of a local derivative operator. Gradient operators, Laplacian (second order derivative) and Marr-Hildreth operators are the most well known edge detection operators [55], [119]. The Marr-Hildreth operator is based on the convolution of an image with the Laplacian of a 2-D Gaussian function ($h(x,y)$)

$$h(x,y) = exp(-\frac{x^2+y^2}{2\sigma^2}) \tag{3.2}$$

where σ, the standard deviation [44], is a free parameter which defines the smoothness of the function $\nabla^2 h$. σ also defines the zero crossings of the function $\nabla^2 h$ ($\sqrt{(x^2+y^2)} = \pm\sigma$). The Laplacian of h (that is, second derivative of h) with respect to x and y is

$$\nabla^2 h = (\frac{(x^2+y^2)-\sigma^2}{\sigma^4})exp(-\frac{x^2+y^2}{2\sigma^2}) \tag{3.3}$$

One of the properties of the Marr-Hildreth operator is the smoothness it introduces in the image which has the effect of reducing the noise and of providing better performance for edge detection.

Generally, edge detection schemes suffer from incorrect detection of edges due to noise, over and under segmentation, and variability in threshold selection in the edge image. These schemes tend to work well in cases involving images with sharp intensity transitions and relatively low noise. As an example, the application of the Marr-Hildreth operator for edge detection and segmentation is presented in Fig. 3.6 The original T1 weighted image of a head is presented in Fig. 3.6(a). The result of convolving that image with the function $\nabla^2 h$ is shown in Figure 3.6(b). The zero crossing operator is used to locate the edges. The result is shown in Fig. 3.6(d). Before applying the zero crossing operator a binary image is created by setting all negative pixel values in Fig. 3.6(b) to black and all positive values to white (Fig.3.6(c)). The zero-crossing operator identifies the boundaries between the black and white regions and locates the edges properly.

Figures 3.7(a), 3.7(c) and 3.7(e) are examples of Marr-Hildreth operator with different values of σ, which shows the degree of blurring and smoothness introduced

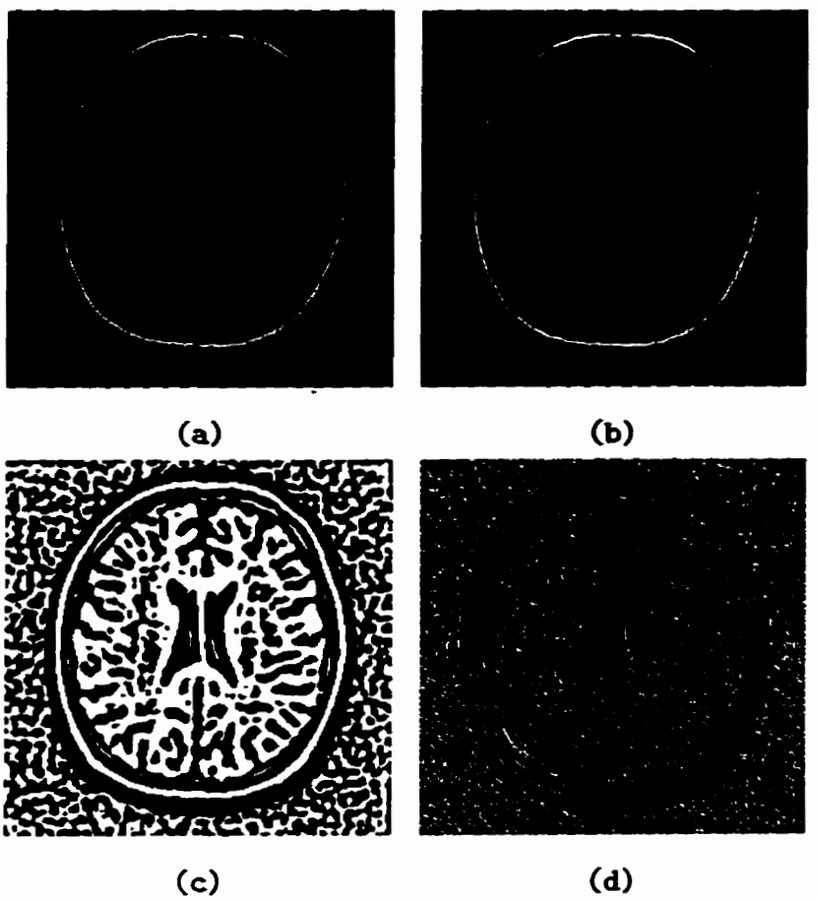

Figure 3.6: (a): Original image, (b) result of convolving (a) with $\nabla^2 h$, (c) result of making (b) binary to simplify detection of zero crossing; (d) zero crossing.

by the Marr-Hildreth operator. As can be seen, the Marr-Hildreth operator provides a "reasonable" estimate of edges. However, it is sensitive to noise and to different threshold settings, and cannot provide a good segmentation result in all cases. The effect of noise can be seen easily in the image background. Generally, edge detection techniques cannot be used by themselves and need to be combined with other techniques to overcome these problems. Bomans *et al.* [9] combined morphological filtering with the Marr-Hildreth operator for edge detection and segmentation of the MR images of the head. The method required manual labeling and editing of

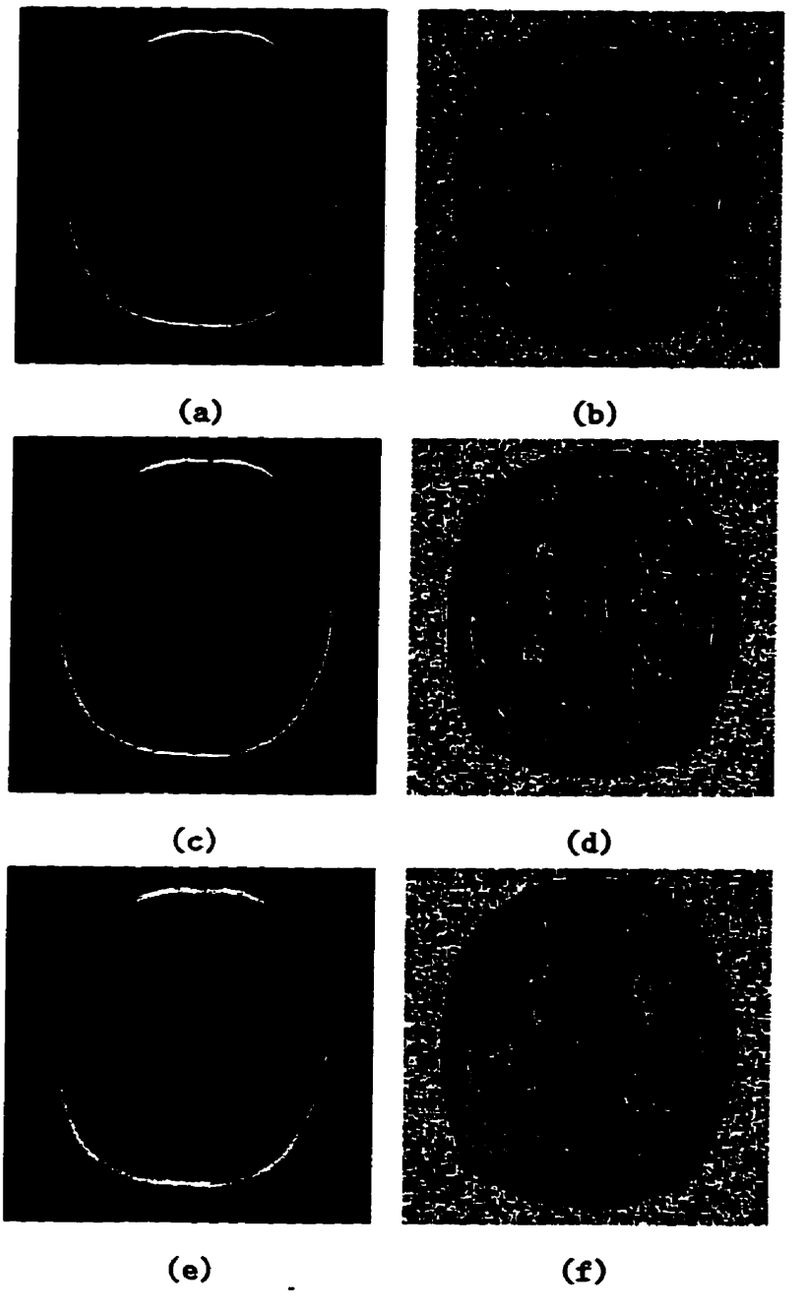

Figure 3.7: (a): Marr-Hildreth operator with $\sigma = 3.5$; (b) zero crossing; (c) Marr-Hildreth operator with $\sigma = 4.5$; (d) zero crossing; (e) Marr-Hildreth operator with $\sigma = 5$ and (f) zero crossing.

the regions to generate satisfactory 3D displays.

A similar approach to edge detection is boundary tracing [8]. The operation is as follows: an operator identifies a pixel in a region to be outlined. The method then finds a point on the boundary of the region and follows the boundary from that point. Other investigators describe a boundary tracing method using similar schemes for noisy brain sections with indistinct boundaries [127], however, a good initial guess for the boundaries is required. In general boundary tracing methods are likely to be restricted to segmentation of large, well defined structures.

3.5.3 Region-oriented segmentation methods

Region growing is a procedure that groups pixels or subregions into larger regions. The simplest of these approaches is pixel aggregation, which starts with a set of "seed" points and from these grows regions by appending to each seed point those neighboring pixels that have similar properties (such as gray level, texture, color).

Cline *et al.*[22], used seed growing to extract the brain surface. A human operator was required to select empirically seeds and thresholds. Pixels around the seeds were examined, and included in the region if they were within set thresholds. Each added pixel then became a new seed whose neighbors were inspected for inclusion in the region. Some researchers have used region growing and connectivity algorithms to enhance the results of segmentation. It can be used as a post-processing step to reduce the noise in the segmentations and improve the appearance of the 3D reconstruction [23]. Results obtained with region growing are generally dependent on the user (operator) settings. As with all single image segmentation methods, in practice only well defined regions can be identified robustly.

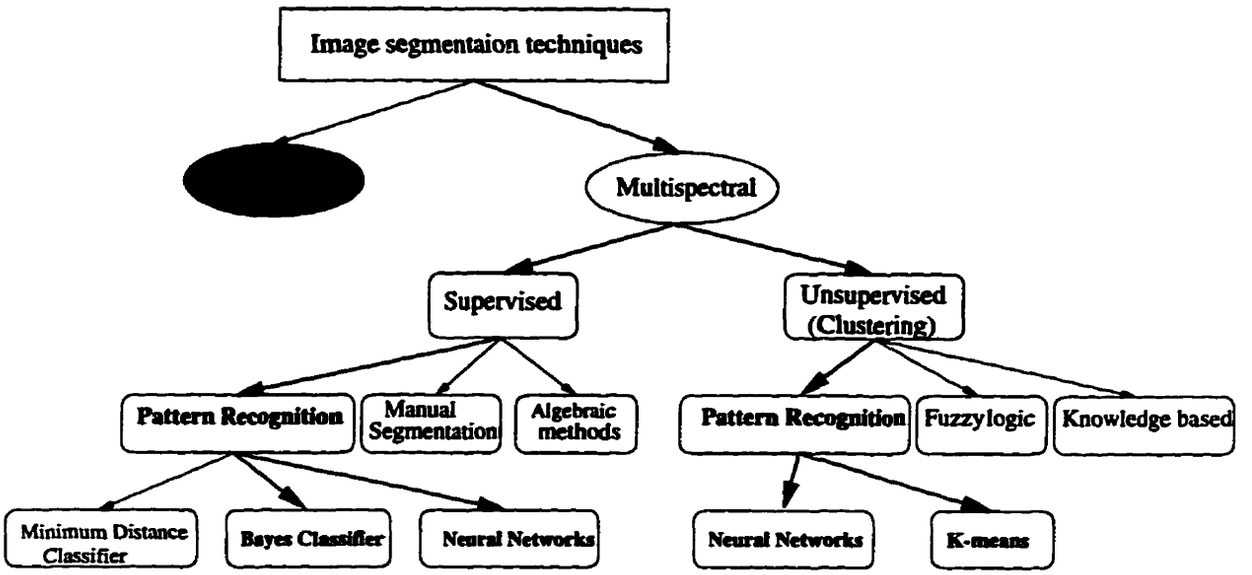

Figure 3.8: Classification of multispectral image segmentation methods.

3.6 Multispectral image segmentation

The approach to the segmentation of multispectral MR studies can be subdivided into two categories: supervised techniques, or unsupervised (clustering) techniques (Fig. 3.8).

The bold arrows in Fig. 3.8 show the approaches which have been considered for MR image segmentations in this thesis. All methods will be discussed in details in the next three chapters. The most common approach for multispectral MR image segmentation, pattern recognition, a supervised technique will be discussed briefly in this section.

3.6.1 Patterns and pattern classes

A pattern is a quantitative or structural description of an object or some other entity of interest in an image. Once patterns have been defined, the next step is to represent patterns in vector form, and then seek approaches for grouping and assigning pattern vectors to different pattern classes. The principal approaches are minimum distance classifiers, Bayes classifiers, and neural networks [55],[44].

A pattern class is a category determined by some given attributes of patterns that are the members of the class. For instance, in our case a pattern is a vector of intensity values corresponding to the same voxel as:

$$X = [T1(x_0, y_0)\ T2(x_0, y_0)\ PD(x_0, y_0)]' \tag{3.4}$$

where $T1(x_0, y_0), T2(x_0, y_0)$, and $PD(x_0, y_0)$ are the intensity values at (x_0, y_0), in T1, T2 and PD MR images respectively. The feature vector can be extended to include some other attributes (i.e. neighboring pixel intensities, other image modalities such as CT or PET), but to have a proper representation of the object the elements of the patterns must belong to the same pixel. Therefore the images used must be registered to the accuracy of a pixel.

Once a pattern representation is defined, the next step is to select a method to discriminate one class from another. If the data are purely numerical, a common way is to use decision functions. Since it is easier to visualize two dimensional intensity space, let us assume that the input patterns have two components, such as T1 and T2. Assume that there are two classes of tissue patterns "*" and "o" which are distributed in the T1-T2 space, as depicted in Figure 3.9. Let $\underline{x} = (x_1, x_2)'$ represent the T1 & T2 parameters and the function $d : \Re^2 \rightarrow \Re$. Let the function $d(x) = w_1 T1 + w_2 T2 + w_3$ be the linear decision boundary, where the $w's$ are the decision function parameters and T1, T2 are the general coordinate variables. In

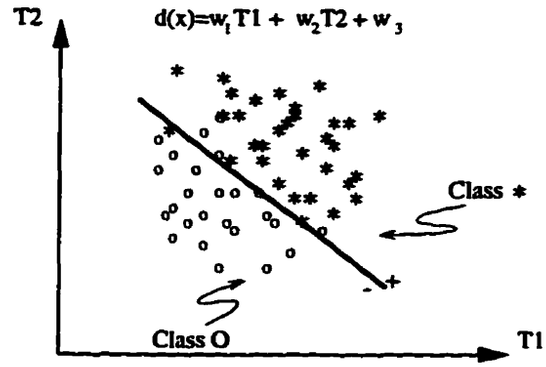

Figure 3.9: A simple decision function for two pattern classes

Figure 3.9, any pattern "*" belonging to class * will yield a positive quantity when substituted into $d(x)$ and similarly patterns "o" that belong to class O will yield a negative quantity when substituted into the function $d(x)$. Therefore $d(x)$ can be used as a *decision (or discriminant) function* for a given pattern y of unknown class. We may say that y belongs to class X if $d(y) > 0$, or to class O if $d(y) < 0$. These concepts are not restricted to two classes or linear decision functions. One can use more classes and non-linear decision functions. The success of this kind of pattern classification scheme, however, depends on two factors: 1) the shape of the decision function $d(x)$, and 2) the ability to determine the coefficients of $d(x)$. If more than two features are used, the decision function can be of the form:

$$d(x) = w_1x_1 + w_2x_2 + ... + w_nx_n + w_{n+1} = W'X \tag{3.5}$$

where $W = (w_1, w_2, ..., w_n, w_{n+1})'$ and $X = (x_1, x_2, ..., x_{n+1})'$. In general vector W is called a *weight* or parameter vector. A weight vector of size n defines a hyperplane in n dimensional space. If there are M classes and each class is separable from all the others by a single decision surface, there will be M decision functions

as:

$$d_i(x) = \begin{cases} W_i'X > 0 & x \in c_i \\ W_i'X < 0 & \text{otherwise} \end{cases} \quad \text{for } i = 1, ..., M \tag{3.6}$$

- where W_i is the weight vector associated with the ith decision function, and c_i is the ith class [119].

In practice however, it is difficult to separate a class from all the others using a single decision function. It is relatively easier to find decision functions that separate the classes pairwise at the cost of increasing the number of decision functions to find. In this case, there are $M(M-1)/2$ (the combination of M classes taken two at a time) decision surfaces. The decision functions here are of the form

$$d_{ij}(x) = W_{ij}'x$$

and have the property that, if x belongs to class c_i, then

$$d_{ij}(x) > 0 \qquad for \quad j = 1, ..., M, \ and \ j \neq i. \tag{3.7}$$

The decision functions also have the property that $d_{ij}(x) = -d_{ji}(x)$. Furthermore $d_{ij}(x)$ can be shown to be composed of two decision functions each of which is expressed as [119]:

$$d_{ij}(x) = d_i(x) - d_j(x). \tag{3.8}$$

In this case, a pattern x belongs to class c_i if

$$d_i(x) > d_j(x) \quad \text{for} \quad j = 1, ..., M, \ and \ j \neq i. \tag{3.9}$$

Theoretically, one can always find decision boundaries, if no two classes share identical pattern vectors. However, the complexity of the boundaries may vary from simple lines to non-linear surfaces.

Often in practical applications the pattern classes are not truly separable within economic or technical constrains, which has led researchers into approximations to the decision functions. One convenient way to generalize the linear decision function concept is to consider decision functions of the form

$$d(x) = w_1 f_1(x) + w_2 f_2(x) + ... + w_k f_k(x) + w_{k+1} \tag{3.10}$$

or

$$d(x) = \sum_{i=1}^{k+1} w_i f_i(x) \tag{3.11}$$

where k is the dimension of the transformed feature space and $f_i(x) : \Re^n \rightarrow \Re$ for $i = 1, 2, ..., k$ are real, single-valued functions of the pattern $x \in \Re^n$. There are an infinite number of decision functions that can satisfy Equation (3.6), using various non-linear functions $f_i(x)$ for a different k and a w vector. However, one can use the fact that these decision functions provide transformation into a new space in which everything can still be treated as linear. The vector pattern x is transformed into a new vector x^* as:

$$x^* = (f_1(x),\ f_2(x),\ ...,\ f_k(x), 1)' \tag{3.12}$$

or

$$d(x) = W'X^*$$

For example, in a two dimensional discrete space, while it is not possible to separate two classes of four points characterized by the "exclusive or" function , addition of a third dimension as a non-linear function of the two inputs allows the separation of the two classes using a linear surface in three-dimensional space (see Fig. 3.10).

The following conclusions can be made from the above (3.11,3.12) equations: 1) If the sample class points can be transformed into a higher dimensional space using non-linear transformation functions of the initial input space in which the

x	y	x⊕y	x&y
0	0	0	0
0	1	1	0
1	0	1	0
1	1	0	1

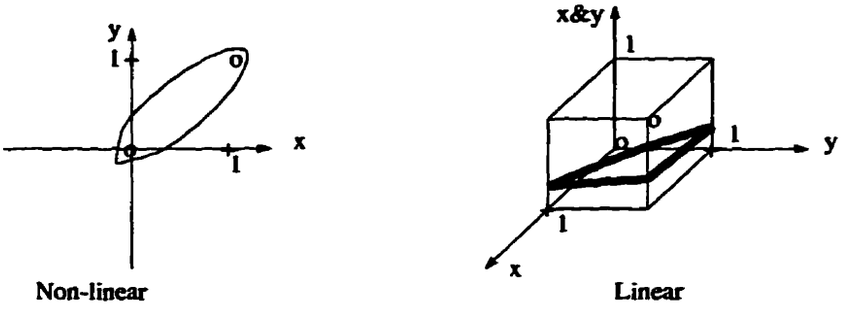

Figure 3.10: Exclusive or problem. Two classes "0" and "1" are not linearly separable in two dimensional discrete space. With an additional nonlinear function it becomes possible to separate the two classes linearly.

transformed points can still be considered as being well distributed, it is easier to find a set of decision functions to discriminate the classes. 2) In order to increase the possibility of finding a decision boundary, the feature space dimension can be increased when the number of classes to be separated is at least one more than the dimensionality of the feature space, provided that the new input is not a linear combination of the existing dimensions.

3.6.2 An example of multispectral image segmentation

In order to illustrate the multidimensional pattern recognition approach that has been introduced, a simple example for segmentation of MR images has been chosen. In the following example the minimum distance (MD) classifier has been applied to the problem in hand. Results using single spectral MR images versus multispectral

MR images are illustrated in Figure 3.11.

In the minimum distance classifier, each pattern class is represented by a prototype which is a mean vector m_i

$$m_i = \frac{1}{N_i} \sum_{x \in w_i} x \qquad i = 1, 2, ..., M \tag{3.13}$$

where N_i is the number of pattern vectors from class w_i and the summation is taken over these vectors. The class membership for an unknown pattern x will be found by measuring the Euclidean distance between vector x and prototypes m_i. Then pattern x will be assigned to class w_j if it has the minimum distance to w_j. The Euclidean distance is

$$D_i(x) = ||x - m_i|| \qquad i = 1, 2, ..., M \tag{3.14}$$

Fig 3.11(a),(b), and (c) show the original PD, T2, and T1 weighted images of the brain respectively. Fig 3.11(d) shows result of segmentation using only PD-weighted image. Figures 3.11(e), and (f) illustrate the results using two and three image spectral respectively. In Fig. 3.11(e) features were selected from PD and T2 weighted images. In Fig. 3.11(f) all three images were used for segmentation. It is obvious from the results that using multidimensional independent features will provide better classification and segmentation results. As can be seen in Fig 3.11(d) only two tissue classes were identified. In Fig 3.11(e), three tissue classes were identified having the same problem and in Fig 3.11(f) five tissue classes are segmented, though results are not completely correct. It should be noted that in this particular example the training data is chosen from the same test data, that is why a simple minimum distance classifier performs well for multispectral image segmentation. More details regarding test and training data will be presented in the

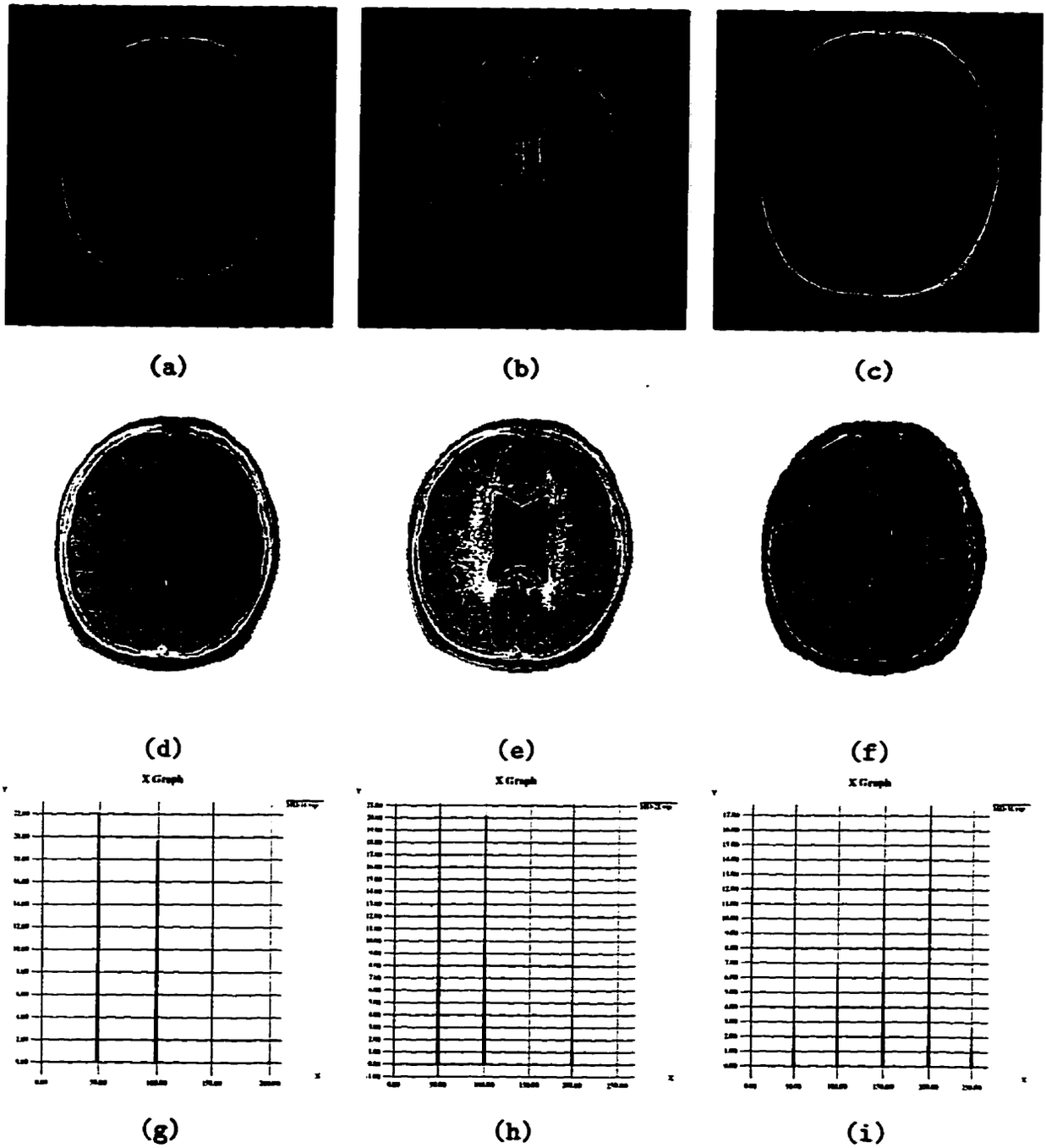

Figure 3.11: (a): Original PD weighted image, (b) T1 weighted image, (c) T2 weighted image (d) Segmentation using a PD-weighted image, (e) segmentation using PD and T2 weighted images (f) segmentation using PD, T2, and T1 weighted images, (g) histogram for image (d), (h) histogram for image (e), and (i) histogram for image (f)

next chapter, for now I close this chapter with a brief summary and conclusion and continue the discussion of multispectral image segmentation in the next chapter.

3.7 Summary

In summary, single spectral image segmentation methods may provide some useful information, but generally are limited to relatively simple structures. For images with complex contrast and texture, such as MR images of the head, more information is required, and this is available in multispectral MRI data sets.

Pattern recognition techniques such as minimum distance classifiers, Bayes classifiers, and artificial neural networks appear generally to be successful, for segmentation of brain MR images however, the important question is which approach can provide better segmentation results. Now that the theoretical aspect of multispectral pattern recognition is introduced, the next step is to find the best methodology for our problem. In the following chapters some of classical pattern recognition techniques for classification and segmentation will be introduced. Results will be compared to the techniques which have been developed in the course of this study.

Chapter 4

Supervised Segmentation with LVQ Networks

4.1 Introduction

In this chapter supervised techniques for classification and segmentation of MR images will be discussed. The application of a Learning Vector Quantization (LVQ) Artificial Neural Network (ANN) will be introduced. Theoretical issues will be discussed, and segmentation results will be presented. A backpropagation ANN and a classical maximum likelihood classifier (MLC) will be considered for comparison. The architecture and design process of the network will be given and results from each technique will be compared.

4.2 Introduction to Vector Quantization (VQ)

Vector quantization (VQ) is a classical signal-approximation method that usually forms an approximation to the probability density function $p(x)$ of stochastic $x \in \Re^n$ using a finite number of so-called *codebook vectors* $w_i \in \Re^n, i = 1, 2, ..., k$. Once the codebook is chosen, x is approximated by finding the codebook vector w_c closest to x . Typically, the codebook will be constructed through a process called *training or learning.* During training, a set of data vectors, which is representative of the data that will be encountered in practice, is used to determine an optimal codebook. Each entry of the codebook is called a codeword. The data used to find the codebook are usually called *training data*, and a set of such data from each class is called a "training set". VQ can be viewed as a form of pattern recognition where an input pattern is approximated by one of a predetermined set of standard patterns, or in other words, the input pattern is matched with one of a stored set of codewords.

A concept that is useful for the illustration of vector quantization methods in pattern recognition and for neural networks in general is called *Voronoi tessellation* [45]. Figure 4.1 shows a two dimensional space where a finite number of codebook or *reference vectors* are shown as points, corresponding to their coordinates. This space is partitioned into regions, bordered by lines (in general, hyper-planes) such that each partition contains a reference vector that is the "nearest neighbor" to any vector within the same partition. These lines, or the mid-planes of the neighboring reference vectors, together constitute the Voronoi tessellation. Note that, all vectors (ξ_1, ξ_2) in the same partition or cell have the same reference vectors as their nearest neighbor.

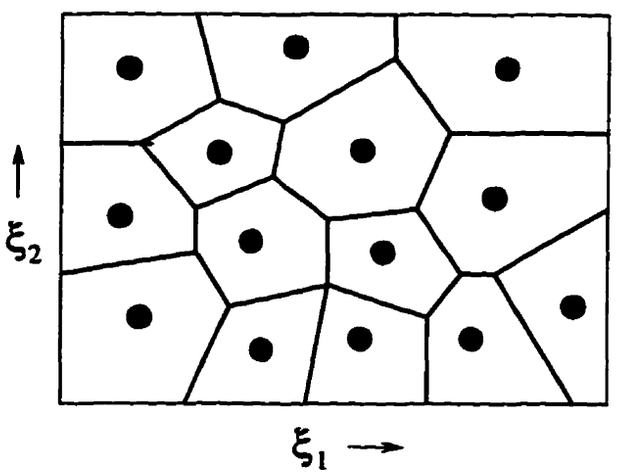

Figure 4.1: Voronoi tessellation partitions for a two dimensional pattern space (ξ_1, ξ_2)

4.2.1 Vector Quantization for Classification

The combination of VQ with classification is a natural one because each technique can be designed and implemented using methods from statistical clustering and classification trees. The goal of such a combination is to incorporate classification information into the codewords by classifying the codewords themselves during code design. By combining VQ and low-level classification, certain features in an image can be classified automatically.

One can use VQ for classification by labeling all known data (vectors) as a training set and using each training vector with its class for classification purpose. A new vector will be classified by finding its nearest Euclidean neighbor in the training set and then assigning the label of that nearest neighbor to the new vector. In this case, the entire training set is a *codebook* which can be extremely large. Although this can be considered as an application of VQ to classifier construction, the reduction of codebook size is needed.

It is not at all obvious how the codebook vectors in Vector Quantization ought to be placed, if this method is used directly for *classification*, [66], [24], [84]. It has been reported in [71] that sometimes even one codebook vector per class may be sufficient to define the optimal border for separating the classes, and sometimes the optimal number and placement of the codebook vectors have no direct correspondence to the density functions of each class taken separately. This issue is still under investigation, but no significant results have been reported yet.

Kohonen *et al.* [66], [71], [68], [69] , [70] proposed a variety of learning vector quantizers (LVQ) to perform classification using a VQ encoder and codebook. The encoder operates as an ordinary minimum mean squared error selection of a representative from the codebook but the codebook is designed to attempt to reduce classification error. Kohonen's general goal is to imitate a Bayes classifier with less complexity than other neural network approaches. Kohonen's approach has been widely used for such disparate applications as the classification of speech sounds [27], objects in clutter in synthetic aperture radar [49], [126], [93] proteins [85], of bird songs [90], and of oceanic signals [42], [91].

4.3 Learning Vector Quantization (LVQ)

Several researchers have demonstrated [66],[68], [3],[11],[27] that Learning Vector Quantization (LVQ) methods constitute a viable alternative to more traditional approaches; their classification accuracy is at least as high as that of any other Artificial Neural Network (ANN) algorithm, while due to the simple computations, their speed in learning as well as in classification can be significantly higher. Moreover they are very easy to use [67],[126]

LVQ is a statistical classification or recognition method, its only purpose is to

define class regions in the input data space. A subset of similarly labeled codebook vectors will be placed into each class region, even if the class distributions of the input samples would overlap at the class borders, the codebook vectors of each class in this algorithm can be placed in and shown to stay within each class region. The quantization regions, like the Voronoi sets in VQ, are defined by the midplane between neighboring codebook vectors. An additional feature in LVQ is that for class borders one can only take such borders of the Voronoi tessellation that separate Voronoi sets into different classes. The class borders thereby defined are piecewise linear.

Fig. 4.2(a) illustrates the distributions of two different tissue classes in (T1, T2 and PD) space. If we assign a subset of codebook vectors to each class as shown in 4.2(b), then the task of assigning x_j to a class is simply the search for that codebook vector w_i that has the smallest Euclidean distance from x_j. The sample x_j is thought to belong to the same class as the closest w_i. The codebook vectors can be placed in a such way that those belonging to different classes are not intermixed, although the class distributions of X overlap. Then only the codebook vectors that lie closest to the class borders are important to the optimal decision, obviously a good approximation of $p(x|x \in C_k)$ is not necessary everywhere. It is more important to place the w_i into the signal space in such a way that the nearest-neighbor rule used for classification minimizes the average expected misclassification probability. Figure 4.2(b) illustrates the distributions of codebooks. The open circles represent the reference vectors of class C_1 and the large black dots are reference vectors of class C_2. The decision border for LVQ and Bayes are shown in the figure by a solid and a broken line respectively.

The segmentation algorithm used in this thesis is based on the LVQ algorithm. Various network topologies were designed and results from each network are pre-

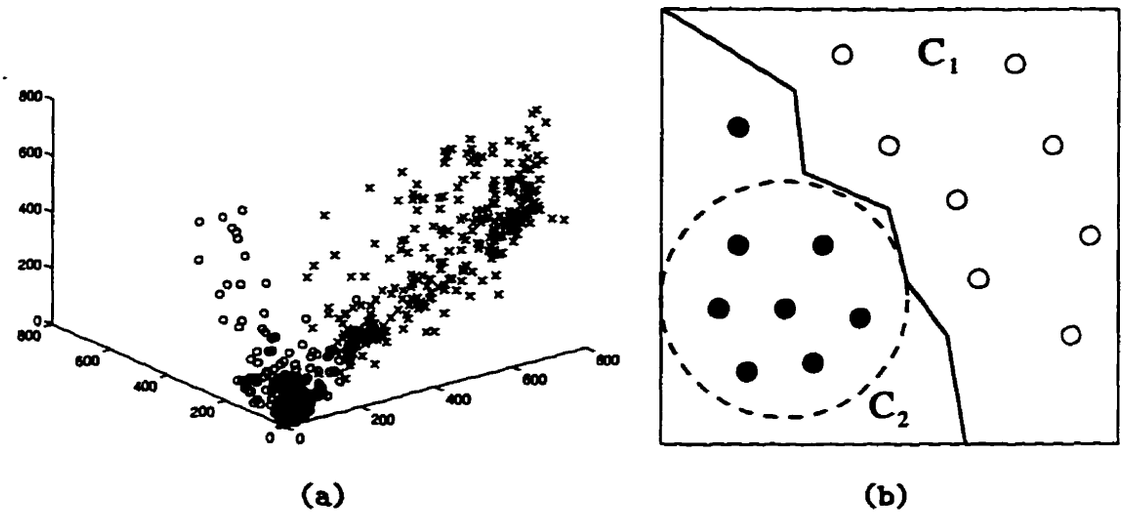

Figure 4.2: LVQ and Bayes decision border

sented in Chapter 5. Different learning coefficients were utilized, and the one which presented faster convergence and better results was adopted. The technique uses a training set which consists of the intensity level of a region of interest in the MRI images. The idea is to generate a training set from expected tissue samples and create a set of *codewords* (entries of codebook). The codeword vectors then will represent each particular tissue. Tissue classification will be possible because each codeword in the codebook can be associated with one of the known tissue classes used to construct the codebook. The manner in which a codebook can be formed to represent effectively the tissue classes will be discussed in the next chapter. In the following sections the theoretical aspects of each classifier used in this thesis will be discussed.

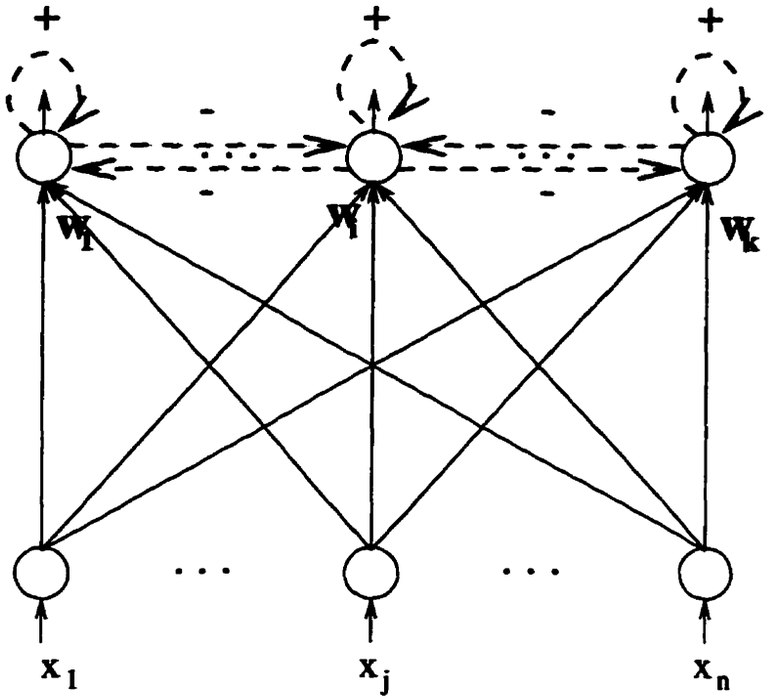

Figure 4.3: Topology of LVQ ANN

4.3.1 LVQ ANN Classifier

LVQ is a classification network that consists of two layers. This ANN classifies patterns by using an optimal set of reference vectors or *codewords*. A codeword is a set of connection weights from input to output nodes (Figure 4.3), (the circle which represents the neuron is called a node or a processing element (PE)). The set of vectors $w_1, w_2, ..., w_k$ is called a codebook in which each vector w_i is a codeword for Vector Quantization. If several codewords are assigned to each class, and each is labeled with the corresponding class symbol, the class region in the x space (input) is defined by simple nearest-neighbor comparison of x with the codewords w_i; the label of the closest w_i defines the classification of x.

To define the optimal placement of w_i in an iterative learning process, initial

values must be set. The next step is to determine the labels of the codewords by presenting a number of input vectors with known classification and assigning the codewords to different classes by majority voting according to the frequency with which each w_i is closest to the calibration vectors of a particular class.

The classification accuracy improves if the w_i are updated according to the algorithm described below [66], [67]. The idea is to pull codewords away from the decision surface to demarcate the class borders more accurately. In the following algorithm we assume w_i is the nearest codeword to the input vector x (Eq. 4.1) in the Euclidean metric; this, then, also defines the classification of x.

$$||x - w_i|| = MIN_{j=1}^{k}||x - w_j|| \tag{4.1}$$

where the Euclidean distance between any two vectors X and Y is defined as

$$||X - Y|| = [\sum_{i=1}^{n}(x_i - y_i)^2]^{\frac{1}{2}}$$

The following algorithm shows how the codewords will be updated.

1. either

$$w_i(t+1) = w_i(t) + \alpha(t)[x - w_i(t)] \tag{4.2}$$

   - if x is classified correctly (if the label agreed with codeword assignment),

2. or

$$w_i(t+1) = w_i(t) - \alpha(t)[x - w_i(t)] \tag{4.3}$$

   - if the classification of x is incorrect (if the label does not agree with the codeword assignment),

3. and

$$w_j(t+1) = w_j(t), \qquad j \neq i \tag{4.4}$$

- (the other codewords are not modified).

Here $\alpha(t)$ is a *learning rate* such that $0 < \alpha(t) < 1$, and is decreasing monotonically in time ($\lim_{t\to\infty} \alpha(t) = 0$). After a sufficient number of iterations, the codebook typically converges and the training is terminated. There are two other options for the LVQ which will be discussed later and the differences between the two versions and original LVQ will be explained.

LVQ2 Algorithm

The classification decision in the LVQ2 algorithm [53], [69] is identical to that in the basic LVQ. While in the original LVQ only one reference vector is updated at a time, in the LVQ2 algorithm two vectors are updated at each step, namely, the winner and the runner-up (one belongs to the correct class and the other to a wrong class). The purpose is to shift the midplane of these two vectors directly to the zone where the Bayes border should lie. An algorithm that can easily be seen to work in that direction is the following.

First define a symmetric *window* (Fig. 4.4) with nonzero width around the midplane of neighboring reference vectors w_g and w_j. Let w_g belong to class C_g and w_j to class C_j , respectively. If the corrections are made according to equation 4.5, it will be easy to see that for vectors falling into the window, the corrections of both w_g and w_j, on the average, have such a distribution that the midplane moves towards the crossing surface of the class distributions, and thus asymptotically approximately coincides with the Bayes decision border.

$$\Delta w_g(t) = -\alpha(t)[x - w_g(t)],$$

$$\Delta w_j(t) = +\alpha(t)[x - w_j(t)] \tag{4.5}$$

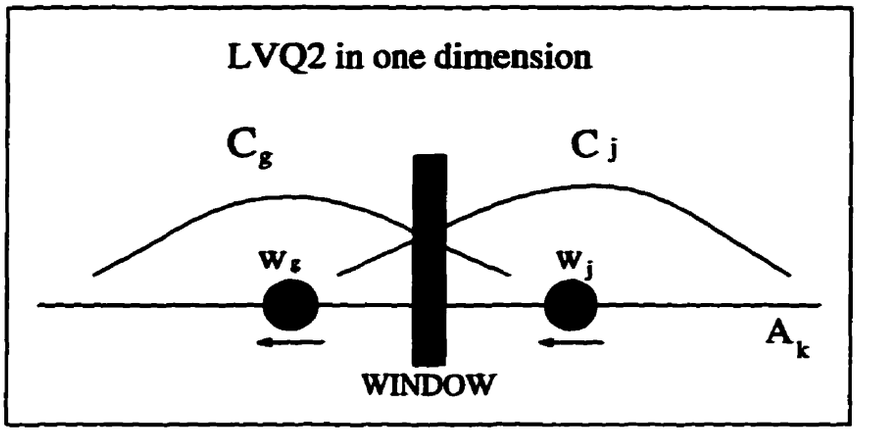

Figure 4.4: LVQ2 in 1 dimension

- where w_g and w_i are the two closest codebook vectors to x, whereby x and w_j belong to the same class, while x and w_g belong to different classes, respectively. Furthermore, x must fall in the "window".

Assume that d_g and d_j are the Euclidean distances of x from W_g and W_j, respectively; then x is defined to fall in a window of width s if,

$$min(\frac{d_g}{d_j}, \frac{d_j}{d_g}) > \epsilon \qquad \text{where} \qquad \epsilon = \frac{1-s}{1+s} \tag{4.6}$$

The size of s depends on the number of available training samples; Values for s around 0.2 to 0.3 are recommended [68]. If the window is made too narrow, the training result will suffer from low statistical accuracy due to the reduced number of corrections.

LVQ3 Algorithm

The LVQ2 algorithm is based on the idea of differentially shifting the decision borders toward the Bayesian limit, while no attention is paid to what might happen

to the location of the w_j in the long run if this process is continued. Therefore a correction is necessary to ensure that the w_j continue approximating the class borders, at least roughly. These ideas have been combined in an algorithm called LVQ3 with improved performance.

The LVQ3 algorithm updates weights according to the following rules:

$$\Delta w_g(t) = -\alpha(t)[x - w_g(t)],$$

$$\Delta w_j(t) = +\alpha(t)[x - w_j(t)], \tag{4.7}$$

- where w_g and w_j are the two closest codebook vectors to x, where x and w_j belong to the same class, while x and w_g belong to different classes, respectively. Furthermore, x must fall into the "window".

$$\Delta w_k(t+1) = w_k(t) - \tau\alpha(t)[x - w_k(t)] \tag{4.8}$$

- for $k \in g, j$, if x, w_j, and w_g belong to the same class.

The value of τ depends on the size of the window; for window sizes of 0.2 to 0.3, values for τ between 0.1 and 0.5 have been recommended [70]. τ can be smaller for narrower windows. This algorithm seems to be self-stabilizing, i.e. the optimal placement of the w_j does not change in continual learning.

4.3.2 Differences between basic LVQ and other options of LVQ

The three options of LVQ were utilized in this thesis for classification and segmentation of MR brain images. From results obtained for each option no significant

differences between accuracies were observed, though the computational time for LVQ2, and LVQ3 were slightly higher than original LVQ. Kohonen [68] also reported similar conclusions when he used LVQ for some statistical pattern recognition tasks. Results of using the LVQ ANN with the modification of learning parameters and initialization will be presented in chapter 5.

4.3.3 Backpropagation ANN classifier

The backpropagation ANN is used in this thesis for segmentation and classification of MR images in order to compare the performance of an LVQ classifier with one of the neural network techniques used in the literature. Backpropagation neural networks are feed-forward neural networks. A backpropagation network can be made of a single or multiple hidden layers of nodes. Figure 4.5 shows the topology of a typical backpropagation neural network. All the nodes that are not used either for input or output are called hidden nodes and the layer they form is called a hidden layer. A backpropagation network has two modes of operation: 1) forward propagation, 2) backpropagation. Both of the modes are executed during the learning (training) phase of a backpropagation network, but only forward propagation is performed during testing, or in actual use of a trained backpropagation network.

Two functions determine the output value of a node. The first one is a linearly weighted summation of the incoming signals from other nodes plus a bias, and the second is a nonlinear activation function (Figure 4.6). Each node computes the weighted sum of the inputs plus the bias weight and passes this sum through the activation function to calculate the output value from the hidden layer as

$$o_{ij} = f(net_{ij}) = f(\sum_{p=1}^{N} w_{jp} x_{ip} + \theta_j) \tag{4.9}$$

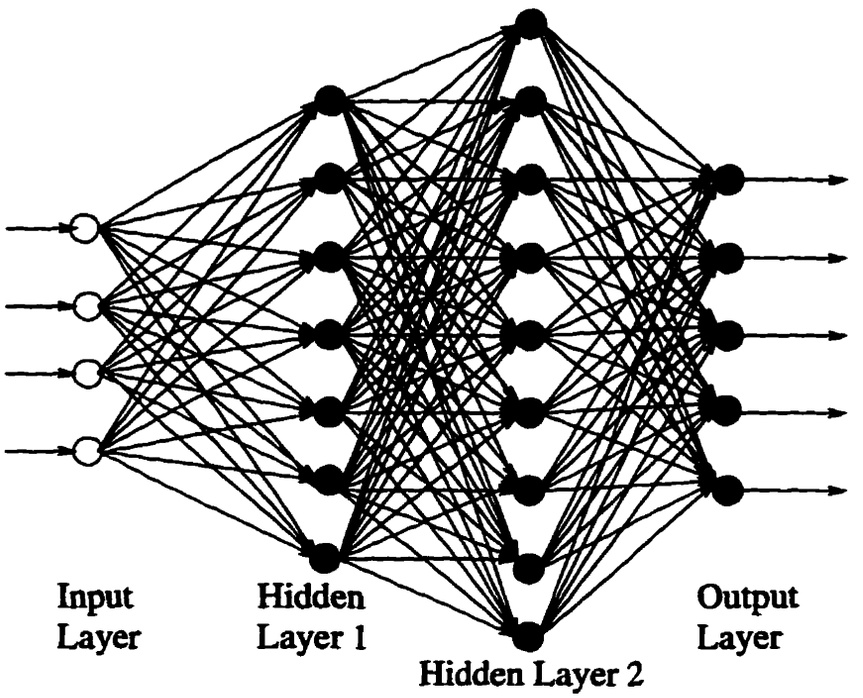

Figure 4.5: Topology of backpropagation ANN

where $X_i = (x_{i1}, x_{i2}, ..., x_{iN})$ is the ith input value for the neuron and W_j is corresponding weight. θ_j is a bias term. The bias term sometimes helps convergence of the weights to an acceptable solution; however, its use is largely a matter of experimentation with the specific application.

The activation function $f(\star)$ typically is a sigmoid function of the form $f(z) = \frac{1}{1+\exp^{-z}}$ (z is an arbitrary variable) which maps the potentially infinite range of the weighted sum to a limited, finite range. During the training phase activations of input units are set to values determined by the training data, and activations of all other units are calculated using $f(z)$. The difference between the desired output value (target) and the actual output (observed) is used to change the weights. The error function E_i for a pattern is defined as:

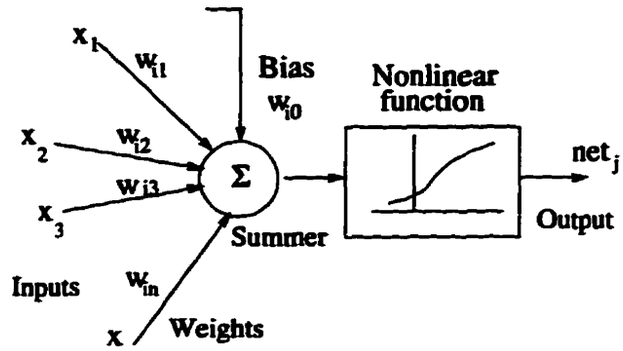

Figure 4.6: Model of artificial neurons in a feedforward neural network.

$$E_i = \frac{1}{2}\sum_{j}^{M}(y_{ij} - o_{ij})^2 \tag{4.10}$$

where subscript "i" refers to the ith training vector, and "j" refers to jth output unit. M is the number of nodes, y_{ij} is the desired output (target) and o_{ij} is the observed output (actual output) from the jth unit. The backpropagation algorithm is a supervised learning algorithm which performs a gradient descent on a squared error energy surface to arrive at a minimum. The key to the use of this method is the calculation of error values for the hidden units by propagating the errors backward through the network. The generalized delta rule implements a gradient descent in E to minimize the error [109]. The gradient of E_i with respect to w_{jp} is

$$\Delta_i w_{jp} \propto \frac{-\partial E_i}{\partial w_{jp}} = (y_{ij} - o_{ij}) f_j'(net_{ij}) o_{ij} \tag{4.11}$$

Let the error $\delta_{ij} = (y_{ij} - o_{ij})$. By using a gradient descent technique [40], weight changes iteratively as:

$$w_{jp}(t+1) = w_{jp}(t) + \Delta_i w_{jp}(t) \tag{4.12}$$

where

$$\Delta_i w_{jp} = \beta \delta_{ij} o_{ip} \tag{4.13}$$

where β is the learning rate. The rule for learning may be modified for faster convergence by adding a momentum rate η as follow:

$$\Delta_i w_{jp}[t+1] = \beta \delta_{ij} o_{ip}[t+1] + \eta \Delta_i w_{jp}[n] \tag{4.14}$$

here η acts like a filter to avoid sudden changes due to conflicting data in the training set.

When a hidden layer is used, the output error δ_{ij} changes as follows:

$$\delta_{ij} = \begin{cases} f'(net_{ij}) \sum_p \delta_{ip} w_{pj} & \text{for a hidden node} \\ (y_{ij} - o_{ij}) f'(net_{ij}) & \text{for an output node} \end{cases} \tag{4.15}$$

With f the sigmoid activation function, equation 4.15 can be rewritten as:

$$\delta_{ij} = \begin{cases} o_{ij}(1 - o_{ij}) \sum_p \delta_{ip} w_{pj} & \text{for a hidden node} \\ (y_{ij} - o_{ij}) o_{ij}(1 - o_{ij}) & \text{for an output node} \end{cases} \tag{4.16}$$

4.3.4 Maximum likelihood classifier

This classifier is based on Bayes decision rule which maximizes the *a posteriori* probabilities. It assigns a pattern X to the class c_i if

$$p(c_i|X) > p(c_j|X) \quad \forall j, j \neq i \tag{4.17}$$

- $p(c_i|X)$ is the conditional probability of class i given the observation X.

Using Bayes' theorem, and assuming equal probability for each class, X is allocated to class i if

$$p(X|c_i) > p(X|c_j) \quad \forall j, j \neq i \tag{4.18}$$

If we assume a normal probability density for X in each class then $p(X|c_i)$ will be

$$p(X|c_i) = (2\pi)^{-n/2}|\Sigma_i|^{-1/2} \exp \frac{-d_i^2}{2}, \tag{4.19}$$

- where n is the dimension of the feature vector X and

d is a distance measure described by

$$d_i^2 = (X - m_i)^T \Sigma_i^{-1} (X - m_i) \tag{4.20}$$

where m_i and Σ_i are the mean vector and covariance matrix for class i respectively. Classification of each pixel is based on the following expression:

$$X \in c_i \quad \text{if} \quad D_i(X) = -\frac{1}{2} ln|\Sigma_i| - \frac{1}{2} d_i^2 > D_j(X) \quad \forall j, j \neq i \tag{4.21}$$

4.4 Summary

In this chapter supervised techniques for classification and segmentation of MR images were discussed. The application of the LVQ Artificial Neural Network (ANN) was introduced. Theoretical issues regarding LVQ ANN, maximum likelihood classifier and backpropagation ANN were discussed. The results of segmentation of MR images using each of these techniques will be presented in chapter 5. The advantages and disadvantages of each technique and part of the contributions of this thesis will be discussed in Chapter 5.

Chapter 5

Results of Supervised techniques

5.1 MR Brain Images

Twenty nine complete studies were obtained from the MRI department at McMaster University Medical Center for the purpose of this thesis. All information identifying the subjects was stripped before we had access to the data. The subjects were studied on a GE 1.5T MR scanner. The axial field of view was either 20 cm for the T1 weighted sequences, or 22 cm for the PD and T2 weighted sequences. Images were reconstructed onto a 256×256 matrix, so that the size of a pixel was either $0.78 \times 0.78\ mm^2$ or $0.86 \times 0.86\ mm^2$. Because the T1 weighted images were acquired with a field of view of 20 cm, they were resampled to ensure accurate registration with the other images. Each slice was 5 mm thick, with a 2.5 mm inter-slice spacing. Typically, 18 slices would cover the brain from the vertex to the base. Three pulse sequences were used: TR/TE = 600 ms / 16 ms for the T1 weighted images; and TR/TE = 2916 ms/ 17 ms for the PD-weighted images; and TR/TE = 2916 ms/ 119 ms for the T2 weighted images. Six selected slices from the brain of a normal

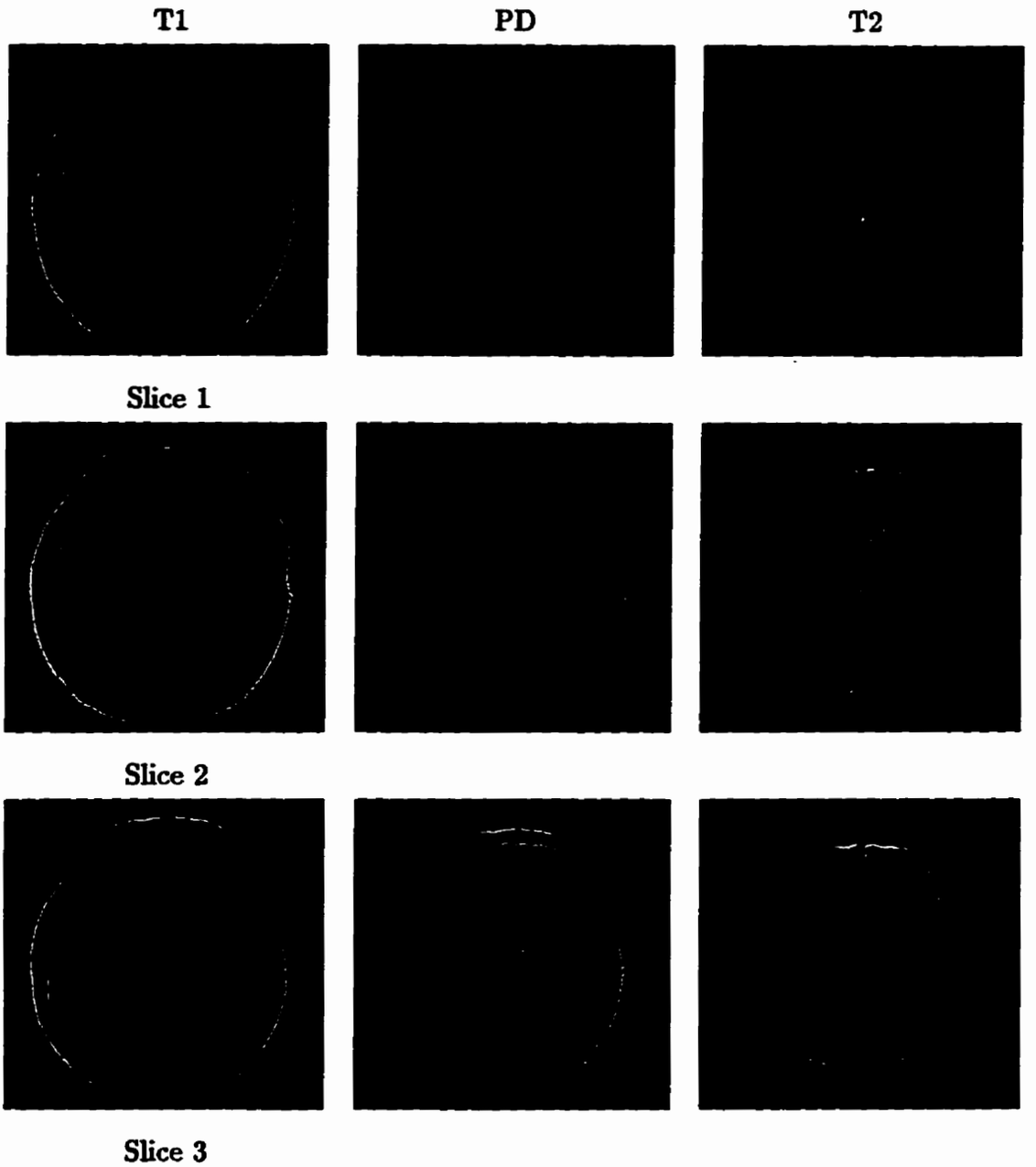

Figure 5.1: Six selected slices from the brain of a normal subject

subject are shown in Figures 5.1, and 5.2.

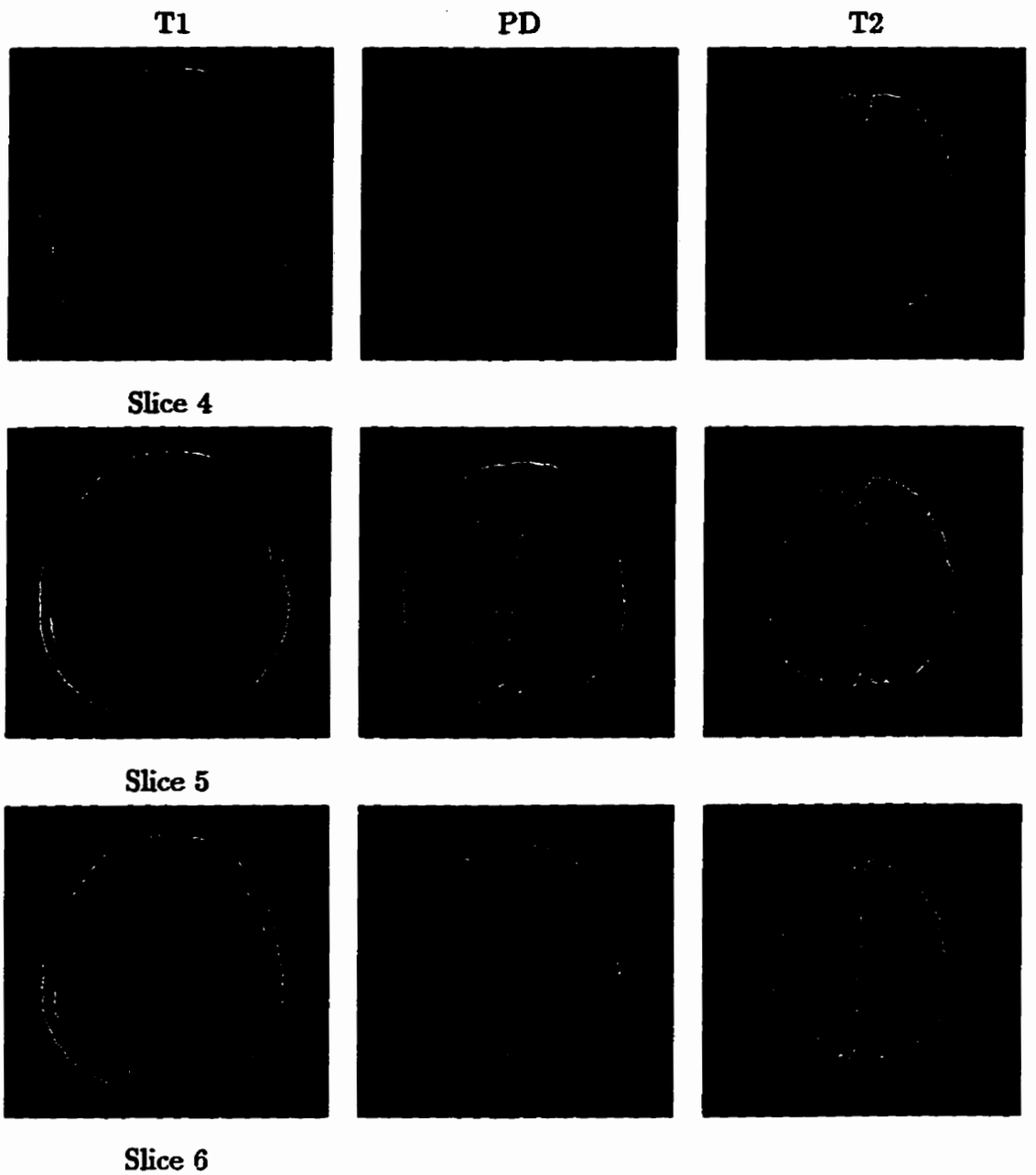

Figure 5.2: Six selected slices from the brain of a normal subject

5.2 Segmentation using LVQ ANN

5.2.1 Generating training data

The first step for supervised tissue classification is to generate training data. In a typical experiment, the T1, T2 and PD-weighted images are displayed on the computer screen, one image at a time. Next, representative regions of interest (ROI's) for the target tissue classes are selected interactively on the computer screen using a mouse-driven interface. By clicking on the mouse each time, a subimage is generated. The size of the subimage is defined by the user. A typical size for a subimage is 3×3 to 5×5 pixels. Subimages are generated for all images at the same anatomical spot when the user clicks on the mouse. It is also possible for the user to select the region of interest from any of the 3 images on the screen. To allow the user to generate more training data from other image slices, the program interactively asks the user for this option. When the ROI's are selected, a data structure containing the labels of the regions and the corresponding intensity vectors is created and stored in a file. The file which is created is then used to train the neural networks. An example of this process is shown in Figure 5.3(a). It illustrates the regions of interest for different classes. The resulting sample statistics are shown in Fig. 5.3(b). Training data were selected from several slices in the same study.

5.2.2 Generating codebook data

Using the algorithm described in Chapter 4, Section (4.3.1), the codebooks were generated from the training data. The following initialization was made to accelerate the process and generate a suitable codebook.

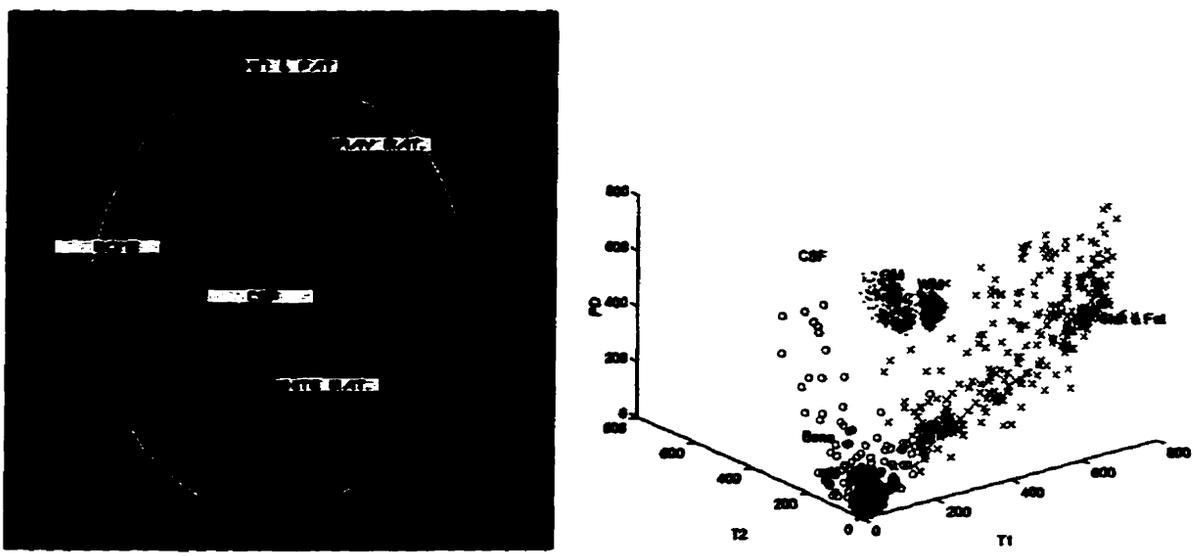

(a) (b)

Figure 5.3: Training regions and statistics for different classes: white matter (WM), gray matter (GM) , CSF, Bone, and skin & fat (scalp)

Codebook initialization

For the initialization of the codebook vectors, a set of vectors is chosen from the training data. All the entries used for initialization must fall within the borders of the corresponding classes, and this is checked by the k-nearest neighbor (k-NN) algorithm. In fact, in this step, the placement of all codebook vectors is determined first without taking their classification into account.

The k-NN method is nonparametric, in that it does not require any knowledge or assumptions about statistical properties of the data [28]. The k-NN rule essentially relies on having a large number of (presumably) correctly labeled samples from each tissue class. Figure 5.4 displays the geometry of this scheme. If we assume n vectors in the feature space which are labeled, then, all that is needed is to choose the number of nearest neighbors (k) that defines the neighborhood of any unlabeled

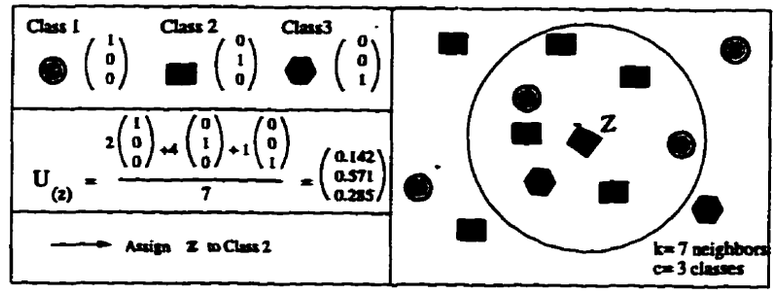

Figure 5.4: The k-NN rule classifier

vector $z \notin X$, and to check some measure of distance, (d) between pairs of vectors in $\Re^p$, usually the Euclidean distance

$$d(z, x_i) = ||z - x_i|| = \sqrt{(z - x_i)^T (z - x_i)}$$

One must also choose a voting scheme, and often this is to accept a simple majority of the votes for any class represented by points in the k-NN neighborhood. In Fig. 5.4, with $k = 7$ nearest neighbors having $c = 3$ class labels, the point z will be labeled as a class 2 pixel, because four of its nearest seven neighbors have this label. It is easy to formulate the implementation used in the example as follows:

1. Store training data X. Let n be the number of vectors and c be the number of classes. Let U be a $(c \times n)$ matrix whose columns $(U_{(j)}, j = 1, 2, ..., n)$ are the known label vectors of X's elements.

2. Choose k=number of neighbors to find.

3. Choose d: any metric (distance measure) on $\Re^p$.

4. For each test pattern z:

   (a) using $x_i \in X$ and $z \notin X$: compute and rank order the distances $d(z, x_i)$ as $d_1 \leq d_2 \leq ... \leq d_k \leq d_{k+1} \leq ... \leq d_n$.

(b) Find the columns in U corresponding to the k-nearest neighbor indices 1,2,...,k.

(c) calculate the label vector U_z for z with the labels of its k-nn's:

$$U(z) = \sum_{j=1}^{k} \frac{u_j}{k}, for \qquad i = 1, 2, ..., c.$$

(d) Calculate

$$D_{k-nn,z}(z) = e_i \leftrightarrow u_{iz} \geq u_{lz} \quad l = 1, 2, .., c, l \neq i$$

5. Continue for next z.

The initialization program then selects the codebook vector based on the desired number of codewords. Note that, the k-NN rule is used here just to filter the training vectors which were labeled mistakenly by the user, or training vectors which were selected from the boundary between tissues. This initialization is important because starting the network with a good estimate of location of each codeword helps speed the learning convergence.

The accuracy of classification may depend on the number of codebook entries allocated to each class. Different sets of codebooks with 60 to 120 codewords for each set have been tested. There does not exist any simple rule to find out the best distribution of the codebook vectors. We used the method of iteratively balancing the medians of the shortest distances in all classes. Our program first computes the medians of the shortest distances for each class and corrects the distribution of codewords so that for those classes in which the distance is greater than the average, codewords are added; and for those classes in which the distance is smaller than the average, some codewords are deleted from the initialized codebook vector.

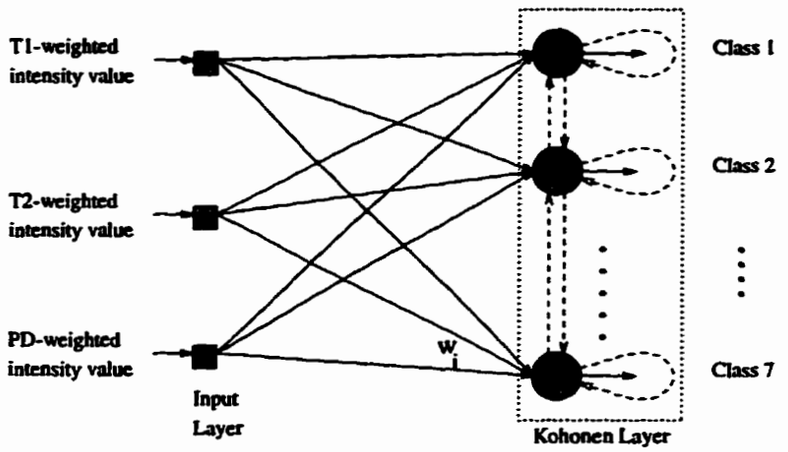

Figure 5.5: Topology of LVQ network

Learning parameter

The learning parameter, $\alpha(t)$, may be constant or may decrease monotonically with time (t). Two different learning factors were tried. It was found from several experiments that the second learning parameter equation, 5.2, produced faster convergence and better results.

$$\alpha(t) = 0.2(1 - \frac{t}{10000}) \tag{5.1}$$

$$\alpha(t) = \frac{\alpha(t-1)}{1 + \alpha(t-1)} \tag{5.2}$$

When the codebook has been initialized properly, training is started.

5.2.3 Segmentation using three pixel intensity value

Two different sets of features were used in this study: 1) intensity values in T1, T2, and PD weighted images 2) neighboring pixel statistics (mean & variance) along intensity values in T1, T2, and PD weighted images.

In Fig. 5.5 the topology and structure of the LVQ network is shown. The three input nodes in the network are the intensity values in T1, T2 and PD-weighted images. Each vector can be written as

$$x = [T1(x_i, y_i), T2(x_i, y_i), PD(x_i, y_i)] \tag{5.3}$$

The number of output nodes is equal to the number of target tissue classes. In each of the cases presented in this chapter, the images were classified into seven classes: background, cerebrospinal fluid (CSF), white matter (WM), gray matter (GM), bone, scalp (fat and skin) and lesion or tumor (if present)

An overall view of the whole segmentation process is shown in Fig. 5.6. Complete segmentation results for those images which were shown in 5.1 and 5.2 are illustrated in Figure 5.9. In Figure 5.10 and 5.11 the three tissues, white matter, gray matter and CSF are shown separately.

5.2.4 Segmentation using neighborhood pixels

To investigate use of other features in the images, in this approach codebooks are formed from a set of features obtained for each pixel in the original image. Input vectors consist of vectors of intensity value for the pixel (i.e., $T1(x_i, y_i)$), mean (μ_{x_i,y_i}), and variance (σ_{x_i,y_i}) of intensity values in a window of size 3×3, presented as follows:

$$x = [T1(x_i, y_i), T1(\mu_{x_i,y_i}), T1(\sigma_{x_i,y_i}), T2(x_i, y_i), T2(\mu_{x_i,y_i}),$$

$$T2(\sigma_{x_i,y_i}), PD(x_i, y_i), PD(\mu_{x_i,y_i}), PD(\sigma_{x_i,y_i})] \tag{5.4}$$

The number of input nodes in the network is equal to the number of features. The number of output nodes is equal to the number of target tissue classes. They

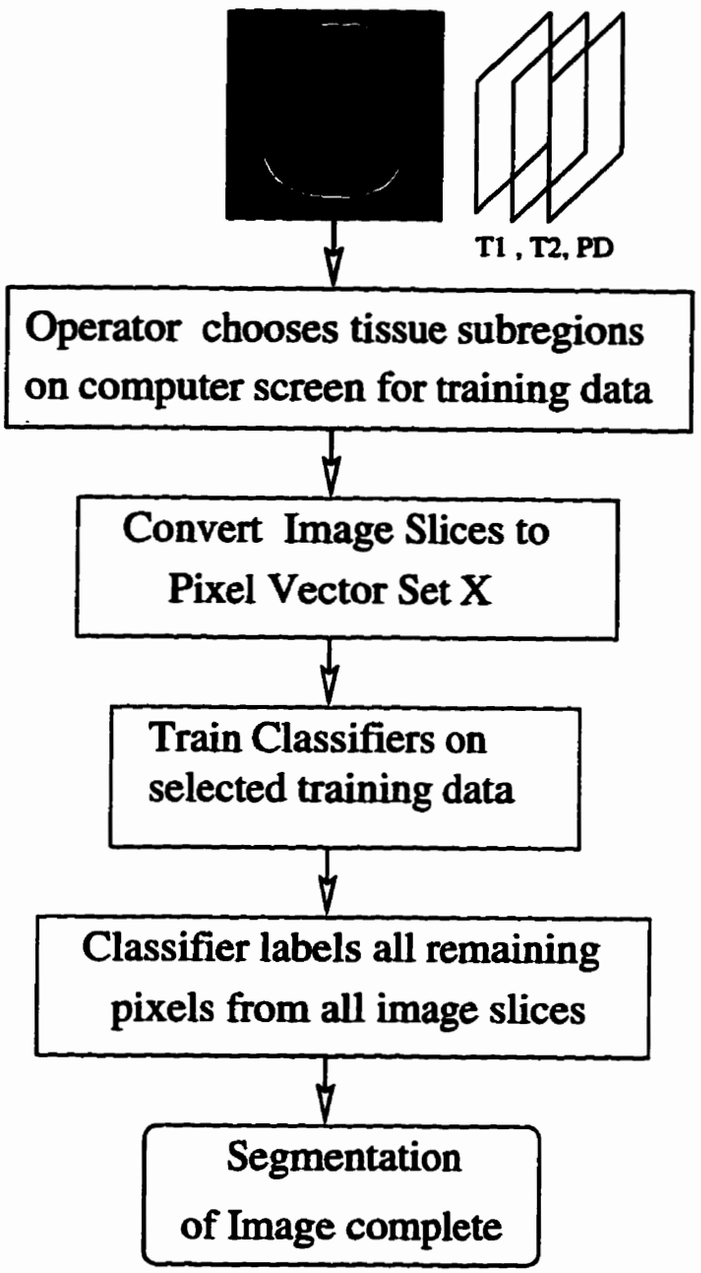

Figure 5.6: Block diagram of entire segmentation process

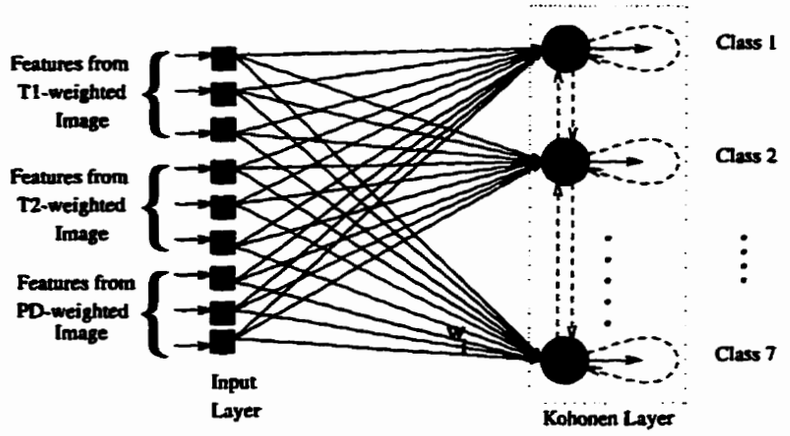

Figure 5.7: Topology of LVQ network for 9 input features

are: background, cerebrospinal fluid (CSF), white matter, gray matter, bone, scalp (fat and skin) and lesion or tumor (if present). The networks were trained using initial codebooks and tested for different sets of image slices from an individual without any brain abnormality, and one with a malignant glioma.

Figure 5.7 shows the topology of our network for nine features for input vector.

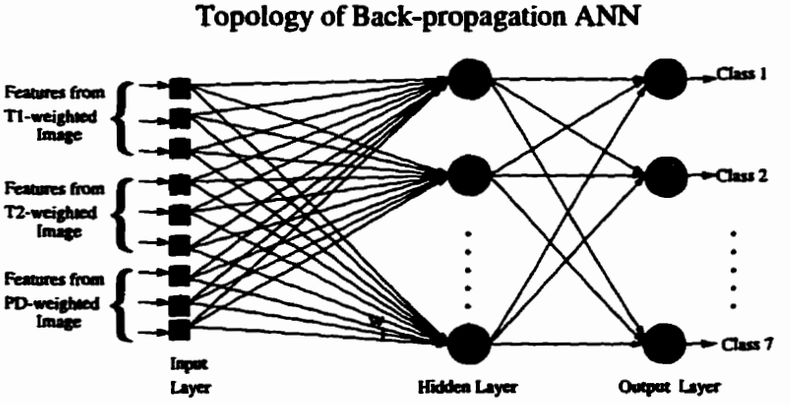

Figure 5.8: Topology of backpropagation ANN

Segmentation of slice 1

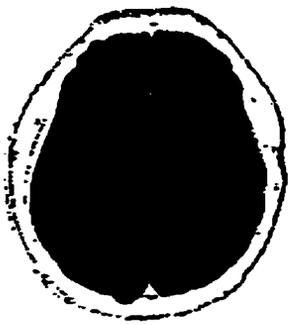

Segmentation of slice 2

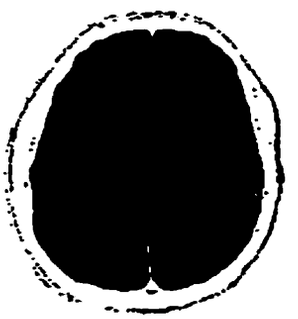

Segmentation of slice 3

Segmentation of slice 4

Segmentation of slice 5

Segmentation of slice 6

Figure 5.9: Segmentation results using LVQ

5.3 Results of backpropagation ANN approach

Fig. 5.8 illustrates the topology of the network for seven classes and nine input features. In general the input values of a backpropagation network is scaled between 0 and 1 or -1 and 1 to operate in the dynamic range of the sigmoid function. We chose the sigmoid function in the 0 to 1 range defined as $f(z) = \frac{1}{1+\exp^{-z}}$. The sigmoid function in the -1 and 1 range is defined as: $f(z) = \frac{1-\exp^{-z}}{1+\exp^{-z}}$ which requires two more operations, a subtraction and an exponential in the numerator which would increase the computational time. Ideally an output node is either one or zero, identifying the class of a pattern when it is one, and zero when it is not. However, the output nodes can take any value between zero and one and the largest valued output node defines the class of the input pattern.

The effect of the learning parameter and the momentum rate on the speed of convergence was investigated, and the best combination was selected for classification and segmentation. The same training and test data were used for training and testing the network. The training was stopped if convergence was not reached after 100,000 iterations. In order to investigate the impact of the topological parameters on both the speed of convergence and the classification accuracy several experiments were undertaken. Neural networks with one and two hidden layers were generated, and the number of nodes in each of the layers was varied from 10 to 30. From results obtained in each test the best combination was selected for classification and segmentation of MR images. For nine input features (neighboring pixels statistics) the backpropagation network with one hidden layer with 18 nodes in each layer and the learning rate of ($\beta = .05$) and momentum rate of ($\eta = 0.2$) provided the best results. Similarly for three input features (pixel intensity values from T1,T2, and PD weighted images) the backpropagation network with one hidden layer with

9 nodes in each layer and the learning rate of ($\beta = .05$) and momentum rate of ($\eta = 0.2$) provided the best results.

The complete segmentation results for those images which were shown in 5.1 and 5.2 are illustrated in Figure 5.12. The three tissues, white matter, gray matter and CSF are illustrated separately in Figures 5.13, and 5.14.

5.4 Results of maximum likelihood classifier

We compared our new technique with a conventional method, the maximum likelihood classifier. Equal *a priori* probabilities and normal probability density functions for the intensity values in each class were assumed. The same training data were used to find the mean and covariance matrix. Results are shown in Figures 5.15, 5.16, and 5.17. The results for the maximum likelihood method depend heavily on the training data.

MR data does not generally support the assumptions that underlie the ML method. Preliminary results published by Dudewicz *et al.* [29] indicate that although the distributions of T1 and T2 values can be considered as jointly normal, the distribution of proton density values is not normal. This is why MLC performs poorly. Although it might be possible to use the MLC using better assumptions or estimations, it is beyond the scope of this thesis to investigate the proper distributions for proton density values.

5.5 Segmentation of abnormal brain images

Figures 5.19, and 5.20 show the results of segmenting the MR images of a patient with malignant glioma. Results are shown for the LVQ and backpropagation approaches discussed in the earlier sections. Only two representative image slices were chosen in this example. The original T1, T2, and PD-weighted images are shown in Fig. 5.18. The first column in Figures 5.19, and 5.20 shows the segmented images and second column shows the extracted regions of tumor.

5.6 Discussion

It has been found that backpropagation neural networks are very sensitive to the training set in MR image segmentation of the brain. From the results presented in sections 5.2, 5.3 and 5.4 it can be shown that results of the backpropagation ANN suffer from noise and mis-classification. Backpropagation nets provide adequate brain segmentations provided that the training data are good. They can learn effectively on as few as 250 pixels per class in a 256x256 image using a multi-layer backpropagation network with between 6 and 18 hidden units, which means that training and testing are relatively fast. Efforts to find a universal training set that would be useful on many different MR images have been made. However, because of the intensity variation across MR images, the backpropagation network could not perform well every time. If backpropagation networks are to be used for segmentation of MR images, at least for now, reliance on operator intervention to select good training data for each tissue and each slice of data is crucial. The advantages of the maximum likelihood classifier is in the noniterative training. However, the assumption of a certain probability distribution of data was a weakness of the

classifier.

The weakness of backpropagation networks is the indeterminate number of hidden units. The convergence of backpropagation networks is dramatically dependent on the number of hidden units, and for most cases it was too difficult to find the optimum number of the hidden units.

The LVQ was also sensitive to selecting the number of codewords, however, changing the number of codewords was not too crucial for acceptable result. Selecting a large set of codewords could increase the misclassification around the border of regions of interest, however, the remaining classified regions were acceptable. Also, LVQ was used in an adaptive fashion to update the codewords from one image slice to another image slice in one complete study. This idea is new and was a key for an accurate segmentation task. Treating the network as described above suppressed the noise and caused the network not to be sensitive to the variations of gray-level for each tissue type between different slices.

The training time required for backpropagation networks was longer than the time required for the LVQ. The computational time for LVQ ANN is on the order of seconds (about 50 seconds learning and 10 seconds testing) while backpropagation ANN requires 10 to 20 minutes. The learning parameter β, and momentum η of backpropagation networks had a crucial role in convergence and accuracy of classification task, and the best combination was found after numbers of experiments.

In case of abnormality, the segmentation of the images is complicated because the image features of the abnormal tissues may be very close to those of their neighbor normal tissues. Therefore, abnormal tissues may be found in a normal tissue component after a segmentation. Abnormal tissues may also deform the geometry of normal tissues.

In summary, in this chapter we have shown that normal and abnormal tissues in the brain can be recognized automatically by multispectral analysis of MR images. We conclude that LVQ ANN is a good choice for segmentation of MR images if implemented in an adaptive scheme. Our technique is adaptive and this allows the user to update codebooks so that classification accuracy can be improved. Results show that tissue segmentation using LVQ ANN produces better and faster results than backpropagation ANN and the Maximum Likelihood method. It also shows the LVQ neural network is a powerful technique for MR image segmentation.

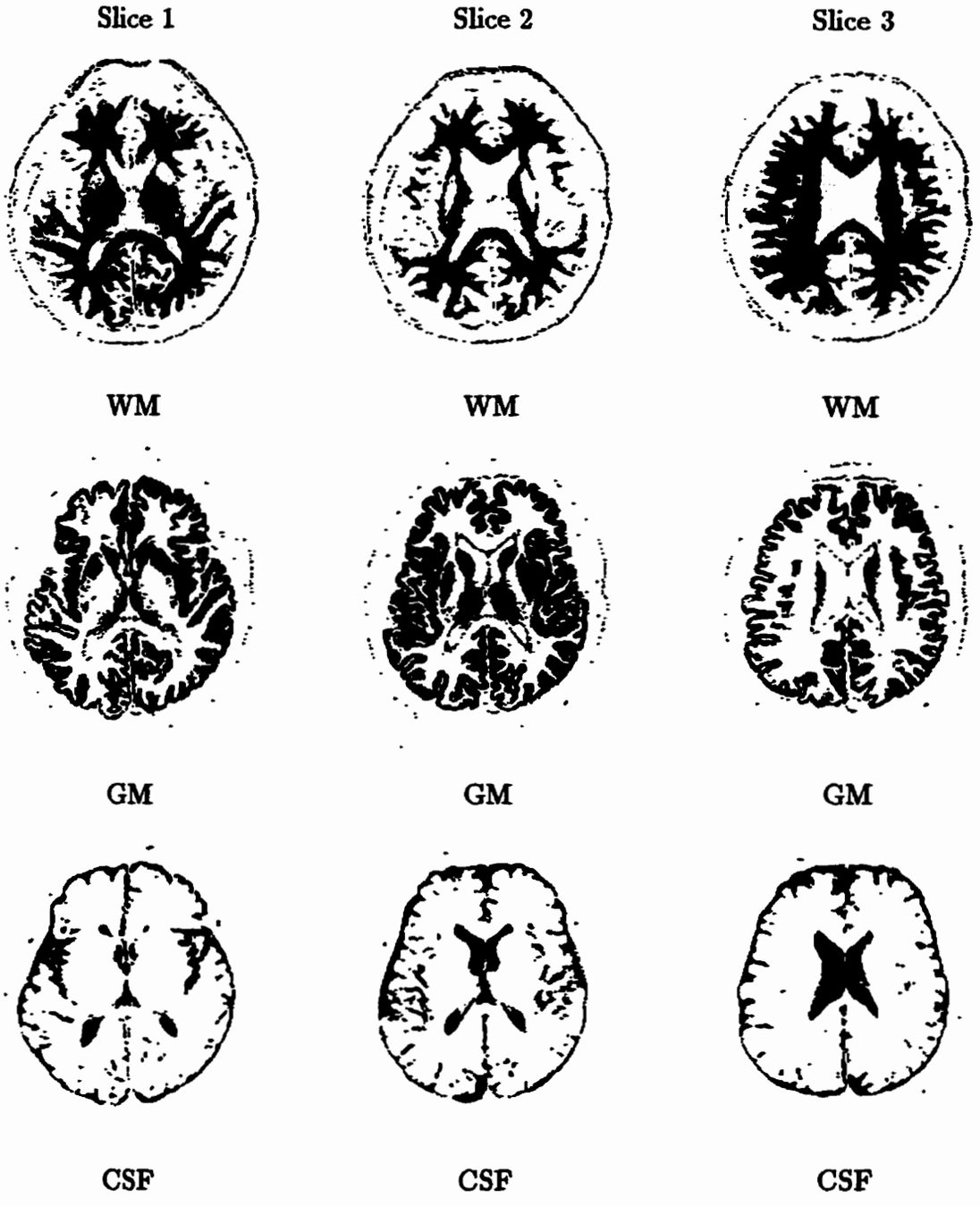

Figure 5.10: Segmentation of images using LVQ. Three tissues: Gray matter (GM), White matter (WM), and CSF are separated

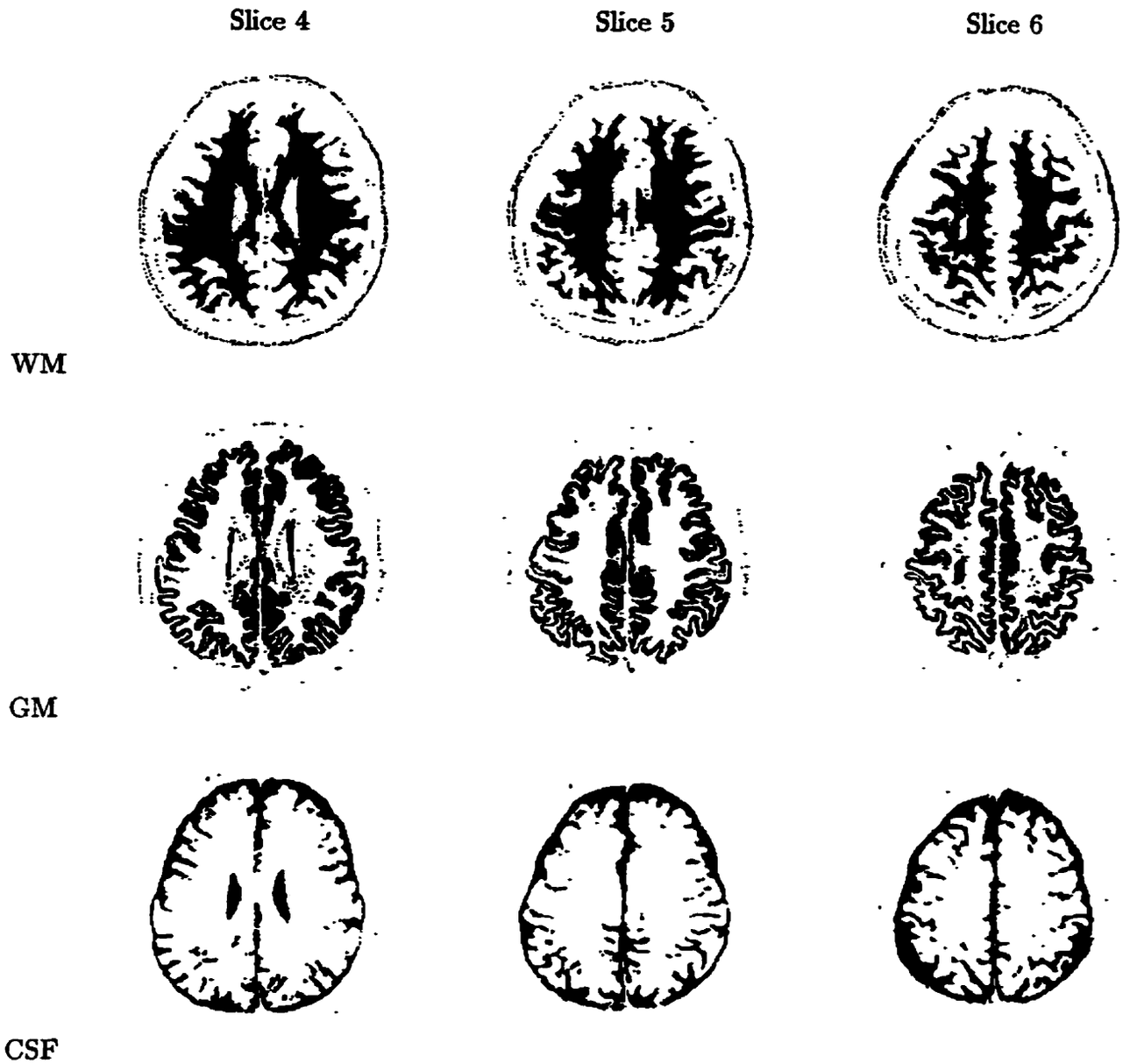

Figure 5.11: Segmentation of images using LVQ. Three tissues: Gray matter (GM), White matter (WM), and CSF are separated

Segmentation of slice 1

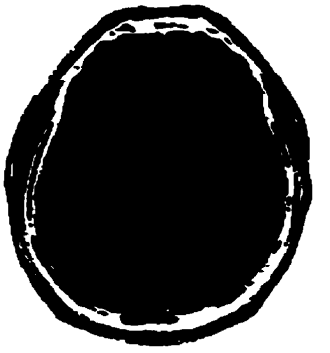

Segmentation of slice 2

Segmentation of slice 3

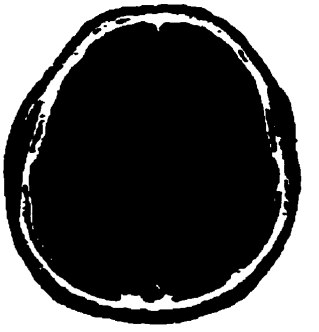

Segmentation of slice 4

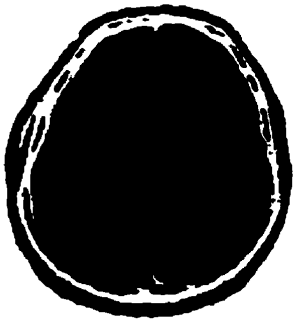

Segmentation of slice 5

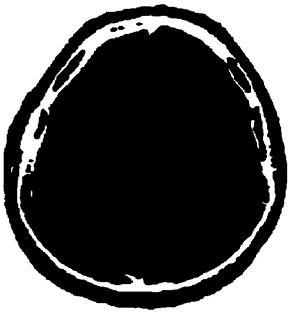

Segmentation of slice 6

Figure 5.12: Segmentation results using backpropagation ANN

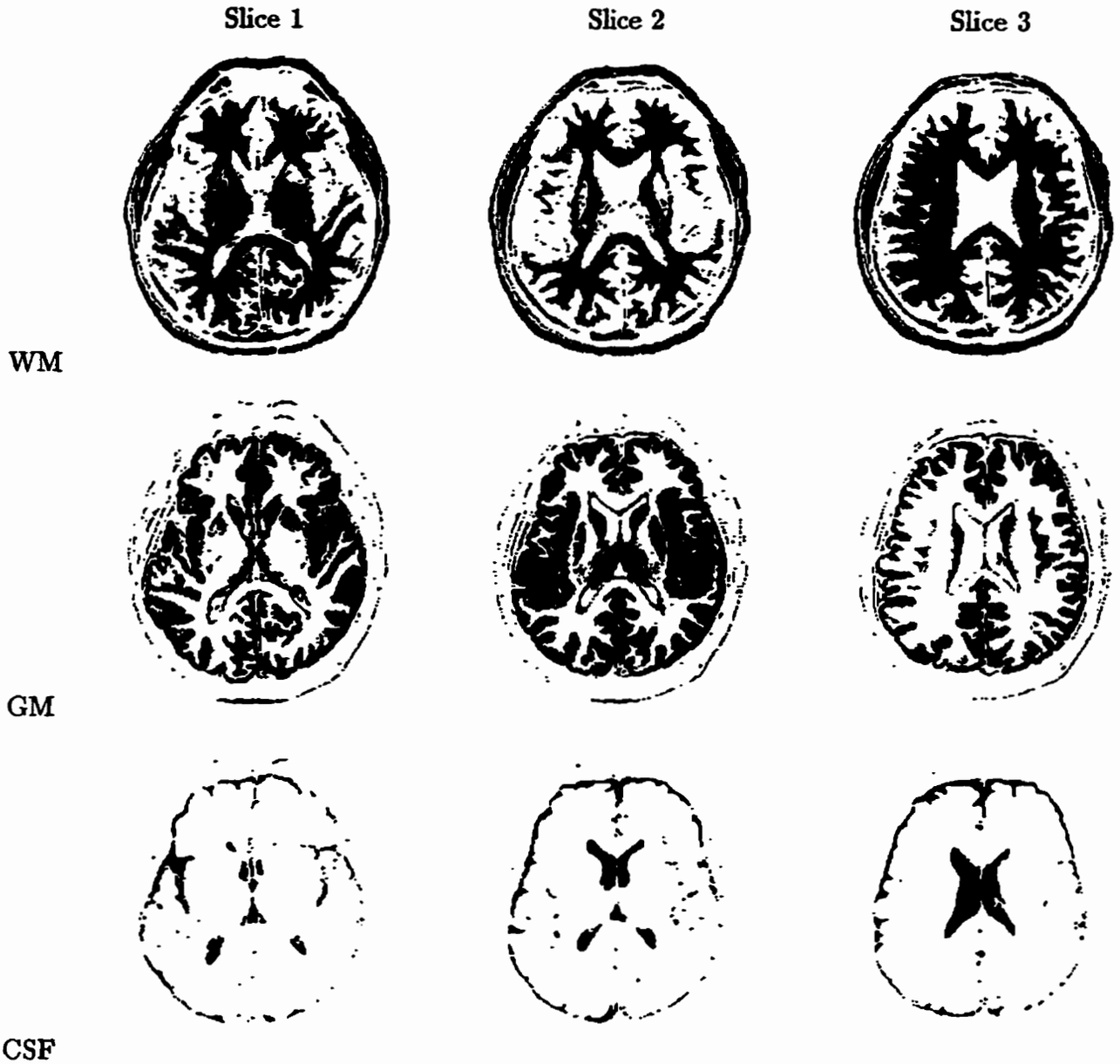

Figure 5.13: Segmentation results using backpropagation ANN, each tissue is shown separately

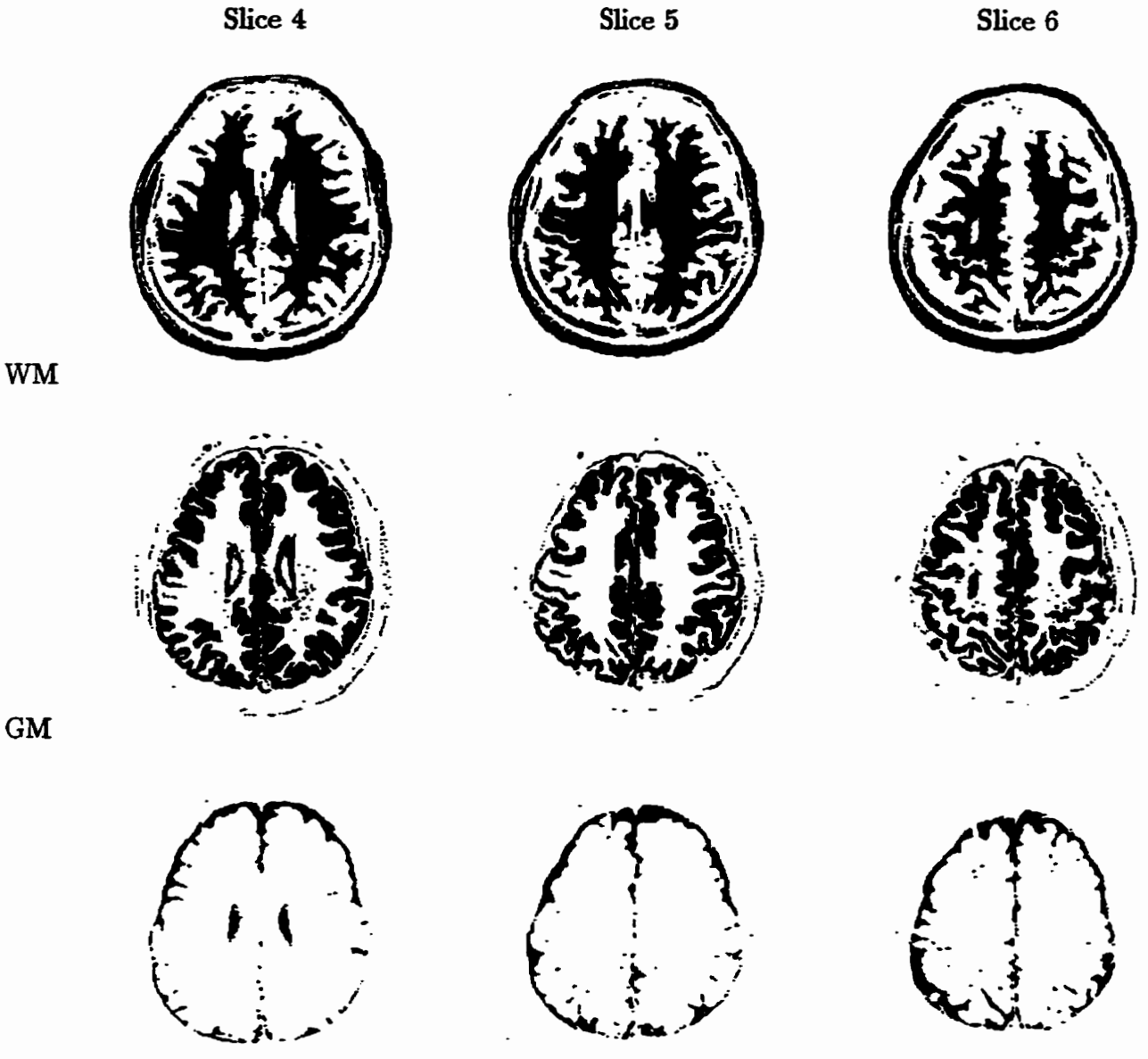

Figure 5.14: A complete segmented image using backpropagation ANN, each tissue is shown separately

Segmentation of slice 1

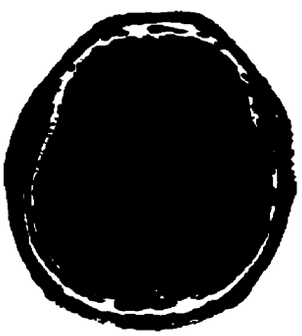

Segmentation of slice 2

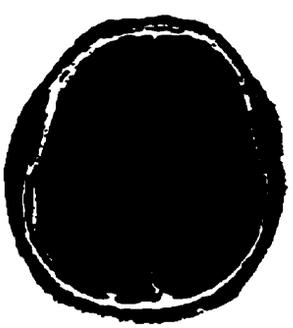

Segmentation of slice 3

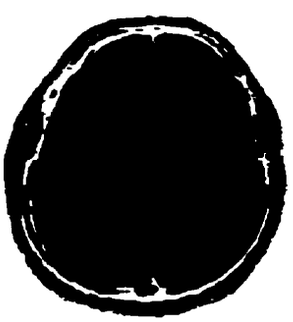

Segmentation of slice 4

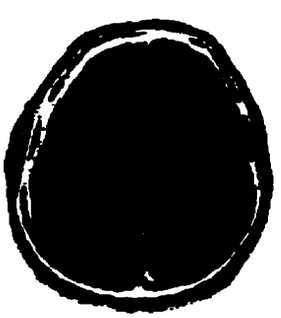

Segmentation of slice 5

Segmentation of slice 6

Figure 5.15: Segmentation results using MLC

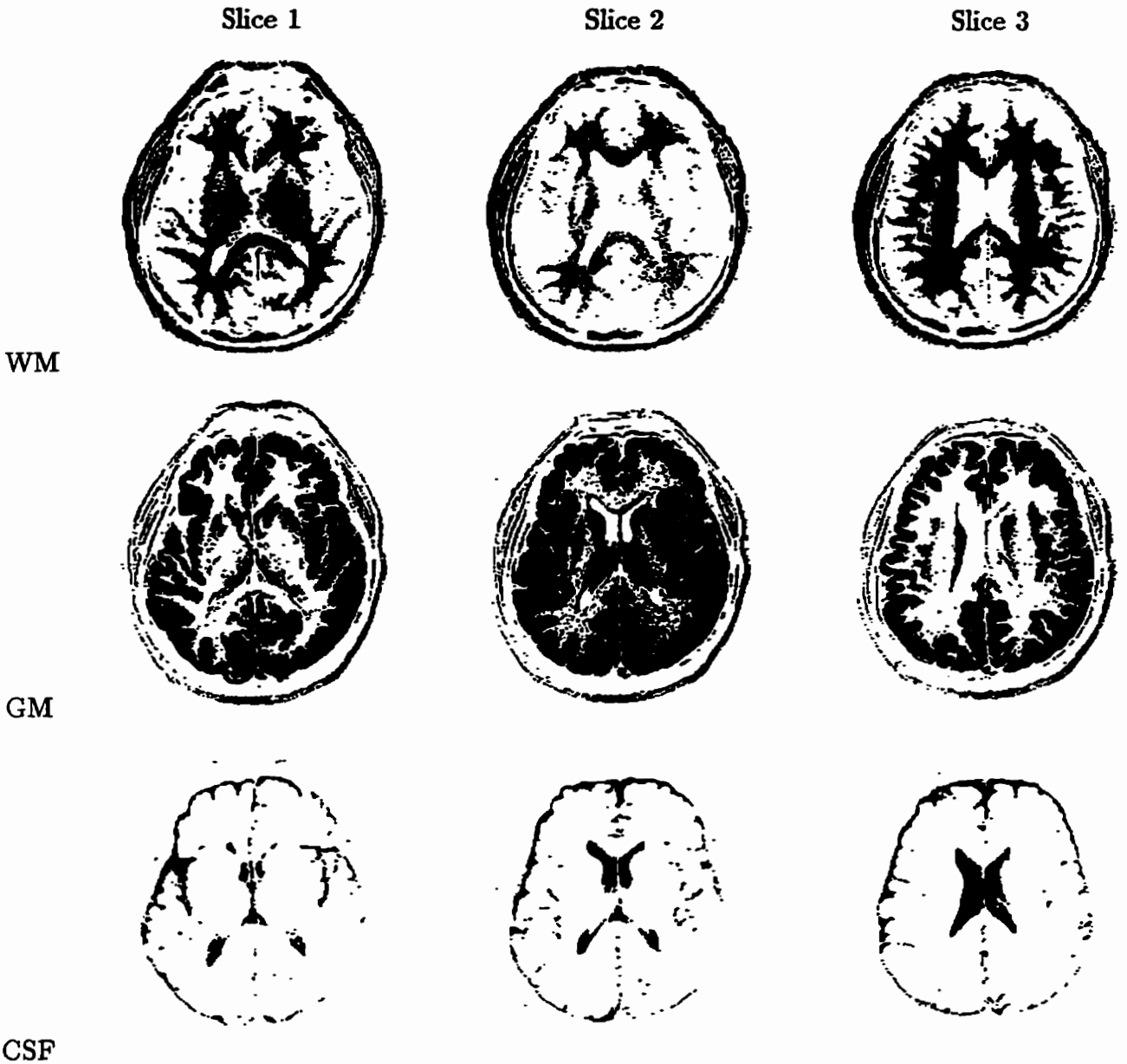

Figure 5.16: Segmentation results using MLC, each tissue is shown separately

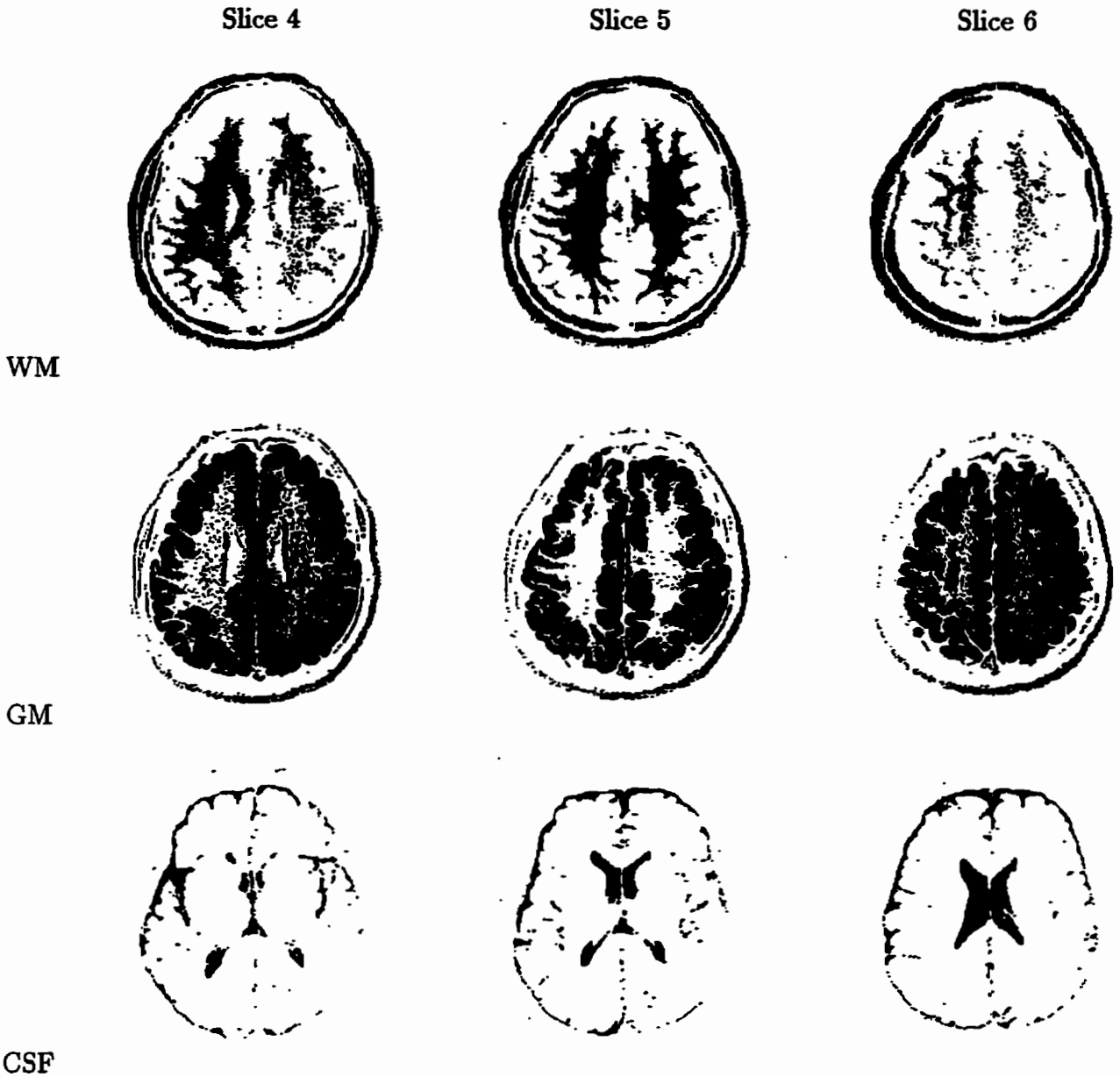

Figure 5.17: Segmentation results using MLC, each tissue is shown separately

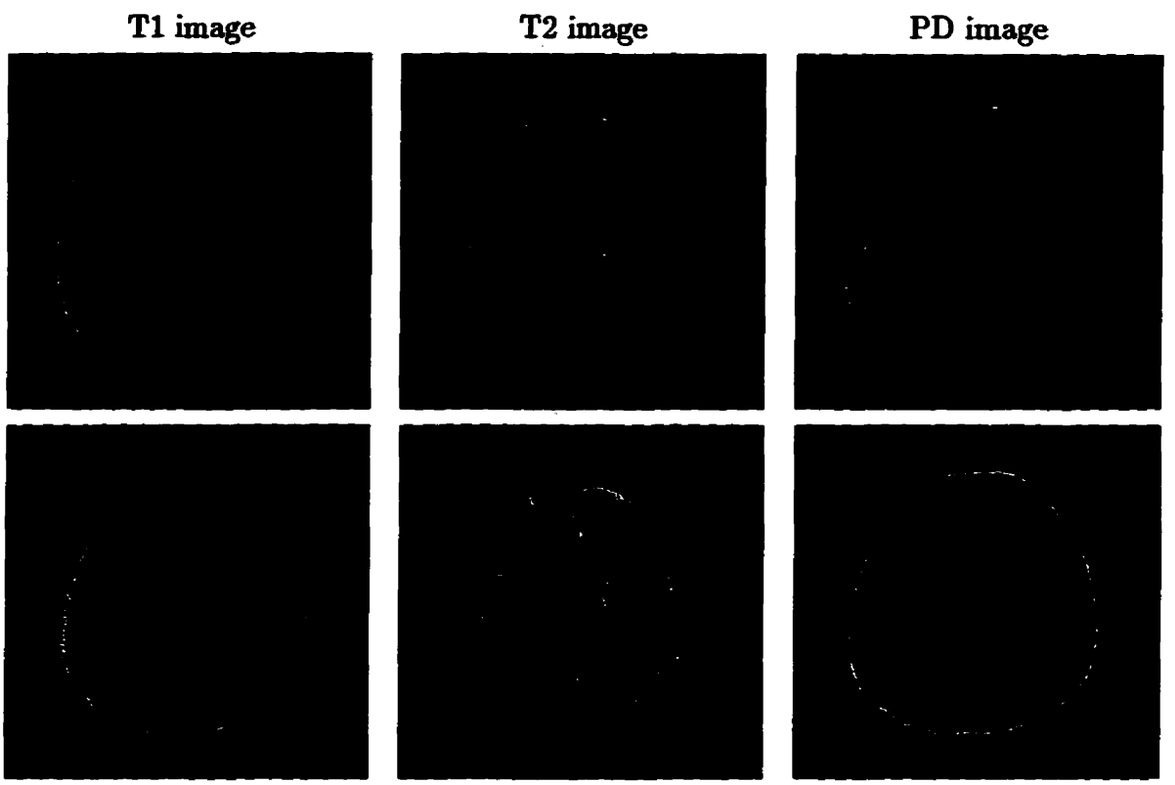

Figure 5.18: Images of a patient with malignant glioma

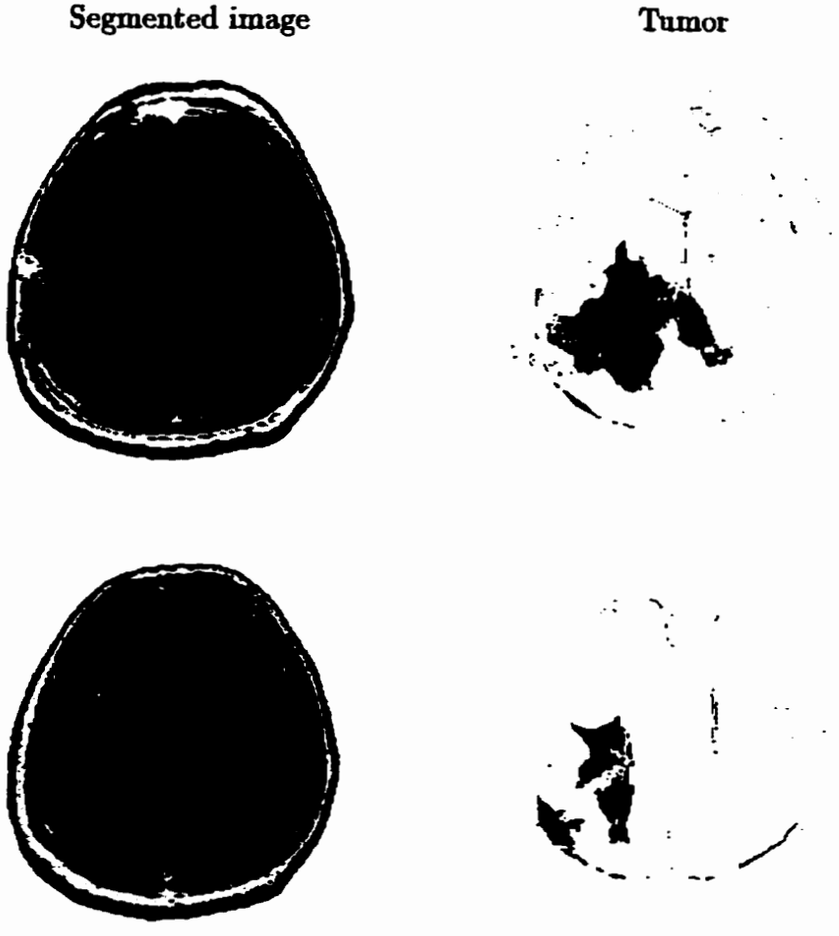

Figure 5.19: Segmentation results for a patient with a malignant glioma using LVQ

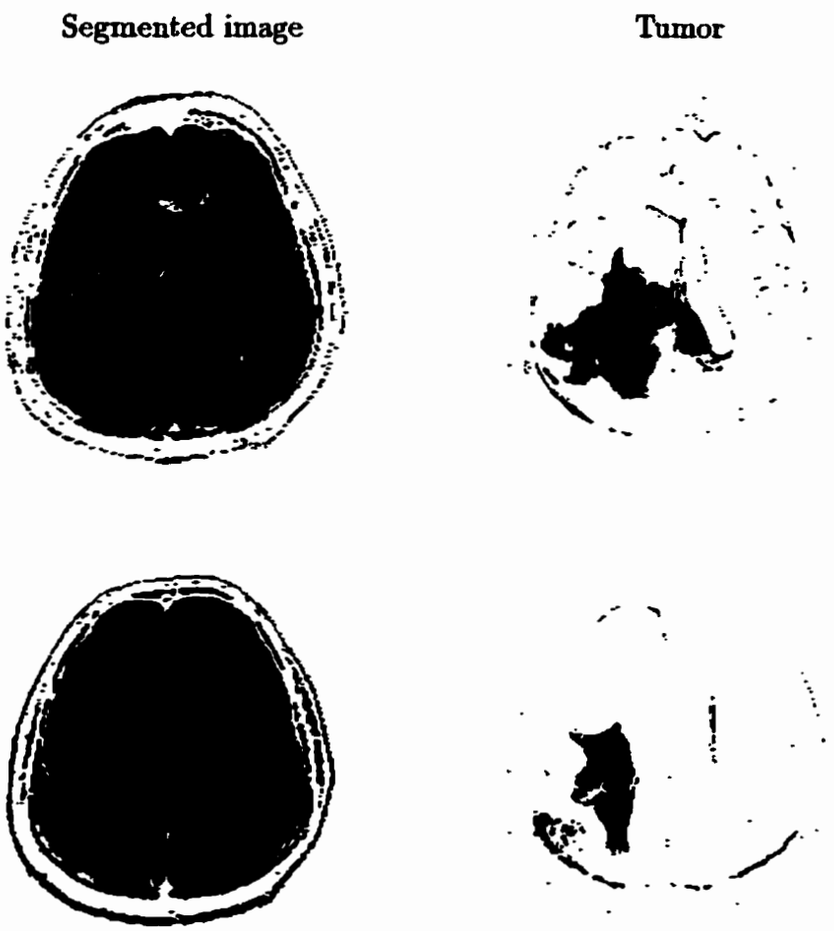

Figure 5.20: Segmentation results for a patient with a malignant glioma using backpropagation ANN

Chapter 6

Unsupervised Segmentation & SOFM Network

6.1 Introduction

Neural network models for pattern recognition can be specified as two types, supervised approaches and unsupervised approaches. The most famous unsupervised approaches are the self organizing feature maps (SOFM) developed by Kohonen [67], and adaptive resonance theory (ART) developed by Carpenter/Grossberg [15]). Systems such as SOFM and ART are based on biological studies of memory organization and dynamics. The ART system has only recently been extended to describe continuous valued input vectors, fuzzy ART, but studies indicate that replicable behavior of the system seems to be sensitive to the exact value of the parameters that need to be initialized to run the system [40]. It has been shown by several researchers [33], [13], [32], [80], [105], [77], [105], [97], [82], [120], [89],[98]. that the SOFM system of Kohonen is a strong candidate for continuous valued un-

supervised pattern recognition. Kohonen's self organizing feature maps use a linear update rule for the weights, which makes this model computationally attractive.

In this chapter the application of SOFM for fully automatic segmentation of MR images is considered. The SOFM network with an additional layer is designed for segmenting and clustering the regions of interest in the brain. To compare results obtained from this scheme with a traditional statistical pattern recognition method, the c-means algorithm is employed. The theoretical basis for each approach is introduced in the following sections.

6.2 Self organizing feature map

"One important organizing principle of sensory pathways in the brain is that the placement of neurons is orderly and often reflects some physical characteristic of the external stimulus being sensed [78]". For example, at each level of the auditory pathway, nerve cells and fibers are arranged anatomically in relation to the frequency which extracts the greatest response in each neuron. This tonotopic organization in the auditory pathway extends up to the auditory cortex [78], [60]. Although much of the low level organization is genetically pre-determined, it is likely that some of the organization at higher levels is created during learning by algorithms which promote self organization. Kohonen [67] presents one such algorithm which produces what he calls self organizing feature maps similar to those that occur in the brain. The algorithm will map a set of input vectors onto output vectors according to some characteristic feature of the input vectors. A brief discussion of this ordering behavior follows. More details can be found in the monograph by Kohonen [70].

The basic self organization feature mapping model consists of two layers. The

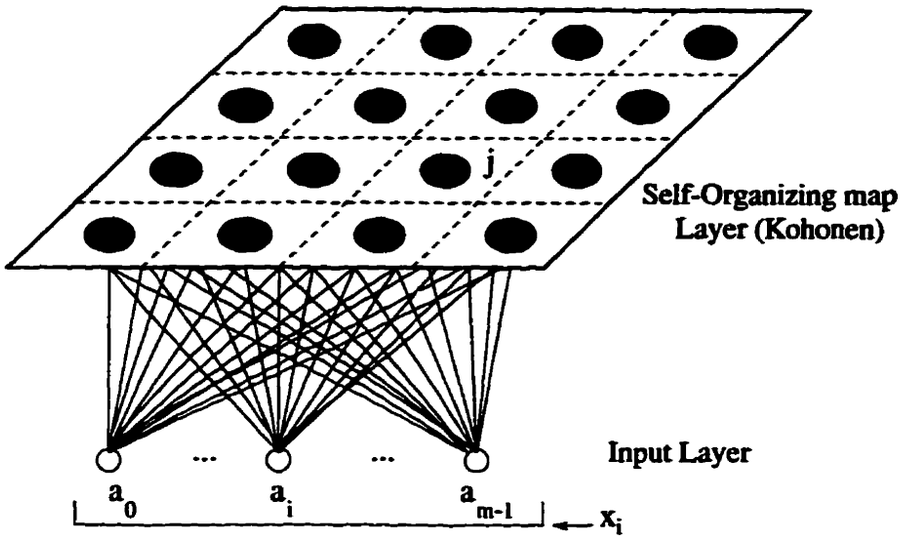

Figure 6.1: Two dimensional array of output nodes used to form feature maps.

first layer contains the input nodes and the second contains the output nodes. The output nodes are arranged in a two dimensional grid as shown in Fig. 6.1. Every input is connected extensively to every output node via adjustable weights.

Let $X = [x_0, x_1, ..., x_{N-1}]^T$ be a set of N inputs in $\Re^m$ such that each x_i has m dimensions (or features). Let m be the number of input nodes and M be the number of output nodes. Let $W_j = [w_{0j}, w_{1j}, ..., w_{(m-1)j}]^T$ denote the weights or *reference vectors*. W_j is the vector containing all of the weights from the m input nodes to output node j. After enough input vectors have been fed to the system, the weights will specify clusters or vector centers that sample the input space such that the point density function of the vector centers tends to approximate the probability density function of the input vectors [67].

Updating the weight for any given input in this model is done only for output units in a localized neighborhood. For each node j, there are NE neighbor nodes that depend on the topological neighborhood selected. A topological neighborhood

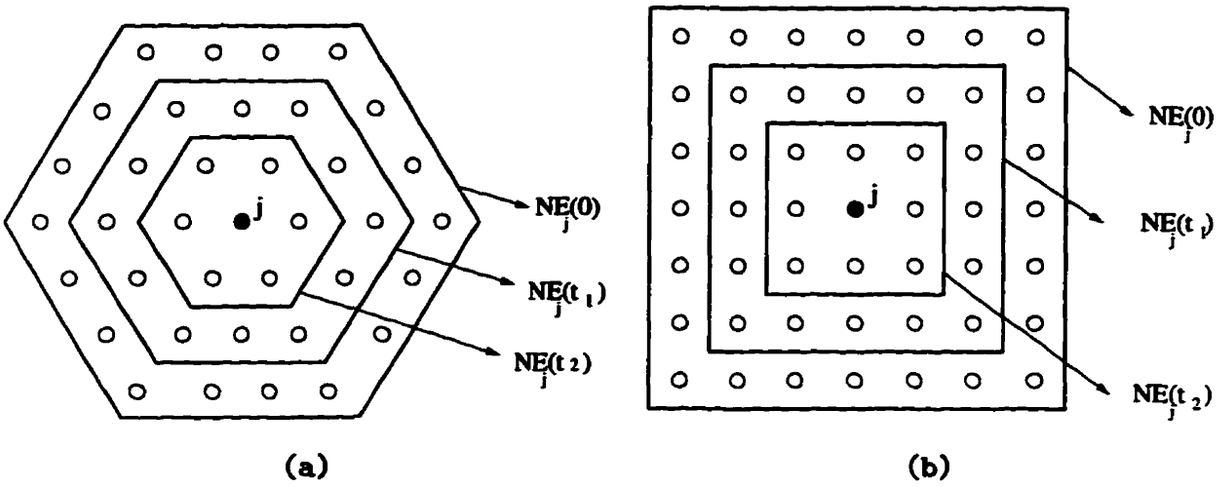

Figure 6.2: Topological neighborhoods at different times as feature maps are formed $(0 < t_1 < t_2)$.

consists of a rectangular, or a hexagonal array of points around the selected node [70]. Figure 6.2(a) and (b) show simple forms of neighborhood sets around node j. The neighborhood is centered on the output node whose distance d_{ij} is minimum. The measurement of d_{ij} is a Euclidean distance, defined as:

$$d_{ij} = \sum_{i=0}^{N-1} (x_i - w_{ij})^2 \tag{6.1}$$

where x_i is the input to node j and w_{ij} is the weight from input node i to output node j.

The neighborhood decreases in size with time until only a single node is inside its bounds. A learning rate is also required which decreases monotonically in time. Convergence to a cluster center will be controlled by the learning rate. As the learning rate decreases with more iterations, movement becomes restricted to smaller distances around the cluster center.

6.2.1 SOFM algorithm

The SOFM algorithm can be described as follows.

- Step1: **Initialize weights.** Randomly initialize weights from N inputs. Set the initial radius of the neighborhood NE.
- Step2: **Present new input**
- Step3: **Compute distance to all nodes**
- Step4: **Select output node with minimum distance.** Select node j^* as that output node with minimum distance d_j.
- Step 5: **Update weights to node j^* and neighbors.** Weights are updated for node j^* and all nodes in the neighborhood defined by $NE_j^*(t)$ following Eq. 6.2. W_j updates as follow,,

$$w_{ij}(t+1) = w_{ij}(t)+h_{ij}(t)(x_i-w_{ij}(t)) \quad \text{for } j \in NE_{j^*}, \quad 0 \leq i \leq N-1 \quad (6.2)$$

  the term h_{ij} is called the neighborhood Kernel and will be discussed later in section 6.2.2.

- Step 5:**if $NE \neq 0$ go back to step 2**

The basic idea behind the SOFM approach is to move the weights towards the center of clusters by updating the weights on each input value. To show this, let us consider a simple example with only one cluster and three inputs in 2 dimensional space (Figure 6.3).

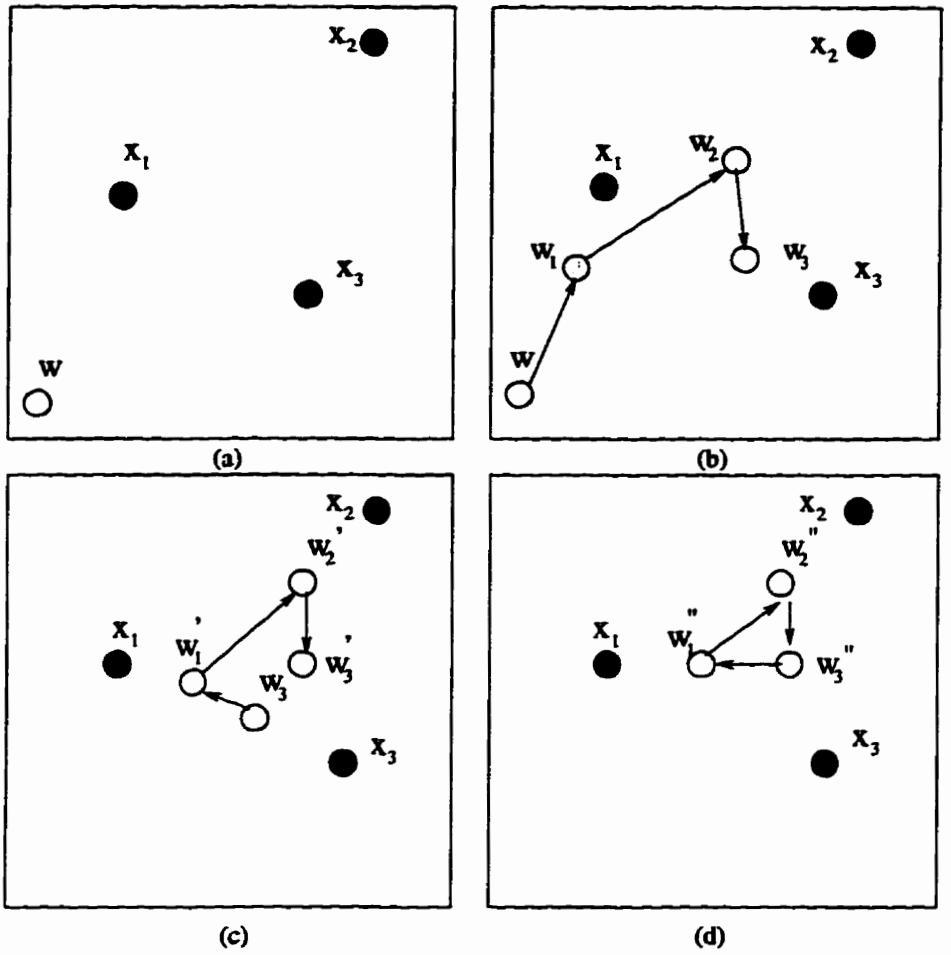

Figure 6.3: Weight movement in SOFM

The dark circles represent the position of input values x_1, x_2, and x_3. The gray circle represents a weight which starts at position w. Once the input x_1 is fed in, the weight is moved to position w_1. When x_2 is input to the net, the weight is moved to position w_2, and so on as shown in Figure 6.3(b). At the end of the iteration, the algorithm checks to see whether a weight has changed (within a tolerance) from the previous iterations or not. If there were no changes, then the last position of the weight will represent the center of the cluster; otherwise, the process will continue

as shown in Fig.6.3(c). Finally, the process will stop, as illustrated in Fig.6.3(d). The center of the cluster will be at the position of w_3^n

6.2.2 Neighborhood Kernel and learning parameters

The neighborhood Kernel h_{ij} is defined over the lattice points and has a very central role for a good feature mapping. Usually $h_{ij} = h(||r_i - r_j||, t)$, where $r_j \in \Re^2$ and $r_i \in \Re^2$ are the radius vectors of nodes j and i, respectively, in the array. With increasing $||r_i - r_j||$, $h_{ij} \to 0$. The average width and form of h_{ij} is important for convergence. In the literature, two simple choices for h_{ij} occur frequently. The simpler form was shown in Fig. 6.2, in which the neighborhood was defined as a set of array points around node j. Then, $h_{ij} = NE_j(t)$ which is decreasing in time monotonically. It can be seen that h_{ij} is acting as a learning rate factor $\alpha(t)$ $(0 \leq \alpha(t) \leq 1)$. Both $\alpha(t)$ and $NE_j(t)$ decrease in time during the ordering process.

Another widely applied neighborhood kernel can be written in terms of the Gaussian function,

$$h_{ij} = \alpha(t) \exp(-\frac{||r_i - r_j||^2}{2\sigma^2(t)}), \tag{6.3}$$

where $\alpha(t)$ is another scaler value, and the parameter $\sigma(t)$ defines the width of the kernel; the later corresponds to the radius of NE_j. Both $\alpha(t)$ and $\sigma(t)$ are some monotonically decreasing functions of time, and their exact forms are not critical. They could be selected as linear functions. Effective choices for these functions and their parameters have so far only been determined experimentally and will be presented in chapter 7.

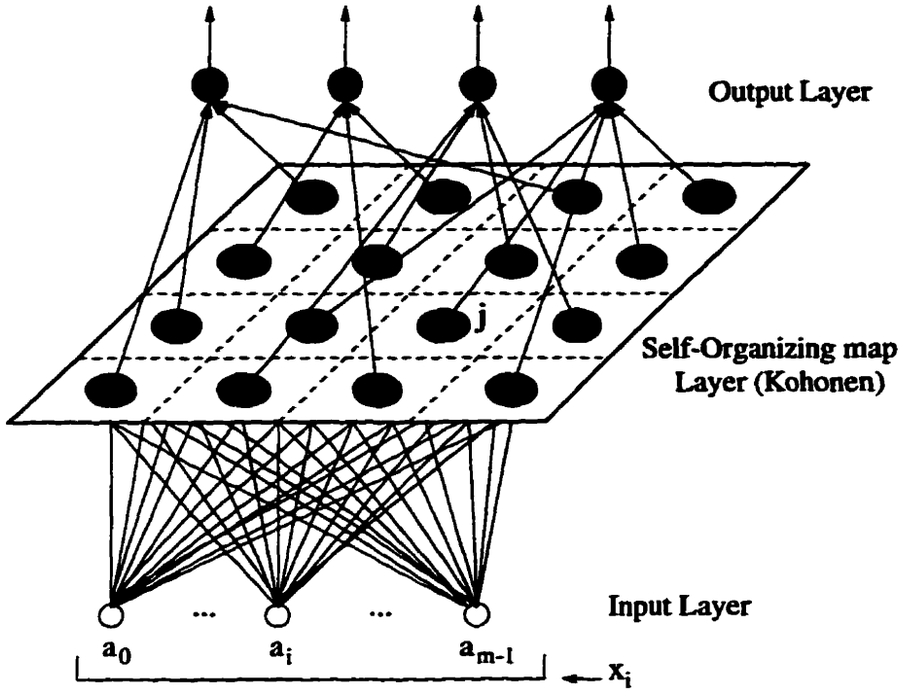

Figure 6.4: SOFM with an additional layer using Maximum likelihood training scheme

6.3 Feature map classification

In order to use the SOFM for clustering and classification we need to extend the network. One way of extending SOFM can be done by adding an associative layer, to the Kohonen layer as shown in Fig.6.4. This additional set of neurons does not participate in weight updating. After the self-organizing network terminates and weights are adjusted, the additional layer finds for each input the weight vector (prototype) closest to it and assigns the input to that class.

The mapping can be accomplished by using maximum likelihood training, a supervised learning scheme. A maximum likelihood approach suggests a simple training algorithm which consists of counting the best matching units in the map

corresponding to the training data. The output units are connected to the output nodes in the Kohonen layer corresponding to that class with greatest frequency of occurrence of training data. Usually the training data is small and for each class few representative are selected.

Another way of extending SOFM is adding an LVQ network at the end of SOFM. The cluster centers or codebooks that have been formed in an unsupervised learning manner using SOFM can be fine-tuned using LVQ. This way requires a much smaller number of samples and performs the classification task well. Figure 6.5 illustrates the topology of the network. This last method should be preferred due to the adaptive nature of classifier; however, results from both methods will be presented in the next chapter.

6.4 c-Means clustering technique

The c-Means algorithm [46] is a well-known clustering procedure, which groups a data set X into c clusters through the minimization of the total inter-clusters variances. In our case, data sets are pixel intensities from three image spectra. The most widely used objective function for clustering a data set X into c classes is the classical within-groups sum of squared error objective function, defined as:

$$J_1(U, v : X) = \sum_{k=1}^{n} \sum_{i=1}^{c} u_{ik} ||x_k - v_i||^2 \tag{6.4}$$

where $v = (v_1, v_2, ..., v_c)$ is a vector of (unknown) cluster centers (weights or prototypes), $v_i \in \Re^p$ for $1 \leq i \leq c$, and U is a hard or conventional c-partition of X. Optimal partitions U^* of X are taken from pairs (U^*, v^*) that are "local minimizers" of J_1. Generalization of 6.4 to the infinite family is called the c-means

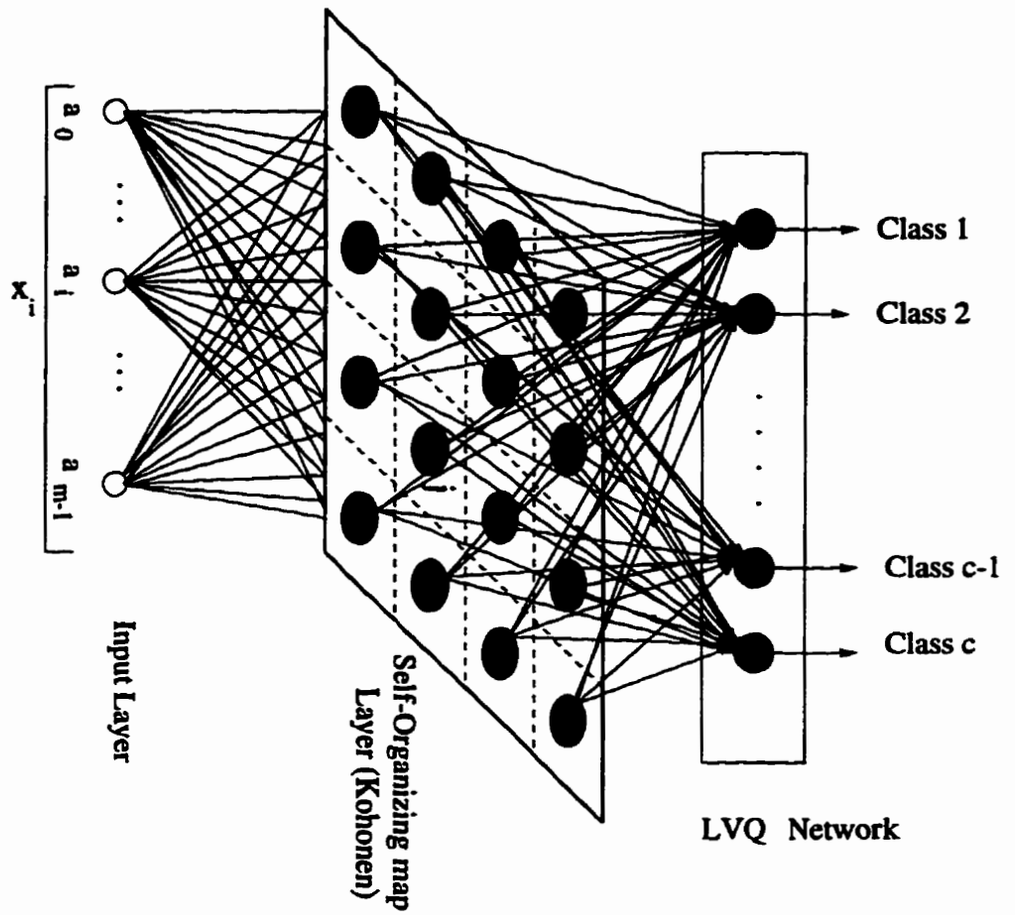

Figure 6.5: SOFM combined with LVQ for an adaptive patter classification.

functionals. Approximate optimization of $J1$ by the c-means algorithm is based on iteration through the following necessary conditions for its local extrema:

c-Means theorem [46]: U, V may minimize J_1 only if

$$u_{ik} = \begin{cases} 1, & ||x_k - v_i|| \leq ||x_k - v_j||, \quad j =, ..., c : j \neq i \\ 0, & otherwise \end{cases} \tag{6.5}$$

$$\text{for all} i, k, \quad 1 \leq i \leq c; 1 \leq k \leq n;$$

$$v_i = \frac{\sum_{k=1}^{n} u_{ik} x_k}{\sum_{k=1}^{n} u_{ik}}, \qquad 1 \leq i \leq c \tag{6.6}$$

c-Means produces a partition U that contains hard clusters, so each pixel will receive a unique class assignment from this method. A brief specification of the procedure is as follow

1. Given unlabeled data $X = \{x_1, x_2, ..., x_n\}$
2. Choose number of classes c and T, number of iteration
3. Compute all (c) weight vectors $\{v_{i,0}\}$ with equation 6.6, for $1 \leq i \leq c$
4. For t= 1, 2, ..., T.
   (a) compute $\{u_{ik,t}\}$ with equation 6.5 for $1 \leq k \leq n$;
   (b) Compute $E_t = ||U_t - U_{t-1}|| = \sqrt{(\sum_{i=1}^{c} \sum_{k=1}^{n} (u_{ik,t} - u_{ik,t-1})^2)}$;
   (c) If $E_t \leq \epsilon$ stop; else compute $\{v_{i,t}\}$ with Eq. 6.6 for the next t.

c-Means and fuzzy c-Means have been used by researchers for MR image segmentation [47],[73]. In this thesis we present results of segmentation using a c-Means algorithm for comparison with our scheme which utilizes SOFM.

6.5 Summary

In this chapter unsupervised techniques for classification and segmentation of MR images have been discussed. The theoretical issues of the SOFM artificial neural network were introduced and the network was designed. Two different schemes were introduced for extending the SOFM network for segmentation and classification.

The topology of the network and its detailed structure will be presented in the next chapter. A traditional unsupervised clustering technique, the c-Means algorithm, was introduced for the purpose of comparison.

The results of segmentation of MR images using each of these techniques will be given in chapter 7. Advantages and disadvantages of each technique will be discussed in chapter 7.

Chapter 7

Results of Unsupervised Techniques

7.1 Introduction

This chapter presents results from two approaches discussed in the chapter 6. The topology of the designed network and the learning parameters will be discussed. Advantages and disadvantages of each technique will be presented. Since the main objective of the segmentation process is to segment white matter, gray matter and CSF from the brain, the proposed automatic approach first strips away pixels of skull and scalp in acquired images. A novel algorithm extracts cerebrum from the head prior to segmentation. For an unsupervised segmentation scheme such preprocessing is needed to avoid too many clustering artifacts and to gain more accurate segmentation results.

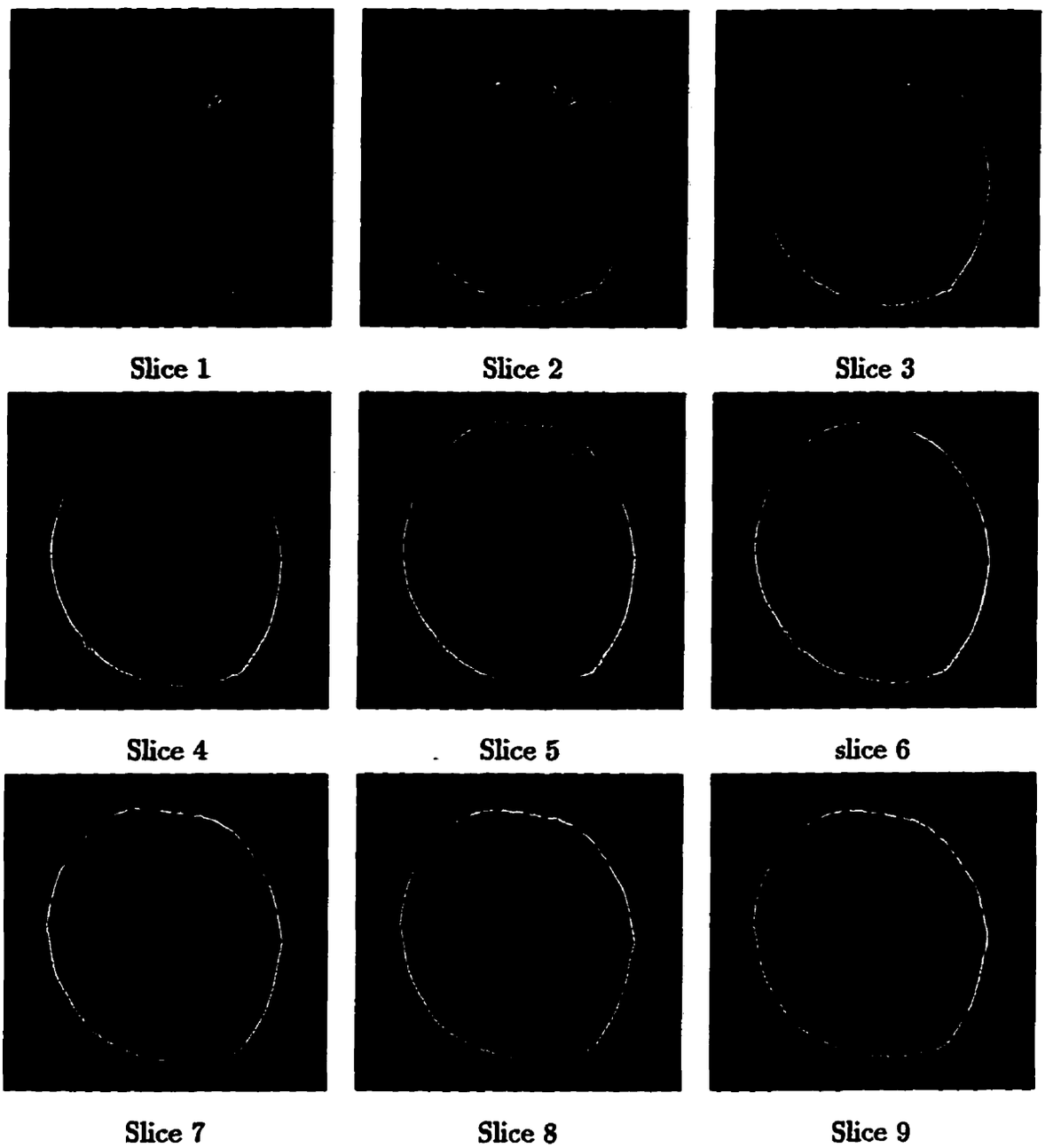

Figure 7.1: A set of nine T1 weighted images from a normal subject

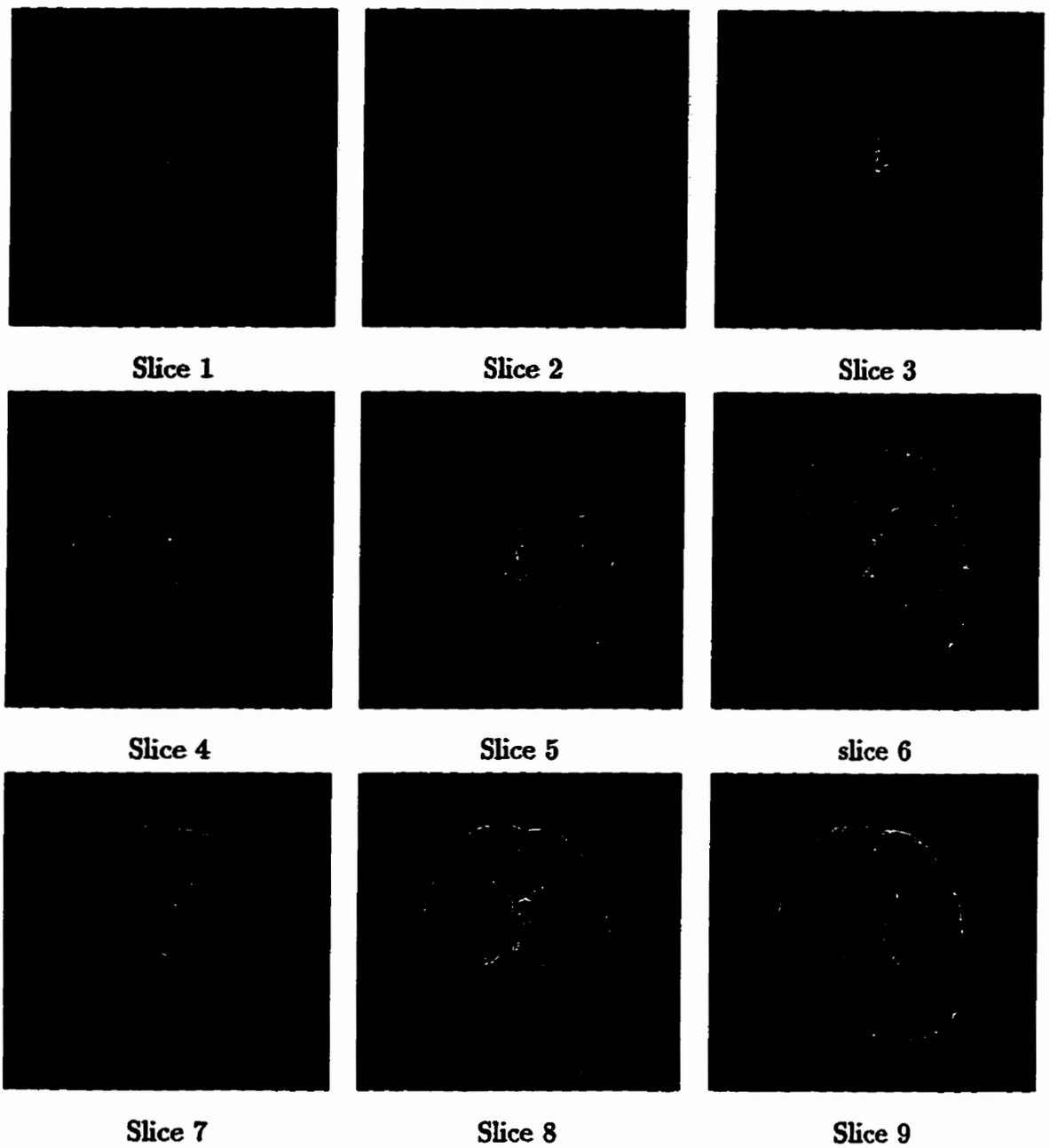

Figure 7.2: A set of nine T2 weighted images from a normal subject

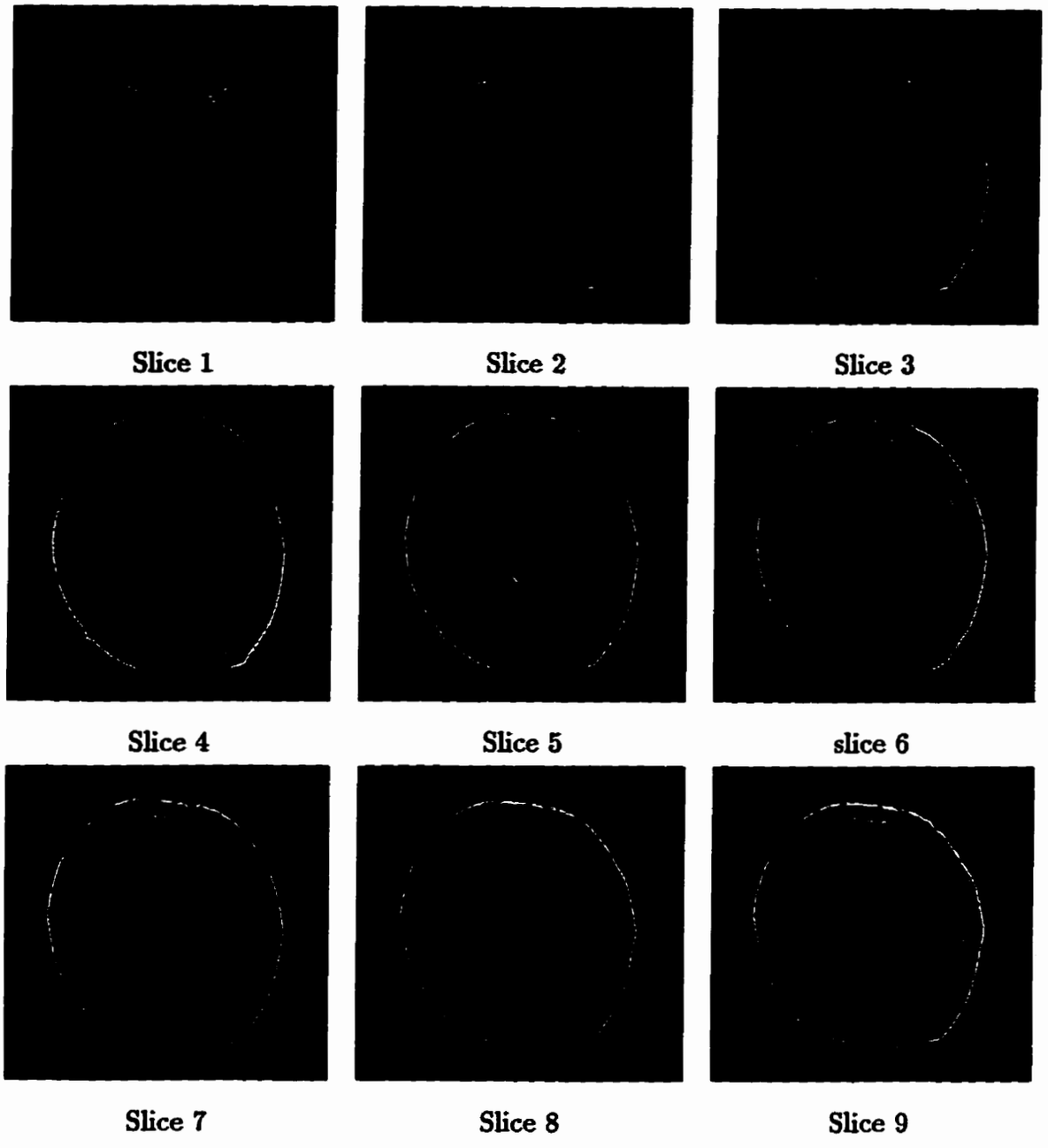

Figure 7.3: A set of nine PD weighted images from a normal subject

7.2 MR brain Images

Nine selected slices from the brain of a normal subject are illustrated in Fig. 7.1 The image slices are $5mm$ thick with no (zero) inter-slice space. The field of view was 22 cm for T1, T2 and PD weighted images. Three pulse sequences were used: TR/TE = 2800/30 ms for the PD-weighted images; for the T2 weighted images; TR/TE = 600/16 ms for the T1 weighted images. Results of segmentation will be shown for some of the representative images in this chapter.

7.3 Extracting the cerebrum

Extracting the cerebrum is performed by stripping away the skull and scalp pixels from the T2 images.

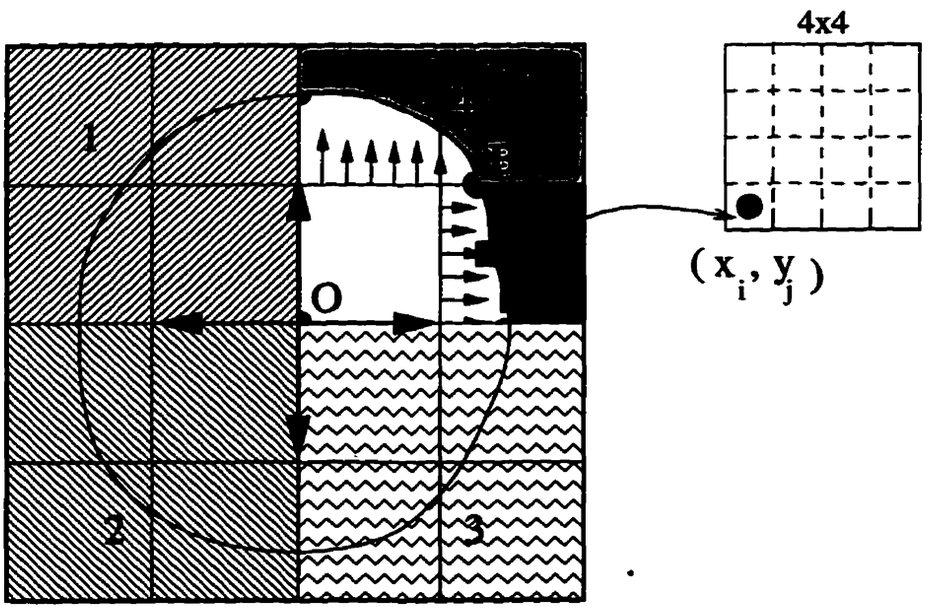

Figure 7.4: Different steps of extracting cerebrum from MR images of the head

The following algorithm describes the technique.

1. **Divide the image into four regions see (Fig. 7.4).**

2. **In region 4:**

   (a) **from the center of the T2 weighted image "o", (x_o, y_o), identify the pixel of bone or air, and background (x_i, y_j) by measuring the threshold of pixel value on each row from left to right . If the pixel value is less than 100, then check the neighborhood pixels in a box of 4x4 or (5x5) (see Fig7.4). If the majority of pixels in the box belong to class of bone then stop and assign (x_i, y_i) as a boundary pixel.**

   (b) **decrement o in the row, go to (a) repeat the process until point B is reached.**

   (c) **From the center of the T2 weighted image "o", (x_o, y_o), identify the pixel of bone or air, and background (x_k, y_l) by measuring the threshold of pixel value on each column from down to up. If the pixel value is less than 100, then check the neighborhood pixels in a box of 4x4 or (5x5) (see Fig7.4). If the majority of pixels in the box belong to the class bone then stop and assign (x_k, y_l)as a boundary pixel.**

   (d) **increment o in the column, go to (c) and repeat the process until point B is reached.**

3. **Process similarly regions 1, 2, and 3 by changing the direction of search:**

   - **in region 1; search right to left in row and down to up in column.**
   - **in region 2; search right to left in row and up to down in column.**
   - **in region 3; search left to right in row and up to down in column.**

By using the detected margin in this stage a mask image is generated to remove skull pixels from the T1 and PD weighted images. A typical example is shown in Fig. 7.5. Figures 7.5(a), (b), and (c) show the T1, T2, and PD weighted images respectively. Figure 7.5(d) shows how the algorithm strips the skull pixels from the T2 weighted image. Figure 7.5(e) shows the mask image. Figure 7.5(f), (g), and (h) show the extracted cerebrum from each image component. Figures 7.6, and 7.7 show the extracted cerebrum from slice 1 to slice 6 which were shown in Fig. 7.1.

7.4 Results of the SOFM network

The theoretical basis of SOFM was discussed in chapter 6. In this section only the network parameters and results of segmentation of MR images will be presented.

One of the parameters which has to be set for a good mapping is the form of the array. From several experiments the hexagonal lattice was chosen because it provided better results than the rectangular lattice. Other parameters were the type of neighborhood function and the map size. The size of map defines the number of codewords or reference vectors. Map sizes of 6×6, 8×8, 10×10, and 11×11 were tested. Results were improved slightly as the map size increased, however, no significant differences were observed when the size was increased from 10×10 to 11×11. Therefore, the size of 10×10 which consisted of 100 codewords was selected. The reference vectors of the map were first initialized randomly. The lattice type of the map and the neighborhood function used in the training procedures were also defined in the initialization. The map was trained by the self organizing feature map algorithm explained in chapter 6.

As discussed in chapter 6, the two different schemes , the Maximum likelihood

and the LVQ, were utilized to classify the map into the desired number of classes. Typical results from both approaches are shown in Figure 7.8. Several experiments showed that adding the LVQ network as an additional layer for feature map classification would produce better results because of the adaptive nature of the classifier. As can be seen in Figure 7.8, the Maximum likelihood layer tends to classify white matter tissue as gray matter.

When the LVQ was utilized in the output layer, training was done in two phases. The first was the ordering phase during which the reference vectors of the map units were ordered. During the second phase the values of the reference vectors were fine tuned. In the beginning the neighborhood radius was taken almost equal to the diameter of the map and was decreased to one during training, while the learning rate decreased to zero. During the second phase the reference vectors in each unit converge to their correct values. The second phase is usually much faster than the first. Figures 7.9, 7.10, and 7.11 show results obtained from this approach. The number of classes was equal to the number of target tissue classes. In each of the cases presented in this chapter the images were classified into four classes: background, CSF, white matter, and gray matter.

7.5 Results of c-means clustering algorithm

The c-means algorithm described in chapter 6 was used for unsupervised classification of MR brain images. The results of the c-means algorithm heavily depend on the number of iterations and classes. Typical results are shown in Figures 7.12, 7.13, and 7.14. To demonstrate how the c-means algorithm performs clustering, different numbers of classes were chosen. In Figure 7.12 results of segmentation are shown for $c = 4$ classes. The different class tissues are shown separately. Figures

7.13 and 7.14 show results for $c = 5$ and $c = 6$ classes respectively.

7.6 Discussion

As can be seen from the results, the c-means algorithm could not provide a reliable result for MR image segmentation. Although the basic theory of the c-means algorithm is similar to the SOFM, two major differences exist; 1) in the SOFM algorithm, each entry (i.e. vector x) is used to update the winning class and its neighboring classes, while in the c-means algorithm each input vector is classified and only the winning class is modified during each iteration. 2) in the SOFM the weights represent the number of reference vectors which are normally several fold of the number of classes, while in the c-means algorithm the number of classes is predetermined as a constant value into the algorithm.

One can claim that if the number "c" in the c-means algorithm is chosen to be the same as the number of codewords in the SOFM, similar results might be achieved when the clusters are merged to the number of desired classes at the end. However, some important issues have to be considered such as computational time, validation, efficiency and complexity of the technique.

Results from the c-means algorithm are discussed below. As shown in Fig. 7.12, for $c = 4$, the algorithm tends to segment the image into 3 tissue classes. Figure 7.12(a) shows white matter and gray matter mixed together as one class, while CSF in Figure 7.12(b), and (c) is classified into 2 tissue classes.

For $c = 5$, the algorithm tends to segment the image into 4 tissue classes, Figure 7.13(a) shows white matter and gray matter mixed together as one class, while part of the gray matter is classified as a separate class in the Figure 7.13(b). The CSF

is classified into 2 tissue classes as in in Fig. 7.13(c),(d).

For $c = 6$, the algorithm tends to segment the image into 5 tissue classes. Although in figure 7.14 results seem to be encouraging, none of the segmented regions are correct. The white matter is classified into one class (Fig. 7.14(a)), while the gray matter and the CSF are each classified into two tissue classes (Fig. 7.14(b),(c) and 7.14(d),(e) respectively). The first class of gray matter is correct while the second class of the gray matter is composed of the gray matter and CSF. An attempt was made to merge the 5 classes to 3 classes, however, similar results were obtained as shown in Figure 7.12. Therefore, it can be concluded that merging classes does not promise improvement of segmentation process.

There are number of important properties which make the SOFM suitable for use as a codebook generator for clustering scheme. They can be summarized as follows:

- The set of reference vectors are a good approximation to the original input space.
- The reference vectors are topologically ordered in the feature map such that the correlation between the reference vectors increases as the distance between them decreases.
- The density of the feature map corresponds to the density of the input distribution so that regions with a higher probability density have better resolution than areas with a lower density.

In summary, this chapter has shown the ability of a new technique for fully automated segmentation of MR images. The characteristics of this artificial neural network scheme which include a massively parallel structure, a high degree of

interconnection and the ability to self organize – parallel many of the characteristics of human visual system. That is why it is a valuable technique for MR image segmentation.

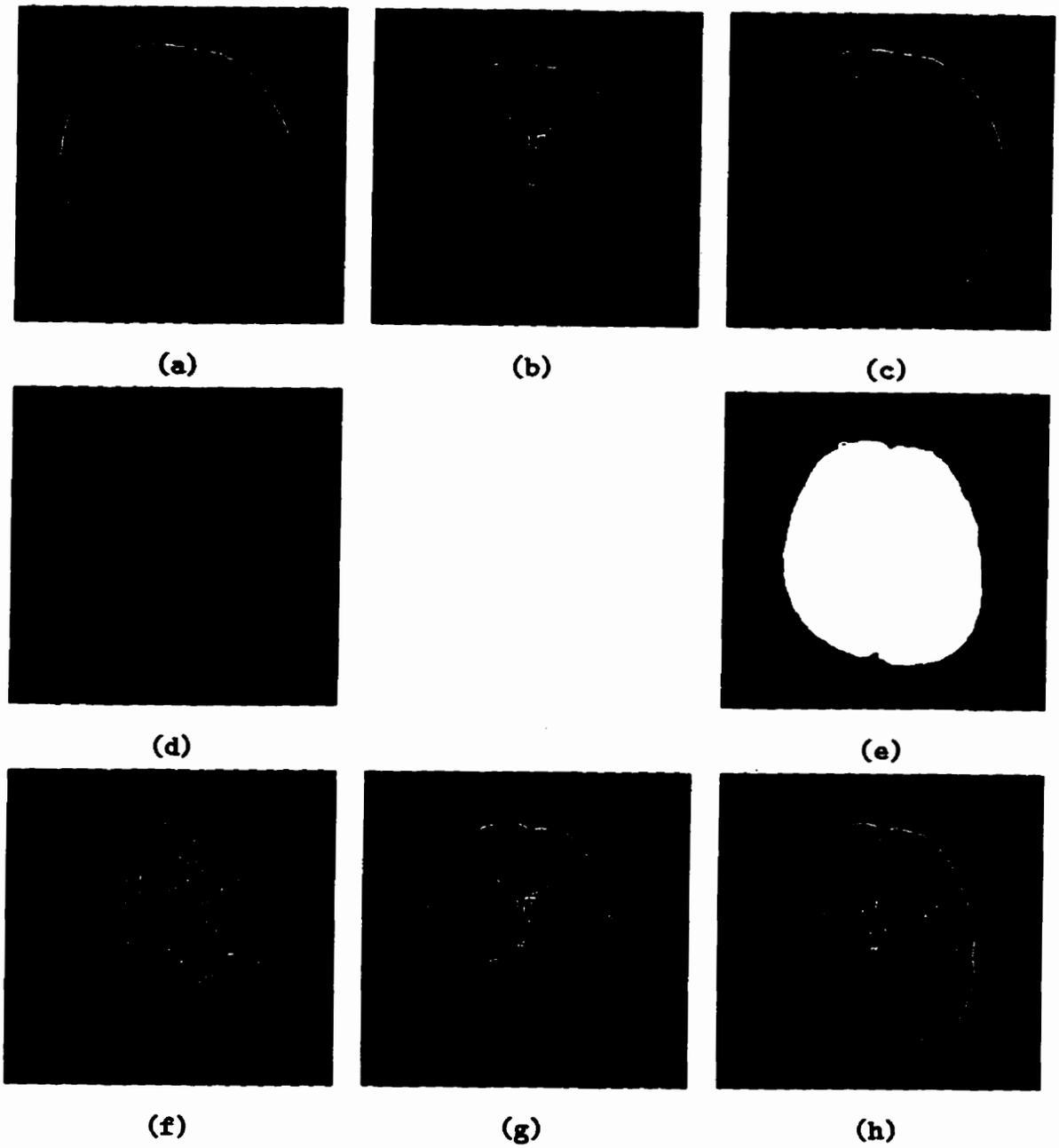

Figure 7.5: (a) T1 weighted image,(b) T2 weighted image, (c)PD weighted image , (d) Stripped T2 image, (e) Mask image, (f) Cerebrum extracted from T1, (g) Cerebrum from T2 and (h) Cerebrum from PD image.

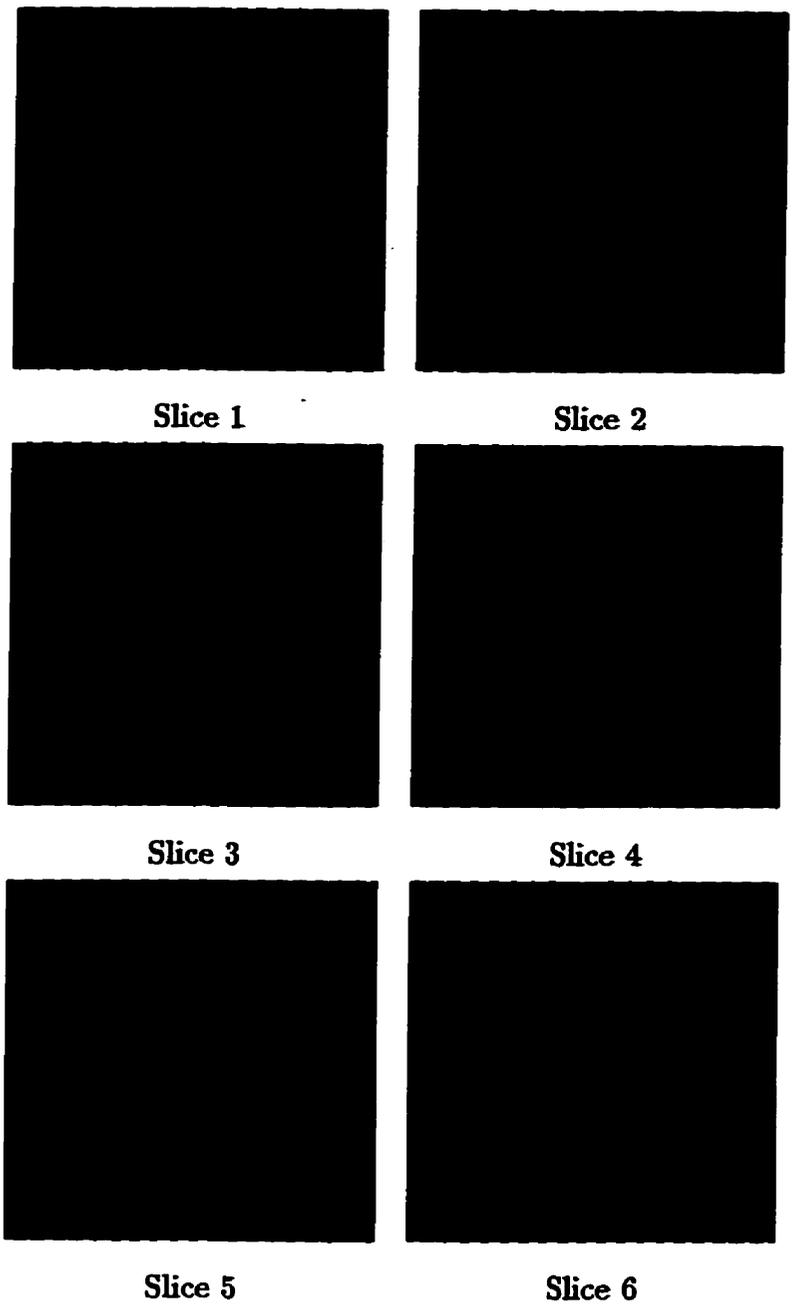

Figure 7.6: Extracting cerebrum from MR images of the head

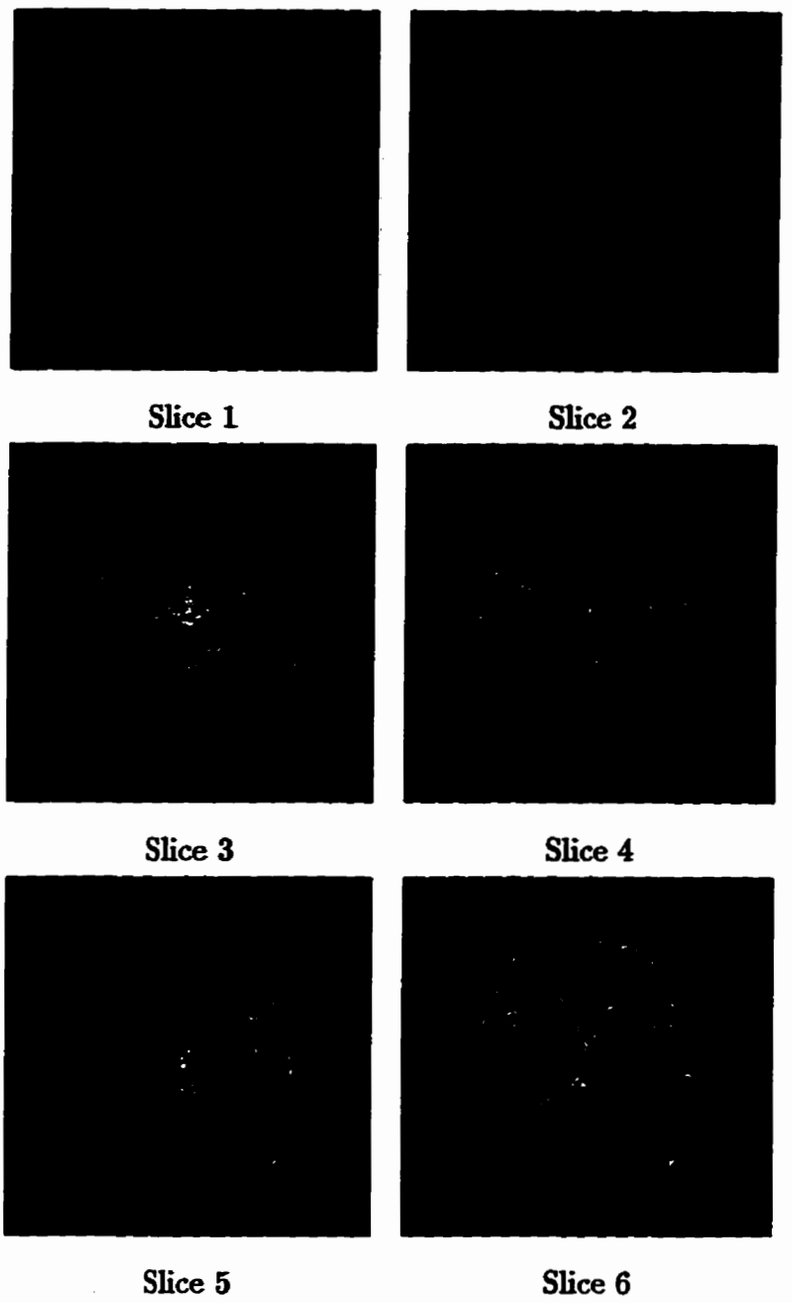

Figure 7.7: Extracting cerebrum from MR images of the head

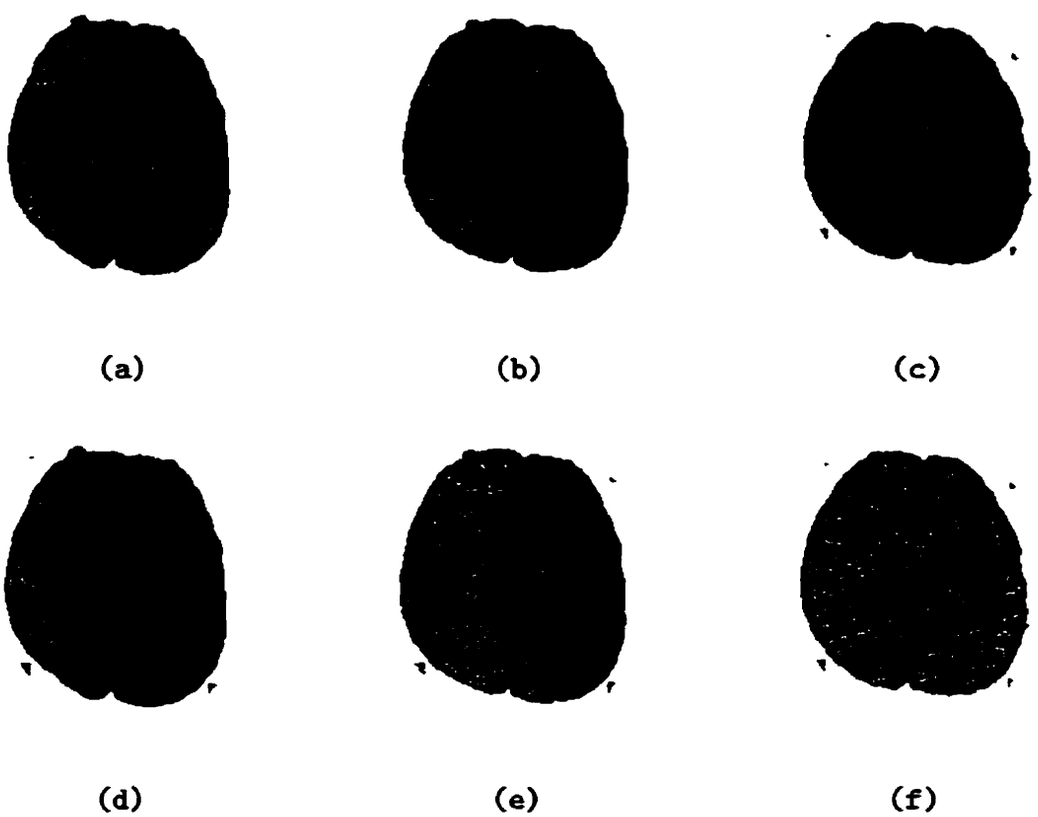

Figure 7.8: Results of segmentation using two different feature map classifiers. Figures (a), (b), and (c) show results of LVQ classifier and Figures (d), (e), and (f) show results from Maximum likelihood classifier

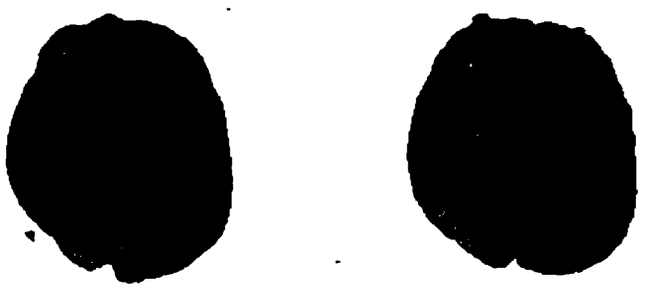

Segmentation of slice 1 Segmentation of slice 2

Segmentation of slice 3 Segmentation of slice 4

Segmentation of slice 5 Segmentation of slice 6

Figure 7.9: Typical results using SOFM and LVQ as feature map classifier

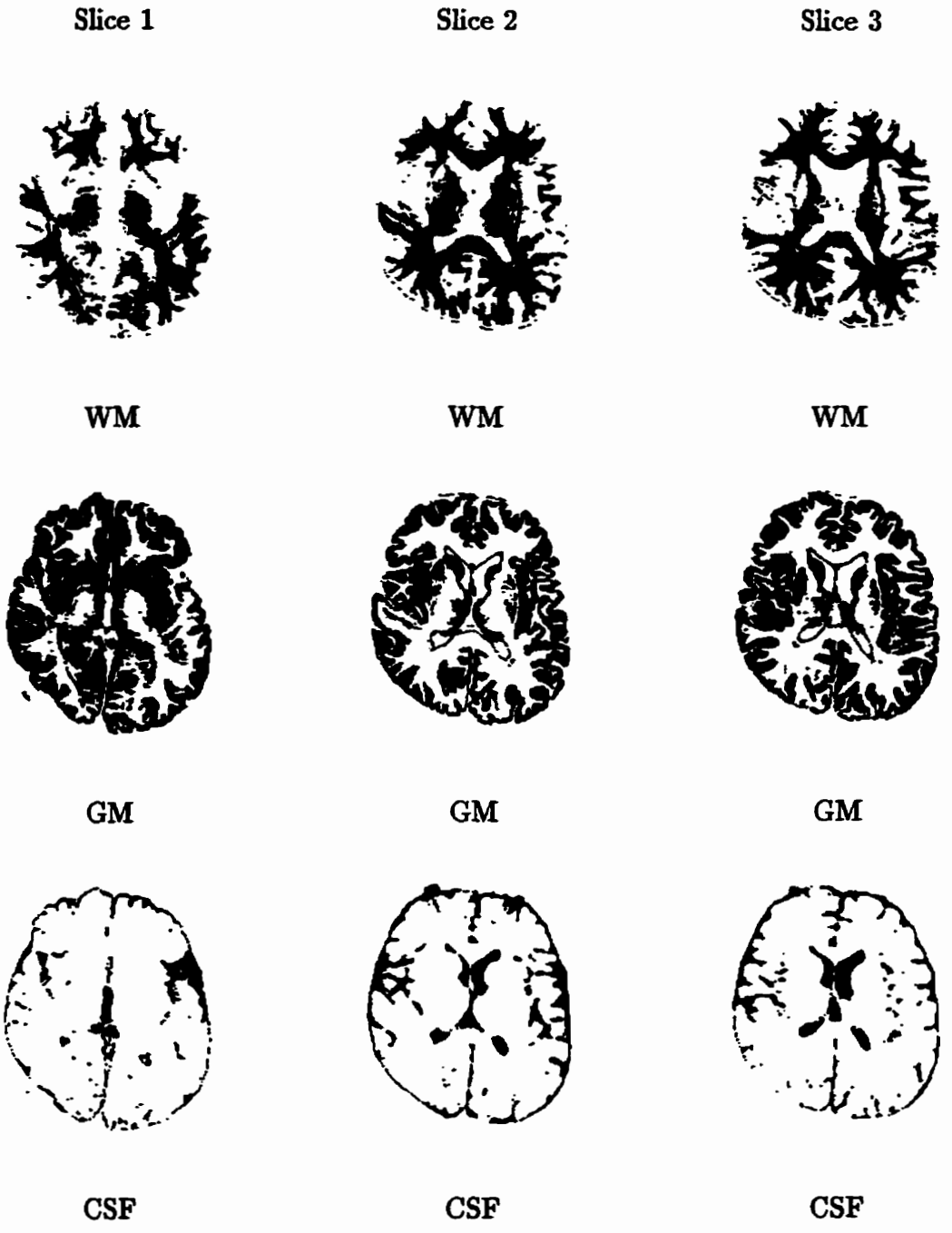

Figure 7.10: Segmentation of images using SOFM. Three tissues: Gray matter (GM), White matter (WM), and CSF are separated

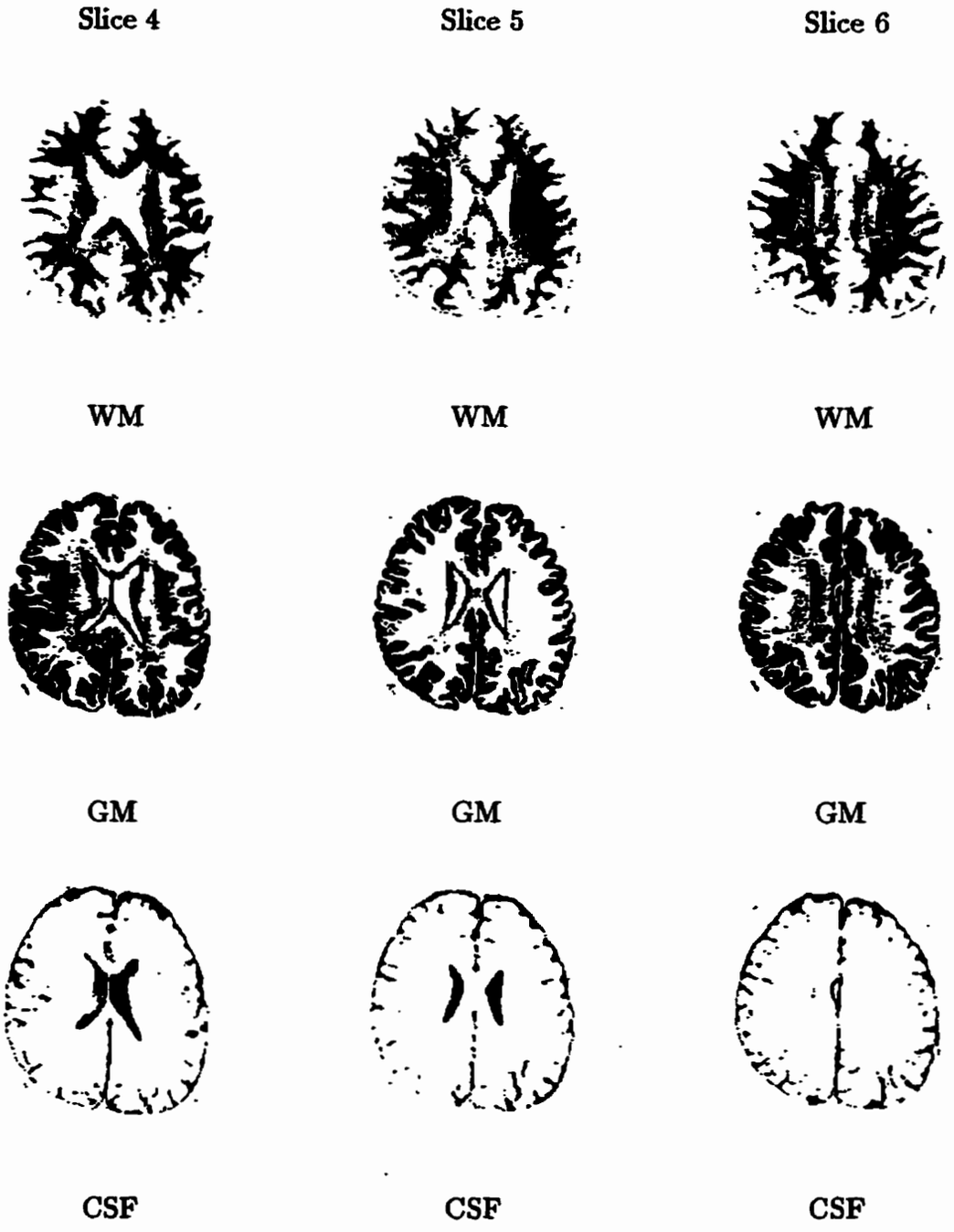

Figure 7.11: Segmentation of images using SOFM. Three tissues: Gray matter (GM), White matter (WM), and CSF are separated

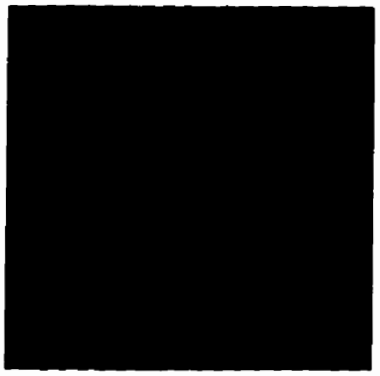

Segmented image

(a)

(b)

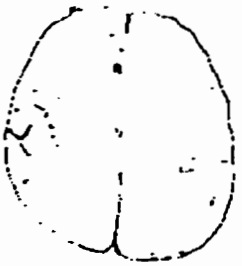

(c)

Figure 7.12: Segmentation of an image using c-Means algorithm. Number of classes, $c = 4$, each class is shown separately (except background)

Segmented image

(a)

(b)

(c)

(d)

Figure 7.13: Segmentation of an image using c-Means algorithm. Number of classes, $c = 5$, each class is shown separately (except background)

Segmented image

(a)

(b)

(c)

(d)

(e)

Figure 7.14: Segmentation of an image using c-Means algorithm. Number of classes, $c = 6$, each class is shown separately (except background)

Chapter 8

Conclusions and Future Directions

This thesis has generated very reliable and interesting results for segmentation of MR brain images. These have been summarized in detail at the end of each of the two testing chapters, chapter 5 and 7. In here, a summary of the major results and their contribution to the research literature are presented.

8.1 Summary of the results

Supervised Segmentation Schemes

- The Maximum likelihood technique was not an acceptable choice since it appeared to be very susceptible to the choice of training data. For reliable results, training data may need to be chosen slice by slice for even one patient which is extremely time consuming and tedious. Further more, techniques that must assume an underlying statistical distribution of the data such as MLC do not appear promising, since tissue regions of interest do not usually obey the distribution tendencies of probability density functions.

- Backpropagation neural networks, on the other hand, were very sensitive to the training data. Their results suffer from noise and mis-classification. Backpropagation neural networks provided adequate brain segmentations when the training data were selected very specifically. If backpropagation networks are to be used for segmentation of MR images, reliance on operator intervention to select good training data for each tissue and each slice of data was crucial. Another weakness of backpropagation networks was the indeterminate number of hidden units. The convergence of networks was dramatically dependent on these numbers, and in most cases it was too difficult to find the optimum number of the hidden units.

- The LVQ technique was sensitive to the selection of the number of codewords, however, changing the number was not too crucial for acceptable results. Selecting a large set of codewords could increase the mis-classification around the border of regions of interest. Also, LVQ was used in an adaptive manner to update the codewords from one image slice to another. That new approach caused LVQ, unlike backpropagation ANN and MLC, not to be sensitive to the variations of gray-level for each tissue type between different slices.

Unsupervised segmentation schemes

- In our new method for automatic tissue segmentation SOFM was utilized to construct an unsupervised clustering scheme. It was further extended by adding a layer to the Kohonen layer to accomplish the classification task. As described previously a novel approach for extracting cerebrum from MR images was introduced and its positive impact on the segmentation of MR images was demonstrated. The simplicity of the method should make it an at-

tractive pre-processing algorithm for automatic or semi-automatic MR image analysis systems. There are two important advantages of the unsupervised procedure. First, the process is completely automatic and there is no need for human interaction. Second, the automated parameter learning is fully reproducible because subjective variations created by selecting different types of training areas are avoided.

8.2 Contributions

- Designed and implemented supervised image segmentation scheme

  VQ has been used mostly in the literature for image coding and compression purposes. Using analogy under VQ design had lead us to implement the VQ in a neural network scheme which is learning vector quantization (LVQ). Implementing LVQ for segmentation of MR images is a novel idea and it has not been tackled by any other researchers in this field. The results of this study were presented in [5], [6].

- In most cases where supervised classification schemes are utilized, training and testing are chosen from the same subject. In this research we developed a new system which utilizes universal training data for classification task. This has been accomplished by using an adaptive training scheme to update the weights in the LVQ network.

- We have presented a modified version of the self organizing feature maps of Kohonen which are capable of generating continuous valued outputs. Extending the output layer by an additional layer allows the network to classify the two dimensional feature maps to a desired number of classes.

- For the first time in the literature extracting cerebrum from the images of the head was performed in this study as a preprocessing step prior to the segmentation. The novel algorithm described in chapter 7, improved the segmentation results significantly when an unsupervised scheme was utilized. Reducing the clustering artifacts made results more accurate, and the post-processing step was avoided.

8.3 Future directions

- The quantitative assessment of performance is complicated by the lack of a gold standard to compare with. However, a receiving operator characteristic (ROC) curve can provide a qualitative evaluation. However, it will take considerable time and substantial assistance from expert radiologists.

- Unsupervised methods need better ways to specify and adjust the number of tissue classes found by the algorithm. Since unsupervised classification techniques are sensitive to good initialization, initialization is an important issue which should be considered in future research direction.

- The Euclidean distance was used in LVQ and SOFM. It would be interesting to compare the use of Euclidean distance versus Mahalanobis distance for each of these two techniques.

- The two new approaches designed and implemented in this thesis can be used for the segmentation of other multispectral images, for example, satellite images obtained with a multispectral scanner.

Bibliography

[1] I. Agartz, J. Saaf, L. O. Vahlund, and L. Wetterberg. Quntitative estimations of cerebrospinal fluid spaces and brain regions in healthy controls using computer assisted tissue classification of magnetic resonance images: Relation to age and sex. *Magn. Reson. Imaging*, 10:217–226, 1992.

[2] J. M. Agris, R. deFigueiredo, G. R. Hillman, and T. A. Kent. A novel method for 3-D segmentation and volume estimation of brain compartments from MRI. *Annual International Conference of the IEEE Engineering in Medicine and Biology Society*, 13(1):68–70, 1991.

[3] S. C. Ahalt, A. K. Krishnamurthy, P. Chen, and D. E. Melton. Competitive learning algorithms for vector quantization. *Neural Networks*, 3:277–290, 1990.

[4] A. Alaux and P. A. Rick. Multispectral analysis of magnetic resonance images: A comparison between supervised and unsupervised classification techniques. In *the International Symposium on Tissue Characterization in MR imaging*, pages 165–169, 1990.

[5] J. Alirezaie, M. E. Jernigan, and C. Nahmias. Neural network based segmentation of magnetic resonance images of the brain. In *Nuclear Science*

Symposium and Medical Imaging Conference. 1995 IEEE Conference record, volume 3, pages 1260–1265, 1995.

[6] J. Alirezaie, C. Nahmias, and M. E. Jernigan. Multi-spectral magnetic resonance image segmentation using lvq neural networks. In *Proceeding of Int. Conf. on System, Man and Cybernetic*, volume 2, pages 1665–1670, Oct. 1995.

[7] S.C. Amartur, D. Piraino, and Y. Takefuji. Optimization neural networks for the segmentation of magnetic resonance images. *IEEE Transactions on Medical Imaging*, 11(2):215–220, June 1992.

[8] M. Ashtari, J. L. Zito, B. I. Gold, J. A. Lieberman, and P.G. Herman. Computerized volume measurement of brain structire. *Invest Rad*, 25:798–805, 1990.

[9] M. B. and M. Riemer. 3-D segmentation of MR images of the head for 3-D display. *IEEE Transactions on Medical Imaging*, 9(2):177–183, June 1990.

[10] A. M. Bensaid and L. O. Hall. MRI segmentation using supervised and unsupervised methods. *Annual International Conference of the IEEE Engineering in Medicine and Biology Society*, 13(1):60–61, 1991.

[11] J. C. Bezdek. Integration and generalization of LVQ and c-means clustering. In *SPIE Vol. 1826, Intelligent Robots and Computer Vision XI: Biological, Neural Net, and 3-D Methods*, pages 280–299, 1992.

[12] J. C. Bezdek, L. O. Hall, and L. P. Clarke. Review of MR image segmentation techniques using pattern recognition. *Med. Phys.*, 20(4):1033–1048, Jul/Aug 1993.

[13] J. C. Bezdek, E. C. Tsao, and N. R. Pal. Fuzzy kohonen clustering networks. In *Proceedings of the first IEEE conference on Fuzzy Systems*, pages 1035–1043, NJ, 1992.

[14] W. Bondareff, J. Raval, B. Woo, D. L. Hauser, and P. M. Colletti. Magnetic resonance imaging and the severity of dementia in older adults. *Arch. Gen. Psychiatry*, 47:47–51, Jan. 1990.

[15] G. Carpenter and S. Grossberg. A massively parallel architecture for a self-organizing neural pattern recognition machine. *Computer Vision, Graphics, and Image Processing*, 37:54–115, 1987.

[16] V. S. Caviness, P. A. Filipek, and D. N. Kennedy. Magnetic resonance technology in human brain science: Blueprint for a program based upon morphometry. *Brain & Development*, 11(1):1–13, 1989.

[17] H. S. Choi and Y. Kim. Partial volume tissue classification of multichannel magnetic resonance images- a mixel mode. *IEEE Transactions on Medical Imaging*, 10(3):395–407, September 1991.

[18] M. C. Clark, L. O. Hall, D. B. Goldgof, L. P. Clarke, R. P. Velthuizen, and M. S. Silbiger. MRI segmentation using fuzzy clustering techniques. *IEEE Engineering in Medicine and Biology*, pages 730–742, Dec. 1994.

[19] L. P. Clarke, A. M. Bensaid, L. O. Hall, J. C. Bezdek, and M. L. Silbiger. MRI segmentation: Supervised, unsupervised and semi-supervised methods. In *Book of abstracts Eleventh annual Scientific Meeting, Society of Magnetic Resonance in Medicine*, volume 2, page 4213. Berlin, Germany, August 1992.

[20] L. P. Clarke, R. P. Velthuizen, M. A. Camacho, J. J. Heine, M. Vaidyanathan, L. O. Hall, R. W. Thatcher, and M. L. Silbiger. MRI segmentation: Methods and applications. *Magnetic Resonance Imaging*, 13(3):343–368, 1995.

[21] L. P. Clarke, R. P. Velthuizen, S. Phuphanich, J. D. Schellenberg, J. A. Arrington, and M. Silbiger. MRI: Stability of three supervised segmentation techniques. *Magnetic Resonance Imaging*, 11:95–106, 1993.

[22] H. E. Cline, C. L. Dumoulin, H. R. Hart, W.E. Lorensen, and S. Ludke. 3D reconstruction of the brain from magnetic resonance images using a connectivity algorithm. *J. Magn. Reson. Imaging*, 5:345–352, 1987.

[23] H. E. Cline, W. E. Lorensen, R. Kikinis, and F. Jolesz. Three-dimensional segmentation of MR images of the head using probability and connectivity. *Journal of Computer Assisted Tomography*, 14(6):1037–1045, November/December 1990.

[24] P. C. Cosman and R. M. Gray. Using vector quantization for image processing. *Proceedings of the IEEE*, 81(9):1325–1341, September 1993.

[25] B. M. Dawant, M. Ozkan, A. Zijdenbos, and R. Margolin. A computer envirnonment for 2D and 3D quantitation of MR images using neural networks. *Annual International Conference of the IEEE Engineering in Medicine and Biology Society*, 13(1):64–65, 1991.

[26] B. M. Dawant, Alex P. Zijdenbos, and Richard A. Margolin. Correction of intensity variations in MR images for computer-aided tissue classification. *IEEE Transactions on Medical Imaging*, 12(4):770–781, December 1993.

[27] A. Duchon and S. Katagiri. A minimum-distortion segmentation/ lvq hybrid algorithm for speech recognition. *J. Acoust. Soc. Japan (E)*, 14(1):37–42, 1993.

[28] R. Duda and P. Hart. *Pattern Classification and Scene Analysis.* Wiley, NY, 1973.

[29] E.J. Dudewicz, G. C. Levy, M. J. Rao, and F. W. Wehrli. Advanced statistical methods for tissue characteristics. *Magnetic Resonance Imaging*, 2:1988, 1988.

[30] R. R. Edelman and S. Warach. Magnetic resonance imaging (first of two parts). *the New England Journal of Medicine*, 328:708–716, March 1993.

[31] H.H. Ehricke. Problem and approaches for tissue segmentation in 3D MR imaging. In *Medical Imaging 1990: Image Processing. Proceedings SPIE*, volume 1233, pages 128–137. 1990.

[32] E. Erwin, K. Obermayer, and K. Schulten. Self-organizing maps: ordering, convergence properties and energy functions. *Biological Cybernetics*, 67:47–55, 1992.

[33] F. Favata and R. Walker. A study of the application of kohonen-type neural networks to the travelling salesman problem. *Biological Cybernetics*, 64:463–468, 1991.

[34] P.A. Filipek and D.N. Kennedy. Magnetic resonance imaging: Its role in the developmental disorders. In D. Gray and D. Duane, editors, *The Reading Brain: The Bilological Basis of Dyslexia*, pages 133–160. York Press, Parkton, Maryland, 1991.

[35] P.A. Filipek, D.N. Kennedy, V.S. Caviness, and P.A. Starewics. MRI-based morphometry: Development and application to normal controls. *Annals of Neurology*, 25:61–67, 1989.

[36] P.A. Filipek, C. Richelme, D.N. Kennedy, J. Rademacher, D.A. Pitcher, S. Zidel, and V.S. Caviness. Morphometric analysis of the brain in developmental language disorders and autism. *Annals of Neurology*, 32(3):475, September 1992.

[37] S. R. Fleagle, W. Stanford, T. L. Burns, and D. J. Skorton. Feasibility of quantitative texture analysis of cardiac magnetic resonance imagery: Preliminary results. In *Medical Imaging 1994: Image Processing. Proceedings SPIE*, volume 2168, pages 23–32. 1994.

[38] S. R. Fleagle, D. R. Thedens, W. Standford, R. I. Pettigrew, N. Reichek, and D. J. Skorton. A multicenter trial of automated border detection in cardiac magnetic resonance imaging. In *Book of abstracts Eleventh annual Scientific Meeting, Society of Magnetic Resonance in Medicine*, volume 2, page 4226. Berlin, Germany, August 1992.

[39] L. M. Fletcher, J. B. Barsotti, and J. P. Hornak. A multispectral analysis of brain tissues. *Magn. Reson. Med.*, 29:623–630, 1993.

[40] J. A. Freeman and D. M. Skapura. *Neural Networks, Algorithms, Applications, and Programming Techniques.* Addison-Wesley Publishing Company, 1991.

[41] G. Gerig, J. Martin, R. Kikinis, and F. A. Jolesz. Automatic segmentation of dual-echo MR head data. *Information Processing in Medical Imaging*, 511:175–185, July 1991.

[42] J. Ghosh, S. Chakravarthy, Y. Shin, and J. Whiteley. Adaptive kernel classifiers for short-duration oceanic signals. In *IEEE Conf. on Neural Networks for Ocean Engineering*, pages 41–48, 1991.

[43] M. Goldbach, W. Menhardt, and J. Stevens. Multispectral tissue characterization in magnetic resonance imaging using bayesian estimation and markov random fields. *Annual International Conference of the IEEE Engineering in Medicine and Biology Society*, 13(1):62–63, 1991.

[44] R. C. Gonzalez and C. Woods. *Digital Image Processing.* Addison-Wesley Publishing Company, 1992.

[45] R. M. Gray. Vector quantization. *IEEE ASSP Magazine*, 1(2):4–29, 1984.

[46] R. M. Gray and Y. Linde. Vector quantization and predictive quantizer for gauss-markov sources. *IEEE Transactions on Communications*, 30:381–389, 1982.

[47] L. O. Hall, A. M. Bensaid, R. P. Velthuizen L. P. Clarke, M. S. Silbiger, and J. C. Bezdek. A comparison of neural network and fuzzy clustering techniques in segmenting magnetic resonance images of the brain. *IEEE Transactions on Neural Networks*, 3(2):672–682, September 1992.

[48] R. M. Haralick and L. G. Shapiro. Survey image segmentation techniques. *Computer Vision, Graphics, and Image Processing*, 29:100–132, 1985.

[49] R. O. Harger. Object detection in clutter with learning maps. In *SPIE- the Int. Soc. for Optical Engineering*, volume 1630, pages 76–86, 1992.

[50] C. A. Harlow and R. W. Conners. Image analysis segmentation methods. In K.S. Fu and T. Pavlidis, editors, *Biomedical Pattern Recognition and Image Processing*, pages 111–130. Verlag Chemie GmbH, Weinheim, 1979.

[51] E. Herskovits. A hybrid classifier for automated radiological diagnosis: preliminary results and clinical applications. *Computer Methods Programs in Biomed*, 32(1):746–749, May 1990.

[52] T. J. Hyman and J. D. Shoop. Characterization of normal brain tissue using seven calculated MRI parameters and a statistical analysis system. *Magnetic Resonance in Medicine*, 11:22–34, 1989.

[53] Peggy Israel and Frank R. Parris. A modified LVQ2 neural network classifier whose performance rivals classical methods for pattern classification. In *Proceedings of the World Congress on Neural Networks*, pages III–445–448, Hillsdale, New Jersey, 1993. INNS, Lawrence Erlbaum Associates.

[54] E. F. Jackson, P. A. Narayana, J. S. Wolinsky, and Timothy J. Doyle. Accuracy and reproducibility in volumetric analysis of multiple sclerosis lesions. *Journal of Computer Assisted Tomography*, 17(2):200–205, March/April 1993.

[55] A. Jain and R. Dubes. *Algorithms that Cluster Data.* Prentice Hall, Englewood Cliffs, 1988.

[56] T. L. Jernigan, G. A. Press, and J. R. Hesselink. Methods for measuring brain morphologic features on magnetic resonance imaging. *Arch Neurol*, 47:27–32, January 1990.

[57] M. Joliot and B. M. Mazoyer. Three-dimensional segmentation and interpolation of magnetic resonance brain images. *IEEE Transactions on Medical Imaging*, 9(2):269–227, June 1993.

[58] M. Jungke, W. V. Seelen, G. Bielke, S. Meindi, G. Krone, M. Grigat, P. Higer, and P. Pfannenstiel. Information processing in nuclear magnetic resonance imaging. *Magnetic Resonance Imaging*, 6(6):683–693, 1988.

[59] M. Just and M. Thelen. Tissue characterization with t1, t2 and proton density values: Results in 160 patients with brain tumors. *Radiology*, 169:779–785, 1988.

[60] E. R. Kandel and J. H. Schwartz. *Principles of Neural Sciences.* Elsevier, New York, 1985.

[61] Y. Kao, J. A. Sorenson, M. M. Bahn, and S. S. Winkler. Dual-echo MRI segmentation using vector decomposition and probability techniques: A two tissue model. *Magn. Reson. Med.*, 32:342–357, 1994.

[62] D. N. Kennedy, J. W. Belliveau, J. Rademacher, B.R. Buchbinder, P. A. Filipek, B. R. Rosen, and V. S. Caviness. Anatomic variability of primary visual cortex. In *Proceedings of the Society of Magnetic Resonance Imaging*, volume 10, page 203, 1991.

[63] D. N. Kennedy and V. S. Caviness. Anatomic segmentation and volumetric calculations in nuclear magnetic resonance imaging. *IEEE Transactions on Medical Imaging*, 8(1):1–7, March 1989.

[64] R. Kikinis, M. E. Shenton, and G. Gerig. Routine quantitative analysis of brain and cerebrospinal fluid spaces with MR imaging. *J. Magn. Reson. Imaging*, 2:619–629, 1992.

[65] M. I. Kohn, R. C. Gur, and G. T. Herman. Analysis of brain and cerebrospinal fluid volumes with MR imaging. *Radiology*, 178(1):115–122, 1991.

[66] T. Kohonen. An introduction to neural computing. *Neural Networks*, 1:3–16, 1988.

[67] T. Kohonen. *Self-Organization and Associative Memory.* Springer-Verlarg, 1989.

[68] T. Kohonen. Improved versions of learning vector quantization. In *IEEE International Conference on Neural Networks (ICNN)*, volume 1, pages 545–550, 1990.

[69] T. Kohonen. The self-organizing map. *Proceedings of the IEEE*, 78(9):1464–1480, 1990.

[70] T. Kohonen. *Self-Organizing maps.* Springer-Verlarg, Berlin, 1995.

[71] T. Kohonen, G. Barna, and R. Chrisley. Statistical pattern recognition with neural networks: Benchmarking studies. In *IEEE International Conference on Neural Networks (ICNN)*, volume 1, pages 61–68, July 1988.

[72] S. Lehar, A. J. Worth, and D. N. Kennedy. Application of the boundary contour/feature countour system to magnetic resonance brain scan imagery. In *Proceedings of the International joint Conference on Neural Networks*, volume 1, pages 435–440, San Diego, June 1990.

[73] C. Li, D. B. Goldgof, and L. O. Hall. Knowledge-based classification and tissue labeling of MR images of human brain. *IEEE Transactions on Medical Imaging*, 12(4):740–750, September 1991.

[74] Z. Liang. Tissue classification and segmentation of MR images. *IEEE Engineering in Medicine and Biology*, 12(1):81–85, March 1993.

[75] Z. Liang, J. R. MacFall, and D. P. Harrington. Parameter estimation and tissue segmentation from multispectral MR images. *IEEE Transactions on Medical Imaging*, 13(3):441–449, September 1994.

[76] Z. Liang, D. Wang, J. Ye, and D.Harri ngton. Development of automatic technique for segmentation of brain tissues from multispectral MR images. In *Nuclear Science Symposium and Medical Imaging Conference. 1994 IEEE Conference record*, volume 3, pages 1453–1456, 1995.

[77] W. Lin, E. C. Tsao, and C. Chen. Constraint satisfaction neural networks for image segmentation. *Pattern Recognition*, 25(7):679–693, 1992.

[78] R. P. Lippmann. An introduction to computing with neural nets'. *IEEE ASSP Magazine*, pages 4–22, 1987.

[79] A. Lundervold and G. Storvik. Segmentation of brain parenchyma and cerebrospinal fluid in multispectral magnetic resonance images. *IEEE Transactions on Medical Imaging*, 14(2):339–349, June 1995.

[80] J. Mao and A. K. Jain. A self-organizing network for hyperellipsoidal clustering (hec). *IEEE Transactions on Neural Networks*, 7(1):16–29, January 1996.

[81] D. Marr. *Vision A Computational Investigation into the Human Representation and Processing of Visual Information.* W.H. Freeman and Company, New York, 1982.

[82] J. D. Mc Auliffe, L. E. Atlas, and C. Rivere. A comparison of the LBG algorithm and kohonen neuarl network paradigm for image vector quantization. In *Proc. IEEE Int. Conf. Acoust. Speech, and Signal Process*, pages 2293–2296, Alburquerqe, NM, April 1990.

[83] K. J. McClain and J. D. Hazel. MR image selection for segmentation of the brain. *J. Magn. Resonance Imaging*, 4(p):88, 1994.

[84] G. F. McLean. Vector quantization for texture classification. *IEEE Transactions on Systems, Man, and Cybernetics*, 23(3):637–649, May 1993.

[85] J. J. Merelo, M. A. Andrade, C. Urena, and F. Moran. Application of vector quantization algorithms to protein classification and secondary structure computation. In A. Prieto, editor, *International Workshop Artificial Neural Networks IWANN'91*, pages 415–421. Spinger-Verlag, New York, 1991.

[86] D. J. Michael and A. C. Nelson. Handx: A model-based system for automatic segmentation of bones from digital hand radiographs. *IEEE Transactions on Medical Imaging*, 8(1):64–69, March 1989.

[87] J.R. Mitchel, S. J. Karlik, D. H. Lee, and A. Fenster. Automated detection and quantification of multiple sclerosis lesions in MR volumes of the brain. In *Book of abstracts Eleventh annual Scientific Meeting, Society of Magnetic Resonance in Medicine*, volume 2, page 4211. Berlin, Germany, August 1992.

[88] J. R. Mitchell, S. J. Karlik, D. H. Lee, and A. Fenster. Computer-assisted identification and quantification of multiple sclerosis lesions in MR imaging volumes in the brain. *J. Magn. Reson. Imaging*, 4:197–208, 1994.

[89] N. M. Nasrabadi and Y. Feng. Vector quantization of images based upon a neural-network clustering algorithm. In *SPIE Visual Communications and Image Processing'88*, volume 1001, pages 207–213, 1988.

[90] E. K. Neumann, D. A. Wheeler, A. S. Bernstein, and J. C. Hall. Artificial neural network classification of drosphila courtship song mutants. *Biological Cybernetics*, 66(6):485–496, 1992.

[91] H. Neumann and K. Ottenberg. Estimating attributes of smooth signal transitions from scale-space. In *Proceedings of IEEE Int. Conf. on Pattern Recognition (ICPR)*, pages 754–758, Netherlands, August 1992.

[92] M.A. Oghabian and A.T. Pokperek. Registration of brain images by a multi resolution sequential method. *Information Processing in Medical Imaging*, 511:165–174, July 1991.

[93] J. R. Orlando, R. Mann, and S. Haykin. Classification of sea-ice images using a dual-polarized radar. *IEEE Journal of Oceanic Engineering*, 15(3):228–237, 1990.

[94] D. A. Ortendhal, N. M. Hylton, and L. Kaufman nad L. E. Crooks. Tissue characterization using intrinsic NMR parameters and a hierarchical processing algorithm. *IEEE Transactions on Nuclear Science*, 32(1):875–879, Feb. 1985.

[95] M. Ozkan and R. J. Maciunas. Neural network based segmentation of multimodal medical images: A comparative and prospective study. *IEEE Transactions on Medical Imaging*, 12(3):534–544, September 1993.

[96] M. Ozkan, H. G. Sprenkels, and B. M. Dawant. Multi-spectral rosonace image segmentation using neural networks. *proc. IJCNN 90 SanDiago*, 1:429–437, June 1990.

[97] N. R. Pal, J. C. Bezdak, and E. C. K. Tsao. Generalized clustring networks and kohonen's self-organizing scheme. *IEEE Transactions on Neural Networks*, 4(4):549–557, July 1993.

[98] T. N. Pappas. An adaptive clustering algorithm for image segmentation. *IEEE Transactions on Signal Processing*, 40(4):901–914, 1992.

[99] J. Parkkinen, G. Cohen, M. Sonka, and N. Andreasen. Segmentation of MR brain images. *Annual International Conference of the IEEE Engineering in Medicine and Biology Society*, 13(1):71–72, 1991.

[100] L. C. Partain, R. R. Price, J. J. Erickson, J. A. Patton, and A. E. James. Nuclear magnetic resonance,. In C. M. Coulman and *et. al.*, editors, *The Physical Basis of Medical Imaging*, pages 213–229. Prentice Hall, 1981.

[101] C. A. Pellizari, K. K. Tan, D. N. Levin, G. T. Y. Chen, and J. Balter. Interactive 3D patient-image registration. *Information Processing in Medical Imaging*, 511:132–141, July 1991.

[102] R. R. Price, W. H. Stephens, and C. L. Partain. NMR physical principles. In C. M. Coulman and *et. al.*, editors, *The Physical Basis of Medical Imaging*, pages 213–229. Prentice Hall, 1981.

[103] Photon Treatment Planning Collaboration Working Group PTPCWG. Three dimensional display in planning radiation therapy: A clinical prospective. *International Journal of Radiation Oncology, Biology*, 21(1):79–89, May 1991.

[104] S. Prasad Raya. Low-level segmentation of 3-D magnetic resonance brain images- a rule-based system. *IEEE Transactions on Medical Imaging*, 9(3):327–337, September 1990.

[105] H. Ritter and K. Schulten. Extending kohonen's self-organizing mapping algorithm to learn ballistic movements. In R. Eckmiller and C. V. Malsburg, editors, *NATO ASI Series*, pages 393–406. Spriger Verlag Berlin Heidelberg, 1988.

[106] L. R. Schad, S. Bluml, and I. Zuna. MR tissue chatacterization of intracranial tumors by means of texture analysis. *Magnetic Resonance Imaging*, 11:889–896, 1993.

[107] L. D. Schertz, M. W. Vannier, M. H. Gado, and R. L. Butterfield. Statistical assessment of MR image classification techniques. In *the Seventh Annual IEEE/EMBS Conference*, pages 585–592, 1985.

[108] A. Simmons, G. J. Barker, P. S. Tofts, and S. R. Arridge. Improvements to dual-echo clustering of neuroanatomy in MRI. In *Book of abstracts Eleventh annual Scientific Meeting, Society of Magnetic Resonance in Medicine*, volume 2, page 4202. Berlin, Germany, August 1992.

[109] P. K. Simpson. *Artificial Neural Systems.* Pergamon Press, 1990.

[110] J. W. Snell and M. B. Merickel. Tissue labelling of MRI using recurrent artificial neural networks. *Annual International Conference of the IEEE Engineering in Medicine and Biology Society*, 13(1):66–67, 1991.

[111] W. Snyder, A. Logenthiran, P. Santago, K. Link, G. Bilbro, and S. Rajala. Segmentation of magnetic resonance images using mean field annealing. In *Information Processing in Medical imageing, Prodeedings , 12th International Conference, IPMI'91*, pages 218–226, UK, July 1991. Wye.

[112] H. Soltanian-Zadeh and J. P. Windham. Mathematical basis of eignimage filtering. letter to the editor. *Magn. Reson. Med.*, 31:465–466, 1994.

[113] H. Soltanian-Zadeh, J. P. Windham, and D. J. Peck. MRI feature extraction using a linear transformation. In *Medical Imaging 1993: Image Processing. Proceedings SPIE*, volume 1898, pages 487–500. 1993.

[114] H. Soltanian-Zadeh, J. P. Windham, D. J. Peck, and A. E. Yagle. A comparative analysis of several transformations for enhancement and segmentation of magnetic resonance image scene sequences. *IEEE Transactions on Medical Imaging*, 11(3):302–318, September 1992.

[115] H. S. Stiehl. 3-D image understanding in radiology. *IEEE Engineering in Medicine and Biology*, 9(4):24–28, December 1990.

[116] H. Suzuki and J. Toriwaki. Automatic segmentation of head MRI images by knowledge guided thresholding. *Computerized Medical Imaging and Graphics*, 15(4):233–240, 1991.

[117] T. Taxt and A. Lundervold. Multispectral analysis of the brain using magnetic resonance imaging. *IEEE Engineering in Medicine and Biology*, 13(3):470–481, Sept. 1994.

[118] T. Taxt, A. Lundervold, B. Fuglaas, H. Lien, and V. Abeler. Multispectral analysis of uterine corpus tumors in magnetic resonance imaging. *Magnetic Resonance in Medicine*, 23:55–76, 1992.

[119] J. T. Tou and R. C. Gonzalez. *Pattern Recognition Principles.* Addison-Wesley Publishing Company, 1974.

[120] K. K. Truong. Multilayer kohonen image coddbooks with a logarithmic search complexity. In *Proceedings of IEEE Int. Conf. Acoust. Speech, and Signal Process*, pages 2789–2792, Toronto, Canada, May 1991.

[121] M. W. Vannier, R. L. Butterfield, D. L. Rickman, and P. R. Bionetti. Multispectral magnetic resonance image analysis. *Critical Reviews in Biomedical Engineering*, 15(2):117–141, 1987.

[122] M. W. Vannier, M. Gado, and R. L. Butterfield. Multispectral analysis of magnetic resonance images. *Radiology*, 154(1):221–224, 1985.

[123] M. W. Vannier, T. K. Pilgram, C. M. Speidel, L. R. Neumann, D. L. Rickman, and L. D. Schertz. Validation of magnetic resonance imaing (MRI) multispectral tissue classification. *Compute. Med. Imaging Graph.*, 15:217–223, 1991.

[124] M. W. Vannier, C. M. Speidel, and D. L. Rickman. Magnetic resonance imaging multispectral tissue classification. *News in Physiological Sciences*, 3:148–154, 1988.

[125] R. P. Velthuizen, L. P. Clarke Lawrence O. Hall, and A. M. Bensaid. Multispectral 3D MRI segmentation using knowledge based systems. *Med. Phys.*, 18(3):622, 1991.

[126] A. Visa. Statistical pattern recognition with neural networks. In *IEEE International Conference on Pattern Recognition (ICPR)*, volume 1, page 101, 1992.

[127] A. Waks and O. J. Tretiak. Recognition of regions in brain section. *Computerized Medical Imaging and Graphics*, 14(5):341–352, 1990.

[128] A. J. Worth and D. N. Kennedy. A recurrent competitive field for segmentation of magnetic resonance brain images. In *Book of abstracts Eleventh annual Scientific Meeting, Society of Magnetic Resonance in Medicine*, volume 2, page 4204. Berlin, Germany, August 1992.

[129] M. X. H. Yan and Joel S. Karp. Segmentation of 3D brain MR using an adaptive K-means clustering algorithm. In *Conference record : IEEE Nuclear Science Symposium and Medical Imaging Conference*, pages 1529–1533, 1995.

[130] A. P. Zijdenbos, B. M. Dawant, R. A. Margolin, A. A. Nimmerrichter, M. J. Levitt, and J. Williams. Computer-aided morphometrics of cerebral ventricles and white matter lesions in MR images. In *Book of abstracts Eleventh annual Scientific Meeting, Society of Magnetic Resonance in Medicine*, volume 2, page 4218. Berlin, Germany, August 1992.